

**LOCAL CALIBRATION OF MEPDG RUTTING MODELS
FOR ONTARIO'S SUPERPAVE PAVEMENTS**

By

Gyan Prasad Gautam,
BEng, Tribhuvan University, Nepal, 2000
MAsc, Purbanchal University, Nepal, 2007

A Thesis
presented to Ryerson University

in partial fulfillment of the
requirements for the degree of
Master of Applied Science
in the Program of
Civil Engineering

Toronto, Ontario, Canada, 2015

© Gyan Prasad Gautam 2015

AUTHOR'S DECLARATION

AUTHOR'S DECLARATION FOR ELECTRONIC SUBMISSION OF A THESIS

I hereby declare that I am the sole author of this thesis. This is a true copy of the thesis, including any required final revisions as accepted by my examiners.

I authorize Ryerson University to lend this thesis to other institutions or individuals for the purpose of scholarly research.

I further authorize Ryerson University to reproduce this thesis by photocopying or by other means, in total or in part, at the request of other institutions or individuals for the purpose of scholarly research.

I understand that my thesis may be electronically available to the public.

**LOCAL CALIBRATION OF MEPDG RUTTING MODEL
FOR ONTARIO'S SUPERPAVE PAVEMENTS**

By

Gyan Prasad Gautam

Master of Applied Science, 2015

Civil Engineering, Ryerson University

Toronto, Canada

ABSTRACT

The rutting models in the AASHTO Mechanistic-Empirical Pavement Design Guide (MEPDG) have been calibrated to Ontario's conditions for flexible pavements of Marshall mixes, and have yet to be calibrated for the Superpave materials. This study differs from previous studies in several counts: First, the local calibration database included both Superpave and Marshall mixes. Second, two of the five local calibration parameters (the temperature and traffic exponents) were pre-fixed based on a secondary study of the NCHRP 719 report. Third, both cross-sectional and longitudinal calibrations were performed and compared. It was concluded that the Superpave and Marshall mix pavements should be separately treated in the local calibration and that the cross-sectional and longitudinal calibrations behaved drastically differently in terms of residual errors. A set of local calibration parameters were recommended for future pavement design. It was recommended that trench investigations be done to further validate the results from the study.

Key words:

Superpave; local calibration; Mechanistic-Empirical Pavement Design Guide (MEPDG); rutting model; longitudinal calibration.

ACKNOWLEDGEMENTS

First of all, my foremost gratitude goes to my mentor and supervisor Dr. Arnold (Xian-Xun) Yuan, who expertly guided me through my graduate studies since my first day at Ryerson University. The suggestions on challenges of study, essential materials, encouragement, continual support, guidance and compassion throughout the work as well as his ideologies and teachings are of immense values for me for which I am indebted. Without his remarkable support and valuable contribution, this dissertation would not be possible to come into this form. His consistent mentoring developed my ethics of scientific research and motivated me to spoil in his attractive domain of civil engineering research.

It is gratefully acknowledged that the research is part of the project funded by the Ministry of Transportation of Ontario (MTO) Highway Infrastructure Innovation Funding Program (FY2013-2015). I would like to extend my gratitude to Mr. Warren Lee from the MTO, Pavement and Foundation Section, for his generous and sincere help. As part of the Ryerson Research Group led by Dr. Yuan on the MEPDG Local Calibration, I would also like to acknowledge the great help from Mr. Afzal Waseem at the early stage of my study. Afzal kindly shared his database passed down from Ms. Gulfam Jannat, and the semi-automated local calibration procedure, which has greatly sped up my local calibration analyses.

I would also like to extend my heartfelt thanks to Mr. Desmond Rogan, the Network Administrator of the Department of Civil Engineering, for his support in Network connections.

I would also like to extend my thanks to Dr. Medhat Shehata and Dr. Joseph Chow, members of the oral examination committee, for their valuable comments and suggestions.

Last but not least, with due respect, I would like to thank my parents and other family members for their financial and moral support and encouragement on my study.

TABLE OF CONTENTS

Title.....	i
Author's Declaration.....	ii
Abstract.....	iii
Acknowledgements.....	iv
Table of Contents.....	v
List of Tables.....	x
List of Figures.....	xv
List of Acronyms.....	xviii
Chapter 1 INTRODUCTION.....	1
1.1 Background.....	1
1.2 Problem Statement and Significance.....	4
1.3 Research Objective.....	5
1.4 Research Methodology.....	5
1.5 Thesis Organization.....	6
Chapter 2 LITERATURE REVIEW.....	8
2.1 Historical Development of Pavement Design Methods.....	8
2.2 AASHTO ME Design Method.....	9
2.2.1 General Framework.....	9
2.2.2 The MEPDG Software.....	11
2.2.2.1 Design Steps.....	12
2.2.2.2 Hierarchical Input Levels.....	13
2.2.2.3 Operation.....	13
2.2.2.4 Output Report.....	13

2.3 Rutting in Pavement	13
2.3.1 Mechanism of Rutting	13
2.3.2 Design Consideration.....	15
2.3.3 Measurement of Rutting	15
2.3.4 Forensic Investigation.....	17
2.3.5 Layer Contribution.....	19
2.4 The MEPDG Rutting Models.....	20
2.4.1 AC Rutting Model	21
2.4.2 Unbound Layer Rutting Model.....	22
2.4.3 Strain Hardening Approach	23
2.5 Global Calibration	24
2.5.1 Calibration in NCHRP 1-37A.....	24
2.5.2 Validation in NCHRP 1-40A.....	26
2.5.3 Recent Development in NCHRP 9-30A	29
2.5.3.1 Effects of Stress State.....	30
2.5.3.2 Effects of Temperature.....	31
2.5.4 Remarks	31
2.6 Efforts on Local Calibration.....	32
2.6.1 The Local Calibration Guide	32
2.6.2 Local Calibration Efforts in USA	33
2.6.3 Local Calibration Efforts in Canada	39
2.6.4 Existing Local Calibration Methodologies	42
2.7 Concluding Remarks	43
Chapter 3 TRAFFIC AND TEMPERATURE EXPONENTS	45
3.1 Introduction	45

3.2 The Traffic Exponent	46
3.3 Temperature Exponent	49
3.4 Concluding Remarks	49
Chapter 4 Local Calibration Methods.....	51
4.1 Guiding Principle	51
4.2 Cross-sectional Calibration and Longitudinal Calibration.....	53
4.3 Validation Methods	54
Chapter 5 Calibration Database	55
5.1 Data Requirement for Local Calibration	55
5.2 Accuracy of Input Data	55
5.3 Sample Selection	56
5.4 Major Input Variables for MEPDG.....	58
5.4.1 General Project Information	58
5.4.2 Traffic Data.....	59
5.4.3 Climatic Data	60
5.4.4 Pavement Material and Structural Data	61
5.5 Calibration Database	62
5.6 Summary	63
Chapter 6 Cross-Sectional Calibration.....	64
6.1 Calibration and Validation Results	64
6.1.1 Results for Superpave Sections.....	64
6.1.2 Results for Marshall Mix Sections.....	66
6.1.3 Discussions	68
6.2 Clustering Analysis	70
6.2.1 Cluster Analysis for Superpave Sections.....	70

6.2.2 Cluster Analysis for Marshall Mix Sections.....	71
6.3 Concluding Remarks	72
Chapter 7 Longitudinal Calibration	74
7.1 Characterization of Rut Depth	74
7.2 Results for Superpave Sections.....	75
7.2.1 Calibration Results.....	75
7.2.2 Discussions	80
7.2.3 Validation.....	81
7.3 Sensitivity Analysis for Local Calibration Results	82
7.3.1 Local Calibration Parameters for $m=0.25$	83
7.3.2 Local Calibration Parameters for $m=0.479$	84
7.3.3 Discussions	86
7.4 Results of Marshall Mix Sections	88
7.4.1 Local Calibration Parameters for $m=0.30$	89
7.4.2 Local Calibration Parameters for $m=0.479$	90
7.4.3 Discussions	92
7.4.4 Validation for Local Calibration Results	94
7.5 Comparison with Global Calibration Results	95
7.6 Second-Stage Factor Analysis.....	96
7.6.1 Superpave versus Marshall mix.....	96
7.6.2 Single factor analysis	97
7.6.2.1 Environment.....	97
7.6.2.2 Highway types.....	98
7.6.2.3 Top AC layer thickness.....	99
7.6.2.4 Total AC layer thickness.....	100

7.6.2.5 Total GB layer thickness	102
7.6.2.6 Sub-grade modulus	103
7.6.2.7 AADTT	104
7.6.2.8 Summary	105
7.7 Methodological Comparison	105
Chapter 8 Summary, Conclusions and Recommendations	108
8.1 Summary	108
8.2 Conclusions	109
8.3 Recommendations	110
APPENDIX A: Derived Plastic Deformation Coefficients Under NCHRP Project 9-30A	112
APPENDIX B: Pavement Sections Selected for Analysis	115
APPENDIX C: Traffic Data for AASHTOWare Analysis	119
APPENDIX D: Climatic Data for AASHTOWare Analysis	134
APPENDIX E: Pavement Material and Structural Data for AASHTOWare Analysis	139
Reference List	148

LIST OF TABLES

Table 2.1: Examples of analytically-based design procedure (Source: Monismith 2004) .	9
Table 2.2: Summary of release dates for MEPDG software version (Source: NCHRP 2013)	12
Table 2.3: Hierarchy of input levels.....	13
Table 2.4: Recommended threshold values of rutting for flexible pavement	15
Table 2.5: Comparison of results under a pilot study	19
Table 2.6: Average layer contribution to rutting.....	20
Table 2.7: Slope coefficient (source: NCHRP Report 719).....	28
Table 2.8: Fine aggregate angularity index (<i>Findex</i>) (source: NCHRP Report 719)	28
Table 2.9: Coarse aggregate angularity index (<i>Cindex</i>) (source: NCHRP Report 719) ..	28
Table 2.10: Proposed calibration parameters from past local calibration studies.....	38
Table 2.11: Local calibration results for new/reconstructed pavements by Waseem (2013)	41
Table 2.12: Local calibration results for rehabilitated pavements by Waseem (2013).....	42
Table 3.1: Test statistics between observed traffic exponents under NCHRP Project 9-30A.....	46
Table 3.2: Statistical results for total predicted rut within the global value of traffic exponent	47
Table 3.3: Statistical results for total predicted rut beyond the global value of traffic exponent	48
Table 5.1: Summary of general project input used for AASHTOWare in this study	58
Table 5.2: Summary of traffic input requirements and the accuracy level used in this study	59
Table 5.3: Climate input requirement used for AASHTOWare in this study.....	60
Table 5.4: AC layer material input requirements and the accuracy level used in the study	61
Table 5.5: Unbound layer material input requirements and the accuracy level used in the study	62

Table 6.1: Statistical results between calibration and validation sets of Superpave sections	64
Table 6.2: Statistical results between calibration and validation sets of Marshall mix sections	66
Table 6.3: Comparison of statistics of Global and Local calibration.....	68
Table 6.4: Cluster analysis results for Superpave Sections.....	70
Table 6.5: Cluster analysis results for Marshall mix Sections	71
Table 6.6: Comparison of cross-sectional calibration results for Marshall mix sections .	73
Table 7.1: Longitudinal calibration results for the Superpave sections (with $\beta r_2 = 1.0$ and $\beta r_3 = 0.6262$).....	75
Table 7.2: Longitudinal calibration results for the Superpave section (with $\beta r_2 = 1.0$ and $\beta r_3 = 0.5218$).....	83
Table 7.3: Longitudinal calibration results for the Superpave section (with $\beta r_2 = 1.0$ and $\beta r_3 = 1.0$)	85
Table 7.4: Comparison of statistical analysis with different value of traffic exponent	86
Table 7.5: Longitudinal calibration results for the Marshall mix section (with $\beta r_2 = 1.0$ and $\beta r_3 = 0.6262$).....	89
Table 7.6: Longitudinal calibration results for the Marshall mix sections (with $\beta r_2 = 1.0$ and $\beta r_3 = 1.0$)	91
Table 7.7: Comparison of statistical analysis with different value of traffic exponent	92
Table 7.8: Comparison of statistics of Global and Local calibration.....	96
Table 7.9: Summary of the t-test statistics for calibration parameters.....	97
Table 7.10: Test statistics of calibration parameters of Superpave mix for effect of environment.....	98
Table 7.11: Test statistics of calibration parameters of Marshall mix for effects of environment.....	98
Table 7.12: Test statistics of calibration parameters of Superpave mix for effects of highway type	99
Table 7.13: Test statistics of calibration parameters of Marshall mix for effects of highway type	99
Table 7.14: Summary of the regression analysis for effect of top AC layer thickness..	100

Table 7.15: Summary of the regression analysis for effect of total AC layer thickness	101
Table 7.16: Summary of the regression analysis for effect of total GB layer thickness	102
Table 7.17: Summary of the regression analysis for effect of sub-grade modulus.....	103
Table 7.18: Summary of the regression analysis for AADTT	104
Table 7.19: Effects of single factors on calibration coefficients.....	105
Table A.1: Field-derived plastic deformation coefficient for AC overlay test sections (source: NCHRP Report 719, Table 9)	112
Table A.2: Field-derived plastic deformation coefficient for new construction test sections (source: NCHRP Report 719, Table 8)	113
Table A.3: Laboratory-derived plastic deformation coefficient from repeated-load tests of reconstituted specimens (source: NCHRP Report 719, Table 24 and Table 25).....	114
Table B.1: Summary of the Superpave pavement sections from western region	115
Table B.2: Summary of the Superpave pavement sections from central region.....	115
Table B.3: Summary of the Superpave pavement sections from eastern region	116
Table B.4: Summary of the Superpave pavement sections from northeast region	117
Table B.5: Summary of the Superpave pavement sections from northwest region	117
Table B.6: Summary of the Marshall mix pavement sections	118
Table C.1: Recommended percentage of truck in design lane for Ontario.....	119
Table C.2: Standard speed for different highway class in Ontario	119
Table C.3: Summary of TTC and FHWA vehicle class distribution used in AASHTOWare.....	120
Table C.4: Axial per truck for southern Ontario.....	121
Table C.5: Axial per truck for northern Ontario	121
Table C.6: Single axial load distribution for southern Ontario.....	122
Table C.7: Single axial load distribution for northern Ontario	123
Table C.8: Tandem axial load distribution for southern Ontario.....	124
Table C.9: Tandem axial load distribution for northern Ontario	125
Table C.10: Tridem axial load distribution for southern Ontario	126
Table C.11: Tridem axial load distribution for northern Ontario.....	127
Table C.12: Quad axial load distribution for southern Ontario	128
Table C.13: Quad axial load distribution for northern Ontario.....	129

Table C.14: Ontario’s traffic information for Superpave pavement sections from western region.....	130
Table C.15: Ontario’s traffic information for Superpave pavement sections from central region.....	130
Table C.16: Ontario’s traffic information for Superpave pavement sections from eastern region.....	131
Table C.17: Ontario’s traffic information for Superpave pavement sections from northeast region.....	132
Table C.18: Ontario’s traffic information for Superpave pavement sections from northwest region.....	132
Table C.19: Ontario’s traffic information for the Marshall mix pavement sections.....	133
Table D.1: Ontario’s weather stations.....	134
Table D.2: Location parameters for selected Superpave pavement sections from western region.....	135
Table D.3: Location parameters for selected Superpave pavement sections from central region.....	135
Table D.4: Location parameters for selected Superpave pavement sections from eastern region.....	136
Table D.5: Location parameters for selected Superpave pavement sections from northeast region.....	137
Table D.6: Location parameters for selected Superpave pavement sections from northwest region.....	137
Table D.7: Location parameters for Marshall mix pavement sections	138
Table E.1: Ontario’s typical superpave and SMA properties	139
Table E.2: Ontario’s typical Marshall mix properties.....	139
Table E.3: Ontario’s recommended asphalt stabilized material properties.....	140
Table E.4: Ontario’s typical granular material properties.....	140
Table E.5: Ontario’s typical chemically stabilized base material properties	140
Table E.6: Ontario’s typical fine sub-grade soil properties	140
Table E.7: Material and structural information for the selected Superpave sections from western region	141

Table E.8: Material and structural information for the selected Superpave sections from central region..... 142

Table E.9: Material and structural information for the selected Superpave sections from eastern region 143

Table E.10: Material and structural information for the selected Superpave sections from northeast region..... 144

Table E.11: Material and structural information for the selected Superpave sections from northwest region..... 145

Table E.12: Material and structural information for the Marshall mix pavement sections 146

LIST OF FIGURES

Figure 1.1: Prediction performance of globally calibrated rutting models	2
Figure 1.2: Comparison of total rutting for Superpave and Marshall mix sections	3
Figure 2.1: Overall concept of MEPDG	10
Figure 2.2: ME design procedure	11
Figure 2.3: Typical rut progression curve in log scale (source: AASHTO 2004)	14
Figure 2.4: Manual and ANAR method of measuring the rut depth (Source: Li 2011) ...	16
Figure 2.5: Typical transverse profile	17
Figure 2.6: Trench profile analysis (Source: Hussan 2013).....	19
Figure 2.7: Concept of strain hardening approach	24
Figure 2.8: Generalized basic steps of local calibration methodology	32
Figure 3.1: Comparison between the predicted rutting with different value of m.....	47
Figure 3.2: Frequency evaluation for traffic exponent under NCHRP Project 9-30A (Data source: Table A-1, A-2 and A-3)	48
Figure 3.3: Frequency evaluation for temperature exponent under NCHRP Project 9-30A (a) repeated load triaxial test and (b) repeated load shear test (Data source: Table A-3) .	49
Figure 4.1: Typical example for longitudinal calibration methodology	54
Figure 5.1: Distribution of number of available sections by climatic zone	57
Figure 5.2: Distribution of number of selected sections by climatic zone.....	57
Figure 6.1: Predicted versus observed plots for (a) calibration (b) validation.....	65
Figure 6.2: Residual error for Superpave sections	65
Figure 6.3: Predicted versus observed plots for (a) calibration (b) validation.....	67
Figure 6.4: Residual error for Marshall mix sections	67
Figure 6.5: Comparison of longitudinal trend of rutting for Superpave pavements	69
Figure 6.6: Comparison of longitudinal trend of rutting for Marshall mix pavements	69
Figure 7.1: Longitudinal plots for predicted and observed rut	79
Figure 7.2: Predicted versus observed plots (with $\beta r_2 = 1.0$ and $\beta r_3 = 0.6262$)	81
Figure 7.3: Predicted versus observed plots for validation (with $\beta r_2 = 1.0$ and $\beta r_3 = 0.6262$).....	82
Figure 7.4: Predicted versus observed plots (with $\beta r_2 = 1.0$ and $\beta r_3 = 0.5218$)	84

Figure 7.5: Predicted versus observed plots (with $\beta r_2 = 1.0$ and $\beta r_3 = 1.0$).....	85
Figure 7.6: Histograms of local calibration coefficients for $m = 0.25$ (or $\beta r_3 = 0.5218$)	87
Figure 7.7: Histograms of local calibration coefficients for $m = 0.30$ (or $\beta r_3 = 0.6262$)	87
Figure 7.8: Histograms of local calibration coefficients for $m = 0.479$ (or $\beta r_3 = 1.0$). 87	
Figure 7.9: Histogram for average calibration coefficients	88
Figure 7.10: Variation of layer contribution with section specific calibration coefficients	88
Figure 7.11: Predicted versus observed plots for marshal mix sections with $m = 0.30$ (or $\beta r_3 = 0.6262$).....	89
Figure 7.12: Predicted versus observed plots for marshal mix sections with $m = 0.479$ (or $\beta r_3 = 1.0$)	91
Figure 7.13: Histograms of local calibration coefficients for $m = 0.30$ (or $\beta r_3 = 0.6262$)	93
Figure 7.14: Histograms of local calibration coefficients for $m = 0.479$ (or $\beta r_3 = 1.0$). 93	
Figure 7.15: Histogram for average calibration coefficients	93
Figure 7.16: Variation of layer contribution with section specific calibration coefficients	94
Figure 7.17: Validation - predicted versus observed plots with $m = 0.30$ (or $\beta r_3 =$ 0.6262).....	95
Figure 7.18: Effects of top AC layer thickness on calibration coefficients for Superpave mix	100
Figure 7.19: Effects of top AC layer thickness on calibration coefficients for Marshall mix	100
Figure 7.20: Effects of total AC layer thickness on calibration coefficients for Superpave mix	101
Figure 7.21: Effects of total AC layer thickness on calibration coefficients for Marshall mix	101
Figure 7.22: Effects of total GB layer thickness on calibration coefficients for Superpave mix	102

Figure 7.23: Effects of total GB layer thickness on calibration coefficients for Marshall mix 102

Figure 7.24: Effects of sub-grade modulus on calibration coefficients for Superpave mix 103

Figure 7.25: Effects of sub-grade modulus on calibration coefficients for Marshall mix 103

Figure 7.26: Effects of AADTT on calibration coefficients for Superpave mix 104

Figure 7.27: Effects of AADTT on calibration coefficients for Marshall mix 104

Figure 7.28: Residual error for total predicted rut depth for Superpave sections 106

Figure 7.29: Residual error for total predicted rut depth for Marshall mix sections 106

Figure 7.30: Typical longitudinal trend of rutting for (a) Superpave (b) Marshall..... 107

LIST OF ACRONYMS

AADT	Annual Average Daily Traffic
AADTT	Annual Average Daily Truck Traffic
AASHO	American Association of State Highway Officials, the predecessor of AASHTO
AASHTO	American Association of State Highway Officials
AC	Asphalt Concrete
ADOT	Arizona Department of Transportation
AI	Asphalt Institute
ARAN	Automatic Road Analyzer
CBR	California Bearing Ratio
CDOT	Colorado Department of Transportation
CSC	Cross-sectional Calibration
CSV	Cross-sectional Validation
DOTs	Departments of Transportation
ESALs	Equivalent Single-Axle Loads
FE	Finite element
FHWA	Federal Highway Administration
GAO	Genetic Algorithm Optimization
GB	Granular base
GPS	General Pavement Section
GRG	Generalized Reduced Gradient
GWT	Ground Water Table
HMA	Hot Mix Asphalt
HRB	Highway Research Board
IRI	International Roughness Index
JULEA	Jacob Uzan Layered Elastic Analysis
LC	Longitudinal Calibration
LTPP	Long Term Pavement Performance
LV	Longitudinal Validation
MASc	Master in Applied Science

ME	Mechanistic-Empirical
MEPDG	Mechanistic-Empirical Pavement Design Guide
MLE	Multilayer-elastic
MLVE	Multilayer-viscoelastic
MMPS	Marshall Mix Pavement Section
MnDOT	Minnesota Department of Transportation
MnRoad	Minnesota Road
MoDOT	Missouri Department of Transportation
MTO	Ministry of Transportation of Ontario
NCDOT	North Carolina Department of Transportation
NCHRP	National Cooperative Highway Research Program
NO	Northern Ontario
PMS	Pavement Management Systems
PR	Public Roads
RLPD	Repeated Load Permanent Deformation
RSS	Residual Sum of Square
SAS	Statistical Software
SHRP	Strategic Highway Research Program
SMA	Stone Matrix Asphalt
SO	Southern Ontario
SPS	Specific Pavement Studies
SPPS	Superpave Pavement Section
ST	Shear Test
TT	Triaxial Test
TTC	Truck Traffic Classification
TxMLS	Texas Mobile Load Simulator
UDOT	Utah Department of Transportation
USA	United State of America
WSDOT	Washington State Department of Transportation
WSPMS	Washington State Pavement Management System

CHAPTER 1 INTRODUCTION

1.1 Background

The modern rational pavement design method started with the Public Roads (PR) soil classification during 1920s (Huang 2004). Afterwards, many models were developed and improved but none of them significantly changed the trend of the pavement design before the road tests were conducted by Highway Research Board (HRB) during 1950s. The AASHO Road Test in Ottawa, Illinois is considered as one of the most important research project in the historical evolution of pavement design that shifted the trend of pavement design from stress-based to performance-based by establishing the empirical relationships between axle loads and structural performance of the pavements (Huang 2004). Based on the results of the AASHO Road Test, AASHTO developed its first interim design guide by 1961 and, thereafter, continuously enhanced it in years 1972, 1986, and 1993. Over the past two decades, the AASHTO pavement design guide version 1993 has served well as the primary method of pavement design in majority of highway agencies in North America. Despite its widespread use, the method is purely empirical with a limited range of design conditions that limits the validation of the models only to the original test range of geographic locations, traffic loadings, soil types and construction methods (AASHTO 2008).

However, extrapolation out of the specific range of experimental conditions requires compromise on the accuracy of the method. To address these limitations, AASHTO Mechanistic-Empirical Pavement Design Guide (MEPDG) and the corresponding software had been developed under the National Cooperative Highway Research Program (NCHRP) Project 1-37A by the end of 2004 (AASHTO 2008). Several subsequent updates were performed in the MEPDG and its software during 2005-2013 under the NCHRP Projects 1-40D and 9-30A. Recently in August 2013, AASHTO released the AASHTOWare pavement design software version 2.1 as its latest version for commercial purpose.

The Ministry of Transportation of Ontario (MTO) is currently practicing its own pavement design method for design and rehabilitation of Ontario's highways, but it is anticipated

that the MEPDG method will be the standard pavement design method for the foreseeable future. Under this scenario, MTO also decided to use the MEPDG method for future pavement design. However, the method includes a suite of globally calibrated empirical transfer models that without local calibration, might fail to characterize the local conditions, materials and construction practices. Preliminary studies have shown that the globally calibrated models over-predict the rutting for Ontario's roads (Jannat 2012, Waseem 2013). At the very beginning of this research, the author performed a preliminary evaluation of some selected Superpave sections in order to evaluate the prediction performance of globally calibrated rutting models. The comparison between the observed and predicted total pavement rutting is shown in Figure 1.1 where the predicted values of all the sections are much higher than the field observed values as mentioned by Jannat (2012). Therefore, to implement the method in Ontario's conditions, local calibration is unavoidable.

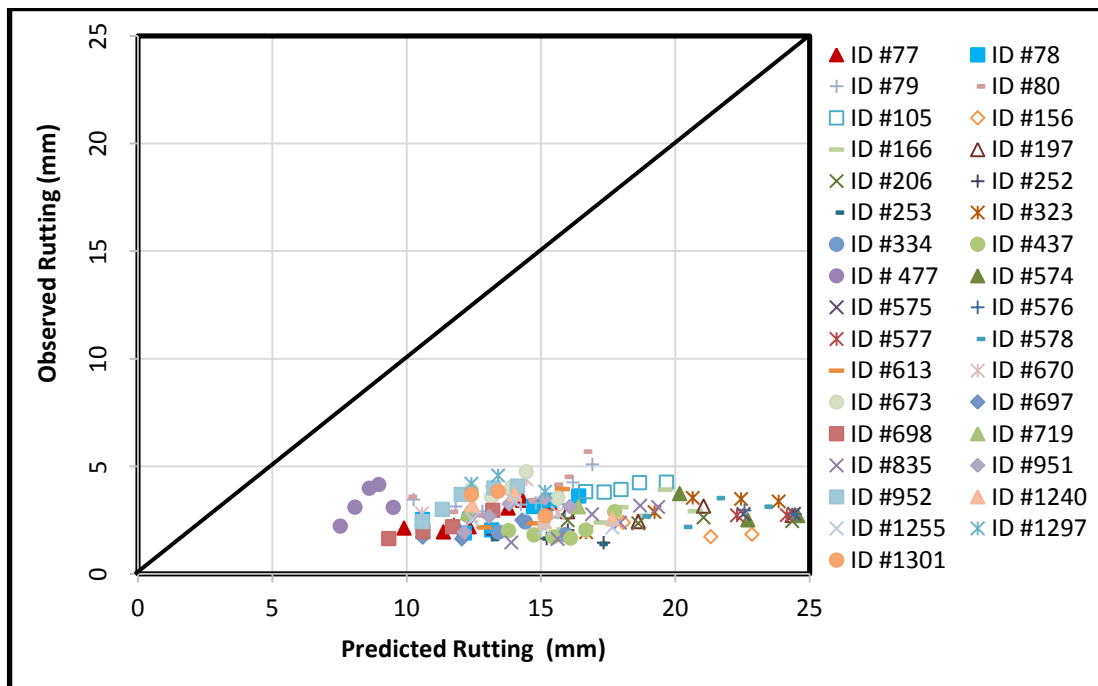


Figure 1.1: Prediction performance of globally calibrated rutting models

The MEPDG Local Calibration Guide (AASHTO 2010) elaborates the step by step procedure in a structured format; however, the universally agreed local calibration methodology is still indistinct. In addition, the performance data collected by MTO under Pavement Management Systems (PMS) are not necessarily appropriate to use directly for the local

calibration. Therefore, there is also an urgent need to pay adequate attention to the development of local calibration methodology along with database development under the Ontario's conditions.

Jannat (2012) contributed on database development for Ontario's local calibration of MEPDG distress models. In particular, she developed a database of 101 section cycles integrated with high quality section specific material, pavement performance and traffic data. Using the database, Waseem (2013) developed a semi-automated local calibration methodology and performed local calibration for the MEPDG rutting models. However, a major constraint of the database was that it included only flexible pavements with Marshall mixes.

Rutting as an important decision parameter of the pavement design has a significant impact on the performance of pavements by causing hydroplaning phenomena, difficulties in driving, formation of ice in the wheel path, roughness and structural damages (Xu et al. 2012). Superpave material was invented in 1993 mainly to improve the rutting resistance. A preliminary observation of total rut depth to some typical Superpave pavement sections (SPPS) and Marshall mix pavement sections (MMPS) from same location of Ontario (refer to Tables B1 to B6) are shown in the Figure 1.2. The curves demonstrate that the rutting is significantly lower in Superpave rather than Marshall mix sections. This has proved the better rutting performance of the Superpave mix. However, whether a separate sets of rutting models is required for the different mix types in the MEPDG remains to be an open question, because albeit the observed difference in rutting, this difference might be able to explained and captured by the mechanistic models in the MEPDG (for example, through the different dynamic modulus models for the different mixes).

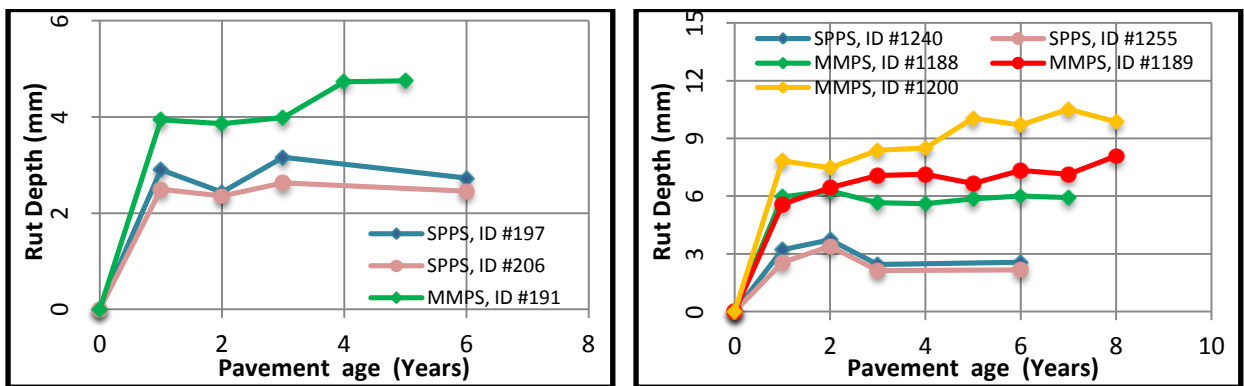


Figure 1.2: Comparison of total rutting for Superpave and Marshall mix sections

On the other hand, pavement design requires clear projection of rutting to ensure the structural and functional requirements. The current cross-sectional calibration method that is suggested by the AASHTO Local Calibration Guide may be able to reduce both the bias and residuals to an acceptable level from the whole database perspective, but the rutting models that were so locally calibrated might still systematically over or under predict the rutting along the life cycle for a *specific* pavement section. This means that although the overall system bias might have been reduced to a minimal level, the section-specific bias across the life cycle may be still substantial. Calibrating the rutting models so as to reduce, if not eliminate, both the system-wide bias and section-specific bias, remains to be a challenging issue. And this involves development of some innovative local calibration method.

1.2 Problem Statement and Significance

Although MEPDG method provides a rational design approach with a solid foundation of engineering mechanics, the empirical models that relate mechanistic structural responses to predicted distresses are globally calibrated using Long Term Pavement Performance (LTPP) and Pavement Management Systems (PMS) database and fail to characterize the local conditions, materials and construction practices. The former studies pointed out that the globally calibrated models compromise on the accuracy of predicted pavement performance under the local circumstances. The recent studies by Jannat (2012) and Waseem (2013) also verified the result of former studies and concluded that the globally calibrated models over-predict the rutting to Ontario's road. The same conclusion is drawn from the study of prediction performance of the rutting models for Ontario's Superpave sections under this research. So, the local calibration of rutting models are essential for realistic representation of evolution of rutting before implementation of MEPDG method to Ontario conditions.

The rutting models have been recently calibrated by Waseem (2013) to Ontario's pavements with AC layers of Marshall type. Although Superpave mix has been almost exclusively used in Ontario's roads since 2001, it is still unknown whether a separate set of calibration parameters are required for Superpave pavements or not. Also, the database developed by Jannat (2012) are limited to Marshall mix types. Therefore, there is also an urgent need to pay adequate attention for database development, methodology development and local calibration of MEPDG rutting models for Superpave mixes under the Ontario's conditions.

This research used the Ontario's PMS database for local calibration of rutting models in contrast to LTPP or road test data that most of the former studies used. This thesis is also significant as the rutting models have yet to be calibrated to Ontario's pavements with AC layers of Superpave mixes. All these issues are to be addressed in this thesis study.

1.3 Research Objective

The primary objective of this study is to conduct a comprehensive local calibration study of the empirical rutting models of the MEPDG method for the Ontario's highway pavement design and maintenance practices. The research consist of:

1. A thorough review of previous efforts on local calibration.
2. Development of a local calibration database that includes a number of selected, typical pavement sections under MTO's jurisdiction with input data and observed rutting data from MTO's PMS database.
3. Development and comparison of local calibration procedures to increase the accuracy and efficiency of the local calibration study.
4. Recommendation of one or several sets of local calibration coefficients of the rutting models for future pavement design in Ontario using MEPDG.

1.4 Research Methodology

This research used both the cross-sectional and longitudinal calibration strategies. In the first type of model calibration, all rutting data from different sections are pooled together to obtain a single set of local calibration parameters, whereas, in the second type of model calibration, each section with a relatively long series of rut records was individually calibrated, thus, a section-by-section calibration. The Residual Sum of Square (RSS) minimization process is used during the both types of model calibration by considering the equal weight for each observed rut depth.

A comprehensive literature review was performed on previous efforts for local calibration. This study raised a plenty of specific issues related to the behavior of the models (such as layer contribution, model exponents) and the type of models for new/reconstructed and rehabilitated pavement sections for full local calibration. These issues were resolved by performing a number of tests (such as t-tests and sensitivity analysis) based on the available

information. A local calibration database for a number of selected, typical pavement sections under MTO's jurisdiction was developed that includes input data and accuracy levels for AASHTOWare pavement design software along with the observed rutting data from MTO's PMS database.

Two different local calibration methods were compared in the literature review and the optimization procedure was developed using the analysis results from the AASHTOWare environment based on least square method. Finally, the proposed cross-sectional and longitudinal method of model calibration were applied to Ontario's Superpave and Marshall mix sections and the results were verified separately.

1.5 Thesis Organization

The thesis is organized into eight chapters. The first chapter introduces the background and elaborates the need and scope of the research.

Chapter 2 provides a comprehensive review of relevant literature to this study. It reviews basic concepts of rutting, historical developments of pavement design methods, overall concept and design process of the MEPDG method and the corresponding design software, the rutting models used in MEPDG, and the current practices of local calibration and the methodology used by previous local calibration studies.

Chapter 3 is devoted to a discussion of the nature of field and laboratory derived plastic deformation coefficients obtained under the NCHRP Project 9-30A, particularly, the temperature and traffic exponents used in the AC rutting model of the MEPDG. Specific values of the temperature and traffic exponents are proposed for the subsequent local calibration analyses.

Chapter 4 discusses the local calibration methodology used by the author for the calibration of rutting models to Ontario's roads. With a fixed set of temperature and traffic exponents, simultaneous linear equations derived from the least square principle are established for both cross-sectional and longitudinal calibrations.

Chapter 5 summarizes the calibration database required for local calibration. The detailed input data regarding traffic, climate, pavement material and structure and level of accuracy used for local calibration are discussed.

Chapter 6 discusses the implementation of cross-sectional local calibration methodology and presents the results of locally calibrated parameters for Ontario's Superpave as well as Marshall mix pavement sections.

Chapter 7 discusses the implementation of longitudinal local calibration methodology and presents the results of locally calibrated parameters for Ontario's Superpave as well as Marshall mix pavement sections.

Finally, Chapter 8 summarizes the research with conclusions and recommendations.

Appendix A, B, C, D and E describes the field and laboratory derived plastic deformation coefficients under NCHRP Project 9-30A, characteristics of the pavement sections, traffic, climate and material input data, input level and sources of these input parameters used in AASHTOWare pavement design software.

CHAPTER 2 LITERATURE REVIEW

2.1 Historical Development of Pavement Design Methods

The AASHTO MEPDG has come from a long way of highway design and construction, along which generations of pavement scientists and engineers have strived to develop a rational pavement design method and various efficient construction methods through systematic experiments, sober and often painful lesson learning from failures, and bold engineering innovations of various forms. Huang (2004) provides an excellent summary of the historical development of pavement design methods. According to Huang (2004), rational pavement design method started with the Public Roads (PR) soil classification, which was the first empirical pavement design method proposed by Hogentogler and Terzaghi during 1920s. In 1928, California Bearing Ratio (CBR) method was developed by California Highways Department to estimate the thickness of layers against sub-grade shear failure based on CBR value of the materials. Further, the method was improved under Highway Research Board (HRB) in 1945 by grouping soil for the best estimate of sub-base quality and pavement thicknesses. AASHO Road Test in Ottawa, Illinois conducted by HRB during 1950s is taken as the most imperative research in the historical evolution of pavement design that contributed toward the serviceability design concept by establishing the empirical relationships between axle loads and structural performance of the pavements (Huang 2004).

Based on results of AASHO Road Test, the later renamed AASHTO developed regression equations and published its first interim design guide by 1961 (Dzotepe and Ksaibati 2011). The guide was purely empirical with limited range of design parameters that includes only one climate, one sub-grade, two years life span, limited cross sections and materials, traffic volumes, specifications and construction methods (AASHTO 2008). Clearly, the equations were not compatible for all soil, traffic and climate. Despite of the many subsequent updates to the regression models up to the year 1993, the AASHTO empirical design equations still lack to incorporate complex behavior of different materials and accuracy of performance predictions.

In the meanwhile, many analytically-based mechanistic empirical (ME) design methods were being developed; for example, the Shell, Asphalt Institute and VESYS pavement design methods (Monismith 2004). The methods were mechanistic-empirical, in that they incorporated

multi-layer analysis software such as BISAR, DAMA, VESYS, CIRCLY, and JULEA for the analysis and pavements were designed by limiting rutting and fatigue cracking on the surface of sub-grade and at the bottom of the asphalt layer respectively. Some of those analytically-based design procedure for flexible pavements are listed in Table 2.1.

Table 2.1: Examples of analytically-based design procedure (Source: Monismith 2004)

Design Method	Theoretical Basis	Computer Program	Design criteria	Rutting Estimation
Shell method	MLE	BISAR	Fatigue and rutting	Design Charts
NCHRP Project 1-10B	MLE	MTC093	Fatigue and rutting	Design Charts
AI method	MLE	DAMA	Fatigue and rutting	Design Charts
LCPC	MLE	ELIZE	Fatigue and rutting	Catalogue of designs
CRR, Belgium	MLE	MTC093	Fatigue and rutting	Design Charts
NITRR, South Africa	MLE	ELIZE	Fatigue and rutting	Catalogue of designs
NCHRP Project 1-26	FE, MLE	ELSYM	Fatigue and rutting	Performance model
FHWA	MLE, MLVE	VESYS	Fatigue and rutting	Model using rutting parameters μ and α
Austroroads	MLE	CIRCLY	Fatigue and rutting	Design Charts
NHRP Project 1-37A (Proposed AASHTO Guide)	MLE	JULEA	Fatigue, rutting and cracking	Performance model
Note: MLE - multilayer elastic, MLVE - multilayer viscoelastic and FE - finite element				

2.2 AASHTO ME Design Method

2.2.1 General Framework

Under the joint initiatives of AASHTO and FHWA, the MEPDG and corresponding software were developed under NCHRP Project 1-37A and completed at the end of 2004 (AAHTO 2008). The guide accounts for several advanced modeling concepts by integrating the mechanistic theories of engineering with experimental results and utilizes a user-friendly software with three hierarchical levels of accuracy for input including traffic, climate, and materials during the

analysis and design of new and rehabilitated pavements. The whole concept of the guide is shown in Figure 2.1.

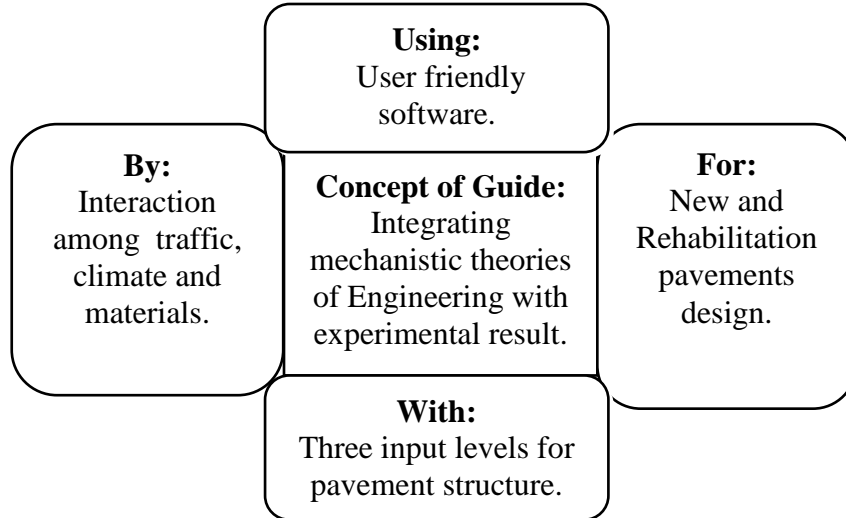


Figure 2.1: Overall concept of MEPDG

The MEPDG method is a hybrid approach, representing a major shift from previous empirical methods of pavement design. It requires inputs of materials, traffic, climate and type of construction, reconstruction or rehabilitation activities. It incorporates the effects of change in inputs parameters during the service life (e.g., traffic loading, temperature, moisture content, air voids, stiffness and density of the materials) and performs the pavement analysis in two steps: engineering mechanistic analysis and empirical transfer models. For flexible pavements, the first step uses multi-layered elastic theory to evaluate structural responses (stresses, strains and deflection), whereas, the second step uses these structural responses to estimate pavement surface distresses through empirical transfer models (NCHRP 2004). The transfer models for flexible pavements includes: fatigue cracking models, thermal cracking models, rutting models and International Roughness Index (IRI) models. These models have been calibrated to actual pavement performance by using the Long-Term Pavement Performance (LTPP) database. Since the database used for the calibration covers a wide range of states in the USA and provinces in Canada, the calibration was called global calibration.

The performance of a pavement is evaluated through the predicted distress. For flexible pavements, the MEPDG method considers AC bottom-up fatigue cracking, AC top-down fatigue

cracking, AC thermal cracking, rutting and International Roughness Index (IRI) to be the major performance prediction indicators. These indicators have certain limiting values established by regional transport agencies to indicate the structural and functional condition of the pavements. The designers should ensure the pavement distresses within the pre-established limit during the design and maintenance practices in a particular jurisdictional region. The flow chart in ME design procedure is shown in Figure 2.2.

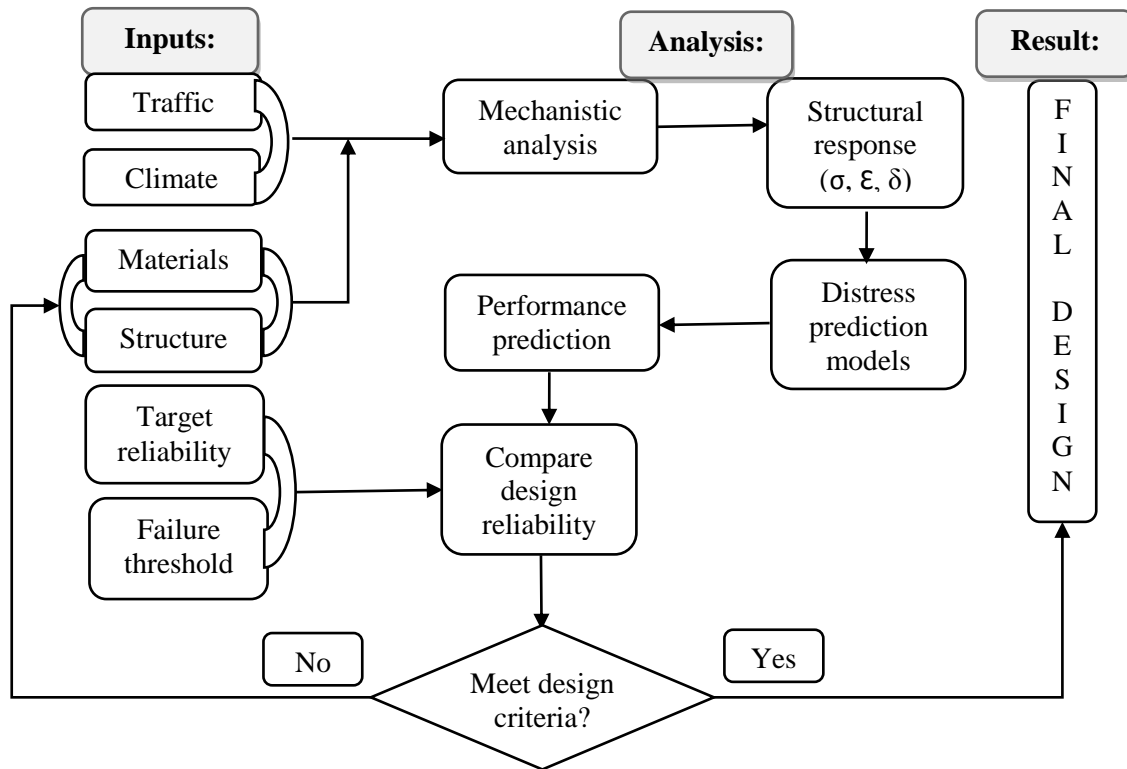


Figure 2.2: ME design procedure

2.2.2 The MEPDG Software

The design software has evolved a lot since it was first introduced to the pavement community. Even the name has been changed a few times. Starting with the name of MEPDG, the software was renamed to DARWin-ME in 2011, and changed again to AASHTOware Pavement ME in 2013. The first publicly available MEPDG software version 0.7 was developed at the end of 2004 as a part of delivery of NCHRP Project 1-37A.

Several updates were performed in the software during 2005-2009 under the NCHRP Projects 1-40D and 9-30A as shown in Table 2.2. The major changes during the period were

related to traffic and other general topics, integrated climatic model, pavement design and analysis approach. The latest research version of user-friendly software, known as AASHTOWare pavement design software, based on the mechanistic-empirical models incorporated in MEPDG version 2.1 is released by AASHTO in August 2013 for commercial purposes. This is a production-ready new generation software that represents a major revolution in the pavement design by providing a direct tie between materials, structure, construction practices, climate, traffic and design features. It is intended to simplify the day-to-day pavement design and analysis.

This study is based on AASHTOWare Pavement ME version 2.1. This version includes a choice on single or multi-layer rutting coefficients for asphalt rutting. It now supports summary reports for backcalculation and allows user to utilize backcalculation data for thickness optimization. It also provides an option to automatically update the system and converts the old files to version 2.0.

Table 2.2: Summary of release dates for MEPDG software version (Source: NCHRP 2013)

Software Version	Release Date	Project
0.700	July 2004	NCHRP Project 1-37A
0.800	November 2005	NCHRP Projects 1-40D and 9-30A
0.900	July 2006	
1.000	April 2007	
1.100	August 2009	
2.100	August 2013	

2.2.2.1 Design Steps

Similar to any engineering design, each pavement design in AASHTOWare pavement design software follows a three-step iterative process. The first step creates a trial design for project. The second step runs the software to predict the key distresses for trial design. In the last step, it compares the predicted performance of the trial design to the performance criteria and modifies the trial design if the performance targets are not satisfied, until a feasible design solution is obtained within the performance criteria.

2.2.2.2 Hierarchical Input Levels

AASHTOWare pavement design software provides flexibility to select hierarchical input levels related to traffic, material, and pavement condition as shown in Table 2.3. This is intended to help reduce the cost of material testing during pavement site investigation. So, selection of input hierarchy primarily depends upon the economic importance of the pavement structure.

Table 2.3: Hierarchy of input levels

Level	Level of accuracy	Reliability	General input source
Level 1	Highest	High	Site specific data
Level 2	Intermediate	Medium	Agency database
Level 3	Minimal	Low	Default or user defined

2.2.2.3 Operation

AASHTOWare pavement design software also provides a database option for enterprise operation (AASHTO 2011). It includes archiving projects, creating data libraries, exporting and importing input data files. It has the capability to run many projects consecutively at same time. It uses the globally calibrated empirical transfer function to estimate the pavement distresses. However, it is also compatible for the use of local calibration coefficients in the transfer models.

2.2.2.4 Output Report

Finally, AASHTOWare pavement design software generates reports in PDF and Excel formats. This report contains the summary of the inputs about the materials, traffic, climates and the calibration coefficients used in the analysis of the project. The report also summarizes the predicted distress of the pavement for entire pavement life.

2.3 Rutting in Pavement

2.3.1 Mechanism of Rutting

The phenomenon of rutting in flexible pavement is the result of material densification and plastic shear deformation in all pavement layers due to repeated traffic load. However, many other internal phenomena such as poor sub-grade and base layers compaction, poor water proofing layers, weak structural design, poor construction quality and weak material stiffness also

contribute to rutting (AASHTO 2008). Despite of these collective and possible synergistic effects of all these factors, present rutting studies for pavement structural design only focus on traffic-induced permanent deformation.

The rutting in the pavement is usually characterized in three stages, known as the primary stage, secondary stage and tertiary stage (Figure 2.3). The main features of three stages mechanism of rutting are listed below (AASHTO 2004).

(a) Primary stage:

- initial stage of loading
- high rate of rutting
- most rutting is due to volumetric changes of the mixture

(b) Secondary stage:

- small and constant rate of rutting
- densification decreases and shear deformation increases
- most rutting is due to the plastic shear deformation

(c) Tertiary stage:

- high rate of rutting
- rutting is due to the plastic shear deformation under no volume change conditions
- shear failure occur and the mixture flows to rupture

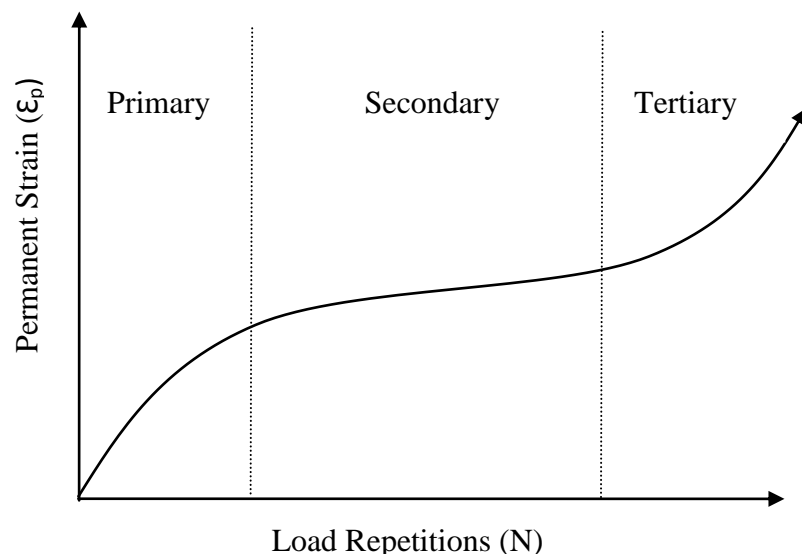


Figure 2.3: Typical rut progression curve in log scale (source: AASHTO 2004)

Modeling of rutting mechanism is required to estimate the true evolution of rutting. The MEPDG rutting models consider only the primary and secondary stages of deformation, assuming that the tertiary stage is not reached in in-service pavements, because the magnitude of rutting associated with tertiary stage yields a very high rut depth compared to the actually accepted level in the practice. Therefore, modeling for true plastic shear deformations in the tertiary stage is a research field mainly to material engineers, but not to design engineers.

2.3.2 Design Consideration

Rutting as a major failure mode has a significant impact on the performance of asphalt pavement. Adding roughness, it reduces not only the service life, but also functional serviceability of the pavement due to hydroplaning, steering difficulty and ice accumulation. Significant amount of rutting adds safety challenges to highway users (Xu et al. 2012). Therefore, to ensure the structural and functional requirements, the pavement requires limiting the maximum rut depth over the pavement lifetime. Table 2.4 shows the limiting value of rutting recommended by the AASHTO MEPDG (AASHTO 2008) for different types of highway pavements. The table also shows the limiting values recommend by MTO. Unlike the AASHTO guide, MTO limits both the total rutting and the AC rutting.

Table 2.4: Recommended threshold values of rutting for flexible pavement

Agency	Highway types	Total or AC rutting	Maximum recommended value
AASHTO (2008)	Primary	Total	0.50" (12.50 mm)
	Interstate	Total	0.40" (10.20 mm)
	Other (< 45mph, or 72.42 kph)	Total	0.65" (16.50 mm)
MTO (2012)	King's and Secondary	Total	0.75" (19.00 mm)
	King's and Secondary	AC	0.24" (6.00 mm)

2.3.3 Measurement of Rutting

In early days, manual methods such as wire method, straight edge method and dipstick method were used to measure rut depth (Gramling et al. 1991, LTPP 2013). An example of straight edge method is shown in Figure 2.4a where the rut depth was measured manually using a 3m straight

edge and displacement transducer (Gramling et al. 1991). However, these measurement approaches are not reliable and may easily result in large error because of their subjective nature. Recently, a modern automated laser scanner method is placed in service in MTO for accurate measurement of rut on the surface of the pavements. The method consists of an advanced pavement data collection vehicle equipped with Automatic Road Analyzer (ARAN). The ARAN technology utilizes a 4m laser transverse profiler with 36 ultrasound sensors as shown in Figure 2.4b to measure the surface profile including rutting, roughness and texture at about 100 mm spacing with an accuracy of 1 mm and reports the average rut depth for each 20 m or 100 m or any desired section length (Li 2011).

MTO has started the use of the ARAN technology for rutting measurement since 2002. The current approach first determines the maximum rut depths in the left and right wheel path, respectively, and then reports the average of these two values as the measured rut depth for a specific pavement section (Li 2011). This research utilizes the MTO's ARAN rut depth for the local calibration of MEPDG rutting model to the local condition. However, the modern ARAN measurements are significantly updated (e.g., number of sensors, compatibility and technology) for higher accuracy. Even in MTO, the new ARAN technology uses 3D laser scan for the rutting, whereas, the old ARAN rutting was based on ultrasonic system. This technological changes can greatly influence the accuracy of the rut depth measurement which can be an issue for local calibration.

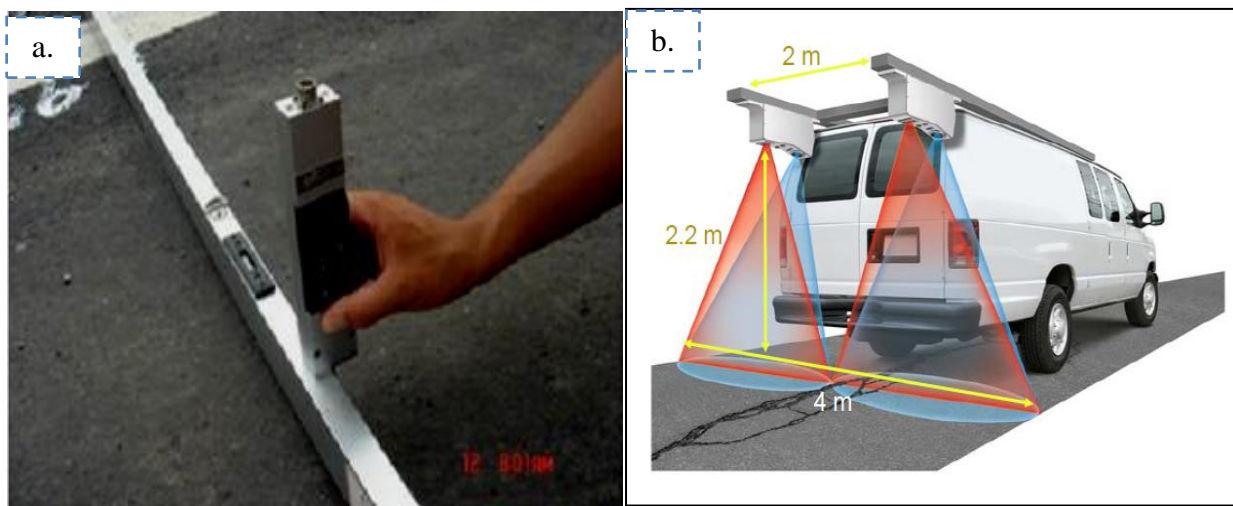


Figure 2.4: Manual and ANAR method of measuring the rut depth (Source: Li 2011)

2.3.4 Forensic Investigation

The concept of forensic investigation in the pavement design is to conduct the investigation of experimental test sections. It mostly focuses on investigating the underlying causes of premature pavement failure, validating pavement performance prediction, or collecting project specific data for calibration of performance prediction models (Rada et al. 2013). The surface rut depth is a general indicator of the structural performance of the pavement but it fails to provide enough information regarding the root cause of the overall rutting.

Independent studies conducted by Villiers et al. (2005) reported inconsistency rut depth with traffic, time and mix properties. Therefore, careful evaluation and identification of the possible source of rutting is an important factor that provide the necessary information to the designers for rehabilitation. In this regard, Simpson et al. (1995) introduced an area technique and later on White et al. (2002) proposed an extension of the Simpson theory to explain the sources of rutting in the pavement section for a NCHRP Project 1-34A. In the report (NCHRP 468), White et al. (2002) proposed the following criteria using the total area (A) and the ratio of the positive to negative area (R) under the transverse surface profile to determine the possible dominating layers to rutting using a typical transverse profile as shown in Figure 2.5. They are:

- i) AC layer rutting failure, if $R \geq 0.05$ and $A > (C_1 + C_2)/2$;
- ii) Base/sub-base layer failure, if $R < 0.05$ and $A > (C_2 + C_3)/2$; and
- iii) Sub-grade layer failure, otherwise.

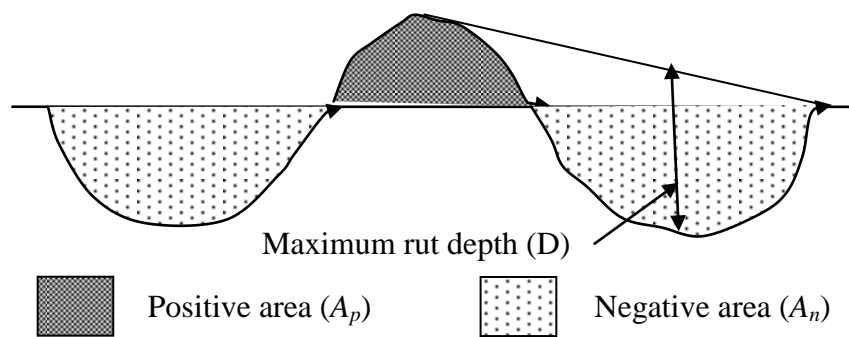


Figure 2.5: Typical transverse profile

The notations used in the above criteria are explained below:

$$A = A_p + A_n \quad (2-1)$$

$$R = \left| \frac{A_p}{A_n} \right| \quad (2-2)$$

$$C_1 = (-858.21)D + 667.58 \quad (2-3)$$

$$C_2 = (-1509)D - 287.78 \quad (2-4)$$

$$C_3 = (-2120.1)D - 407.95 \quad (2-5)$$

where: A_p, A_n = positive and negative area of transverse profile respectively (mm^2), C_1, C_2 and C_3 = theoretical average total area for AC failure, base/sub-base failure and sub-grade failure respectively (mm^2), D = maximum rut depth (mm).

It should be noted that although NCHRP Report 468 is entitled “Contribution of Pavement Structural Layers to Rutting of Hot Mix Asphalt Pavements,” the proposed method would only present a likelihood that a certain structural layer is the dominating rutting failure layer. To make it clearer, the percentage reported from the procedure refers to a probability of the layer being the caprice instead of the quantitative percentage of contribution to the total surface rut depth.

According to NCHRP report 468 (White et al. 2002), percentage of layer contribution to rutting is section specific and depend on material properties, load, and climatic condition. Further, the report used an analysis of transverse surface profile to determine the possible dominating layers to rutting. Under this circumstance, a pilot study is performed using transverse surface profile of some typical pavement sections from LTPP database with long historical performance records used during global calibration in NCHRP 1-37A to identify the link between percentage of dominating layers and percentage of layer contribution to rutting. The result is compared with predicted layer contribution to rutting as shown in Table 2.5. This comparison also rejects the initial assumption of the study. The layer contribution to rutting is still indistinct and thus not used in this research.

In contrast to this non-destructive technique, a destructive technique is the most accurate and widely accepted approach where the rut depth in each layer is directly measured by cutting the trenches on experimental test sections, hence known as trench analysis. The typical example of trench analysis is presented in the Figure 2.6. As shown, the advantage of the trench analysis is that it measures directly the rut depth in each structural layer of the pavement.

Table 2.5: Comparison of results under a pilot study

Layers	Layer failure from transverse profile study based on White et al. (2002) failure criteria (%)					Layer contribution to rutting from globally calibrated rutting models (%)				
	Section 11001	Section 21002	Section 40115	Section 473104	Section 481130	Section 11001	Section 21002	Section 40115	Section 473104	Section 481130
AC	82	79	83	78	77	60	28	48	3	48
Base	13	15	11	20	12	24	37	0	43	25
Sub-grade	5	5	6	2	11	16	35	52	54	27

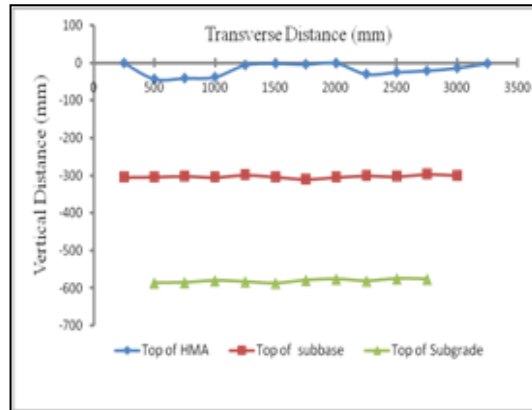


Figure 2.6: Trench profile analysis (Source: Hussan 2013)

2.3.5 Layer Contribution

The information of layer-specific rut depth would eliminate the indeterminacy and interdependency of the rutting models during local calibration through RSS minimization in order to determine a unique solution of the local calibration parameters. The trench analysis discussed in the preceding subsection is a straight approach for determining the actual percentages of layer contribution to rutting. However, no trench analysis data has been available or made available to the research project from the MTO. Therefore, a review of past trench studies were performed. Meanwhile, a typical Superpave pavement structure designed in Ontario (200 mm AC layer, 550 mm granular base and sub-grade with $M_r = 35$ MPa) is analyzed with different software packages under this research to estimate the surface displacement. The results are presented in Table 2.6, showing contradicting observations. The software packages predict much higher rutting in sub-grade and negligible rutting in AC layer, whereas, it is just opposite from trench studies. To resolve the non-uniqueness issue, Waseem (2013) investigated the layer contribution to rutting from several aspects (e.g., global default models, elastic multilayer

computer packages and empirical studies) and also made similar conclusions in this regard. Finally based on literature review, he proposed a pre-set value of layer contribution to rutting for new/reconstructed and rehabilitated pavement sections separately. Because there is no further adequate evidence to support this line of argument, this research takes another approach to resolve the indeterminacy issue; the details are discussed in Chapter 3.

Table 2.6: Average layer contribution to rutting

Study criteria	Source of study	AC layer rutting (%)	Granular base rutting (%)	Sub-grade rutting (%)
Trench studies	AASHO (1962)	32	59	9
	ALF-TxMLS (2002)	67.8	25.9	6.3
	ALF-FHWA (2006)	57	27	16
Software package	WESLEA	3	19	78
	mePADS	7	32	62
	DARWin ME default global models	13	39	48

2.4 The MEPDG Rutting Models

The rutting models for flexible pavement in the MEPDG are based on accumulation of incremental damage for each application of traffic loading. Each material within the pavement system is divided into several analysis sub-layers and different models are used to evaluate the accumulated vertical plastic strain in each sub-layers at the end of each sub-season. The calculated plastic strain is further used to estimate the damage at the mid depth of each sub-layer for each sub-season. Total rutting for a given season is the sum of the rut depth in each layer and expressed mathematically by the following equation.

$$RD(t) = \sum_{i=1}^n \varepsilon_{p,i}(t) h_i \quad (2-6)$$

where: $RD(t)$ = Total pavement rutting at age t

n = Number of computational sub-layers of the pavement structural system

$\varepsilon_{p,i}(t)$ = Accumulative plastic strain at age t in the i^{th} sub-layer and

h_i = Thickness of the i^{th} sub-layer

To evaluate the accumulative plastic strain (ε_p) for each sublayer at different age, MEPDG first calculates the resilient or elastic strain under different seasons at various traffic loads, and then uses a set of empirical equations to calculate the plastic strain by incorporating the strain hardening principle to link the traffic loads, temperature, and age. These empirical equations are collectively called the rutting models. Note that in reality various traffic loadings are applied at different time under different climates and seasons. Thus, accumulation of the permanent deformation under different loading conditions is calculated by using the strain hardening concept discussed next in detail. But before that, the exact forms of the empirical models are explained first.

2.4.1 AC Rutting Model

In 1989, Leahy proposed an AC rutting model based on his laboratory data from repeated load permanent deformation tests. Leahy's model was modified by Ayres (1997) using additional laboratory data. Later, Kaloush (2001) developed several models based on the laboratory test data with many more types of mixtures at multiple levels of temperature and loading stress. In the end, the model with temperature and load repetition term was selected by the team of NCHRP Project 1-37A to be the MEPDG model for global calibration using the Long Term Pavement Performance (LTPP) database. The general form of the AC rutting model in MEPDG, on the basis of the Kaloush model, is expressed as

$$\frac{\varepsilon_p}{\varepsilon_r} = k_z \beta_{r1} 10^{k_{r1}} T^{k_{r2} \beta_{r2}} N^{k_{r3} \beta_{r3}} \quad (2-7)$$

where: ε_p = accumulated plastic strain at N repetitions of load

ε_r = resilient strain of the asphalt material

T = mix (or pavement layer) temperature (°F)

N = number of load repetitions

k_{r1} = global calibration parameter and equal to -3.1552 in the global MEPDG model

k_{r2} = global calibration parameter and equal to 1.7342 in the global MEPDG model

k_{r3} = global calibration parameter and equal to 0.39937 in the global MEPDG model

k_z = depth confinement factor and equal to 1.0 by default

$\beta_{r1}, \beta_{r2}, \beta_{r3}$ = local calibration parameters and equal to 1.0 by default

2.4.2 Unbound Layer Rutting Model

Tseng and Lytton in 1989 developed unbound layer rutting model to estimate the permanent deformation behaviour based upon the type of materials. The model was modified by Ayres (1997) using same but combined data in one database. Later, El-Basyouny and Witczak (2004) modified the model to enhance its overall performance by changing the slope and intercept of the relationship between $\frac{\varepsilon_p}{\varepsilon_r}$ Vs E during NCHRP Project 1-37A. The general form of the unbound layer rutting model in MEPDG is expressed as

$$\frac{\varepsilon_p}{\varepsilon_v} = k_1 \beta_{s1} \left(\frac{\varepsilon_0}{\varepsilon_r} \right) e^{-\left(\frac{\rho}{N}\right)^\beta} \quad (2-8)$$

where: ε_p = accumulated plastic strain of layer or sub-layer

N = number of traffic repetitions

ε_v = average vertical resilient strain in layer or sub-layer obtained from the primary response model

ε_r = resilient strain imposed in laboratory test to obtain material properties $\varepsilon_0, \beta, \rho$

k_1 = global field calibration parameters for unbound granular base and sub-grade material and equal to 1.0 by default for both granular base and fine soil layer in MEPDG model. Hereafter, global calibration parameters for granular base is defined by k_{GB} and that for sub-grade material is defined by k_{SG} .

β_{s1} = local calibration parameters for unbound granular base and sub-grade material. Hereafter, the local calibration factor is denoted by β_{GB} for granular base and by β_{SG} for sub-grade material. Both parameters are set 1.0 by default.

$\varepsilon_0, \beta, \rho$ = material properties. These properties are the function of water content, deviator stress, bulk stress and resilient modulus of the layer and given by the following equations.

$$\log \beta = -0.61119 - 0.017638(W_c) \quad (2-9)$$

$$\rho = 10^9 \left(\frac{C_o}{1 - (10^9)\beta} \right)^{\frac{1}{\beta}} - 0.61119 - 0.017638(W_c) \quad (2-10)$$

$$C_o = \ln \left(\frac{a_1 M_r^{b_1}}{a_9 M_r^{b_9}} \right) = 0.0075 \quad (2-11)$$

W_c = water content (%).

M_r = resilient modulus of the unbound layer.

a_1, a_9 = regression constants; $a_1 = 0.15$ and $a_9 = 0.15$

b_1, b_9 = regression constants; $b_1 = 0$ and $b_9 = 0$

2.4.3 Strain Hardening Approach

For a specific set of pavement conditions (defined by climatic and environmental conditions as well as a particular configuration and combination of tire loading), the total plastic deformation at the end of pavement age t is calculated by using the so-called *strain hardening* concept as shown in Figure 2.7. According to the principle of strain hardening, the total number of load repetitions at the end of pavement age t is estimated by using the equivalent number of load cycle at the beginning of that pavement age expressed as:

$$N(t) = \Delta N + N_{eq}(t - 1) \quad (2-12)$$

where: $N(t)$ = Total number of load repetitions at the end of pavement age t

ΔN = Application of traffic load during pavement age t

$N_{eq}(t - 1)$ = Equivalent number of load cycle at the beginning of pavement age t associated with total deformation at the end of each pavement age $t - 1$

The total plastic strain $\epsilon_p(t - 1)$ for point A at the end of pavement age $t - 1$ is first calculated corresponds to a total number of load repetitions $N(t - 1)$, layer temperature $T(t - 1)$ and resilient strain $\epsilon_r(t - 1)$. But for the beginning of pavement age t as represented by point B, the layer temperature $T(t)$ and the resilient strain $\epsilon_r(t)$ are prevailing conditions. Thus, an equivalent number of load repetitions $N_{eq}(t - 1)$ is to be established corresponding to the total plastic strain at the end of pavement age $t - 1$ but under the new prevailing conditions. Finally, the total plastic strain $\epsilon_p(t)$ at point C is calculated corresponding to the total number of load repetitions $N(t)$ which is obtained by adding the number of traffic repetitions ΔN during pavement age t to the total equivalent number of repetitions $N_{eq}(t - 1)$.

The rutting models in the AASHTO MEPDG include two separate models, one for AC layers and the other for unbound materials, which include base/sub-base layers and sub-grade soils. These models are globally calibrated and need local calibration before use to reduce the bias. Although the predicted rutting of each layer is the explicit function of traffic load, the effects of temperature and moisture content are also included in the prediction of rutting through resilient modulus for granular layers and dynamic modulus for AC layer.

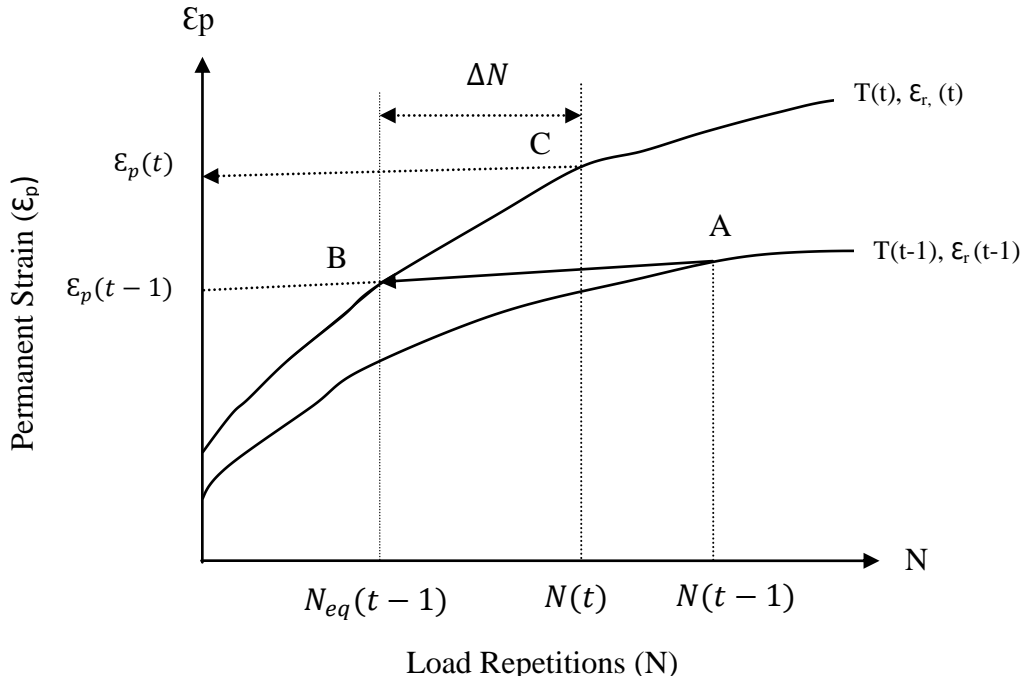


Figure 2.7: Concept of strain hardening approach

2.5 Global Calibration

To understand the local calibration discussed in this study, it is important to establish a good appreciation of the global calibration process, because both calibrations represent a systematic process of eliminating bias and minimizing the residual errors between observed and predicted rut depth by modifying calibration parameters in the model. This section deals with global calibration only.

2.5.1 Calibration in NCHRP 1-37A

The global calibration in the NCHRP Project 1-37A initially included 136 LTPP test sections (94 new and 42 overlay sections) selected from USA and Canada. But only 88 new sections (including 1 from New Brunswick, Canada) that had permanent deformation data were used for global calibration of rutting models. The calibration process also includes 38 AASHO Road Test sections and 7 MnRoad sections. The overall calibration process is summarized in the following three steps.

Step One:

The temperature exponent (β_{r2}) and traffic exponent (β_{r3}) were calibrated using the 88 pavement sections from LTPP database. Eleven combinations of β_{r2} and β_{r3} ranging from 0.8 to 1.2 were used during simulation run in two different optimization approaches for each pavement section. The first optimization was done with a constant value of β_{GB} and β_{SG} and varying β_{r1} to obtain minimum RSS in total rut and zero error in AC rut, whereas the second optimization was done with varying β_{r1} , β_{GB} and β_{SG} simultaneously to obtain minimum RSS and zero error in total rut. The final result was the selection of same set of coefficients ($\beta_{r2}= 0.9$ and $\beta_{r3}= 1.2$) from both approaches.

Step Two:

The unbound layer coefficients β_{GB} and β_{SG} were calibrated using 38 imaginary sections designed by AASHTO 1993 model. The analysis found the values of $\beta_{GB}= 1.05$ and $\beta_{SG} = 1.35$ by comparing the average predicted rut depth of base/sub-base layer with 0.075" (1.9 mm) and sub-grade with 0.2" (5 mm) over 20 years. Here, the average 20 years rut depths were fixed based on a survey among nearly 40 DOT material engineers under the assumption that the rut depth should be same irrespective of the sub-grade support and traffic level. This calibration used the first optimization approach with a constant value of $\beta_{r2}= 0.9$ and $\beta_{r3}= 1.2$ calculated from the first stage and found the value of $\beta_{r1}= 0.551$ using a corrected AC rut model from MnRoad test study. The correction in AC rut model is given by;

$$k_z = 0.328196^D (C_1 + C_2 D) \quad (2-13)$$

$$C_1 = -0.1039 H_{AC}^2 + 2.4868 H_{AC} - 17.342 \quad (2-14)$$

$$C_2 = 0.0172 H_{AC}^2 - 1.7331 H_{AC} + 27.428 \quad (2-15)$$

where: k_z = depth confinement factor as a function of total asphalt layer thickness and depth to computational point

D = depth below the surface

H_{AC} = total AC thickness

Step Three:

Further, the calibration was performed with LTPP pavement sections using second optimization approach taking the previously found coefficients $\beta_{r2}= 0.9$ and $\beta_{r3}= 1.2$ as a constant values. The

calibration process also utilized a corrected AC rut model from MnRoad test study and the final selected result was $\beta_{r1}= 0.509$, $\beta_{GB}= 1.673$ and $\beta_{SG}= 1.35$.

Thus, the results from this three steps global calibration process was used to obtain the calibration parameters for rutting models to equations 2-7 and 2-8 which were,

k_{r1} = plastic deformation factor representing intercept of the log–log relationship between the number of load applications and cumulative plastic strain and equal to - 3.4488 based on the global calibration effort for all AC mixes

k_{r2} = plastic deformation factor related to the effect of temperature on intercept and equal to 1.5606 based on the global calibration effort for all AC mixes

k_{r3} = plastic deformation factor representing steady-state slope related to the effect of wheel loads and equal to 0.4792 based on the global calibration effort for all AC mixes

k_{GB} = global field calibration parameters for granular base/sub-base and is equal to 1.673 based on the global calibration effort

k_{SG} = global field calibration parameters for fine soil layer and is equal to 1.35 based on the global calibration effort

$\beta_{r1}, \beta_{r2}, \beta_{r3}$ = local calibration parameters and equal to 1.0 for the AC mixtures based on the global calibration effort

β_{GB}, β_{SG} = local calibration parameters and equal to 1.0 based on the global calibration effort

From this calibration process, It is noted that the original model developers in Project 1-37A already pointed out the need of trench analysis. Further, a preset value of rutting for base/sub-base and sub-grade layer is fixed from export knowledge during the analysis of the 38 AASHO road test sections because of lack trench analysis.

2.5.2 Validation in NCHRP 1-40A

An independent comprehensive third-party engineering review of the rutting models developed under NCHRP Project 1-37A was performed under the subsequent funding support of NCHRP Project 1-40A. A number of issues were raised regarding the technical aspects, design reliability, nature and calibration of the distress models, and properties of the pavement layers (NCHRP 2006). Based on their study, the reviewer recommended for:

- (i) Local calibration of the distress models rather than continuously adjusting the global calibrations,
- (ii) The use of mixture-specific plastic deformation coefficients to individual AC layers,
- (iii) Recalibration of the AC transfer functions of NCHRP Project 1-37A.

These recommendations all have been considered in the later development and enhancement of the MEPDG. A local calibration manual was developed and released in 2010 (AASHTO 2010). Many state-wide and even municipality-wide local calibration studies have been subsequently conducted; these are reviewed in Section 2.6. The use of mixture-specific coefficients were allowed in the latest AASHTOWare Pavement ME software, although what different coefficients to be used for different mixtures remains unknown.

Validation and recalibration of distress transfer functions were performed under NCHRP Project 1-40D with correct estimation of resilient modulus and expanded database. This calibration effort resulted in a new set of global calibration parameters $k_{r_1} = -3.3541$, $k_{r_2} = 1.5606$, $k_{r_3} = 0.4791$, $k_{GB} = 2.03$ and $k_{SG} = 1.67$ which are incorporated in the later versions of the AASHTOWare.

The study of NCHRP Project 1-40A also recognized a large bias related to AC volumetric properties as a major limitation of using one set of plastic deformation coefficients for all AC mixes. To enhance the rutting prediction accuracy, mixture-specific coefficients as given below were suggested to replace the global calibration parameters.

$$k_{r_1} = \log(1.5093 \times 10^{-3} K_{r_1} V_a^{0.5213} V_{beff}^{1.0057}) - 3.4488 \quad (2-16)$$

$$k_{r_2} = 1.5606 \left(\frac{V_a}{V_{a(design)}} \right)^{0.25} \left(\frac{P_b}{P_{b(opt)}} \right)^{1.25} F_{index} C_{index} \quad (2-17)$$

$$k_{r_3} = 0.4791 K_{r_3} \left(\frac{P_b}{P_{b(opt)}} \right) \quad (2-18)$$

where: k_{r_1} = intercept coefficient based on volumetric properties and gradation

k_{r_2} = temperature sensitivity exponent based on volumetric properties and gradation

k_{r_3} = load sensitivity exponent based on volumetric properties and gradation

K_{r_1} = intercept coefficient, estimated based on void filled with asphalt and gradation

K_{r_3} = slope coefficient, as given in Table 2.7

V_a = air voids after compaction (%)

$V_{a(design)}$ = design air voids used to select optimum asphalt content (%)

V_{beff} = effective asphalt content by volume (%)

P_b = asphalt content by weight (%)

$P_{b(opt)}$ = optimum asphalt content by weight (%)

F_{index} = fine aggregate angularity index, as given in Table 2.8

C_{index} = coarse aggregate angularity index, as given in Table 2.9

Table 2.7: Slope coefficient (source: NCHRP Report 719)

Types of Gradation mix	Gradation Index (GI)	Slope coefficient value
Fine graded mixes	< 20	0.4
Coarse graded mixes	20 - 40	0.7
	> 40	0.8

In Table 2.7, GI represents the gradation index and is expressed as

$$GI = \sum_{i=\frac{3}{8}}^{\#50} |P_i - P_{i(0.45)}| \quad (2-19)$$

where: P_i = percent passing sieve i.

$P_{i(0.45)}$ = percent passing sieve i for the FHWA 0.45 maximum density line.

Table 2.8: Fine aggregate angularity index (F_{index}) (source: NCHRP Report 719)

Gradation - External to restricted zone	fine aggregate angularity	
	< 45	> 45
Dense grading - External to restricted zone	1.0	0.9
Dense grading - Through to restricted zone	1.05	1.0

Table 2.9: Coarse aggregate angularity index (C_{index}) (source: NCHRP Report 719)

Types of Gradation	Percent Crushed material with two faces				
	0	25	50	75	100
Well Graded	1.1	1.05	1.0	1.0	0.9
Gap Graded	1.2	1.1	1.05	1.0	0.9

2.5.3 Recent Development in NCHRP 9-30A

NCHRP Project 9-30A represents a more recent effort of the MEPDG research community to upgrade and enhance the performance of the rutting models (Von Quintus et al. 2012). The research outcomes were summarized in the NCHRP Report 719. Among many useful conclusions, the team concluded that the global value of the traffic (N -term) exponent k_{r3} 0.479 is too high, whereas they observed a contradictory result for the temperature exponent k_{r2} . A detailed analysis of NCHRP Report 719 is discussed in Chapter 3.

The NCHRP Project 9-30A focused on enhancing and populating the database to upgrade the prediction performance of the MEPDG AC rutting model developed under NCHRP Projects 1-37A and 1-40 by recalibration process (Von Quintus et al. 2012). The recalibration process contributed toward the measurement of AC rutting property testing protocols (triaxial test vs. shear test) in the laboratory for fixing the local calibration parameters. Also, the process involved the use of same database for a comparative study of the different AC rut depth transfer models in terms of accuracy, sensitivity and robustness to identify the possibility of their use as alternative models. In this regards, the following three rut depth transfer function were added to the MEPDG software version 9-30A, which unfortunately has not yet been made publicly accessible as of the time the thesis is written.

(i) WesTrack shear strain and stress transfer function,

$$\gamma_p = ae^{b\tau}\gamma_e N^c \quad (2-20)$$

where: γ_p = permanent shear strain at a depth of 2 inches beneath the tire edge

γ_e = corresponding resilient or elastic shear strain

τ = corresponding elastic shear stress

N = number of load cycles

a, b, c = regression coefficients, recommended $a = 2.114$, $b = 0.04$, and $c = 0.124$

for conventional AC mixtures

(ii) Verstraeten deviator stress transfer function,

$$\varepsilon_p = A \left(\frac{\sigma_1 - \sigma_3}{E^*} \right) \left(\frac{N}{1000f} \right)^{b_{AC}} \quad (2-21)$$

where: ε_p = permanent or plastic strain

σ_1 and σ_3 = vertical and radial stresses

E^* = dynamic modulus of asphalt mixture

N = number of load cycles

f = frequency of load, Hz

A and b_{AC} = regression coefficients

(iii) Asphalt Institute vertical strain and deviator stress transfer function,

$$\log\left(\frac{\varepsilon_p}{\varepsilon_r}\right) = -6.631 + 0.435 \log(N) + 2.767 \log(T) + 0.110 \log(\sigma_d) - 0.118 \log(\eta) + 0.930 \log(V_{beff}) + 0.501 \log(V_a) \quad (2-22)$$

where: ε_p = plastic strain

ε_r = resilient strain

T = mix (or pavement layer) temperature

N = number of load repetitions

σ_d = deviator stress

η = viscosity of the asphalt binder

V_{beff} = effective asphalt content by volume

V_a = air void volume

All these models have a traffic term, all in exponential form. Some models do not have temperature term, arguing that the temperature effects have been considered in the dynamic modulus model. The use of these different transfer models resulted in insignificant error in predicted rut depths. However, there are some other important differences, such as the consideration of confining pressures and testing protocols. Therefore, Von Quintus et al. (2012) performed a study on the effect of stress state (confining pressure, deviator stress) and temperature on plastic deformation coefficients by triaxial repeated-load permanent deformation test as a part of NCHRP Project 9-30A.

2.5.3.1 Effects of Stress State

The study showed that a small confining pressure of 10 psi (689.5 KPa) considerably reduces the plastic strains throughout the test but it remains almost same to 20 psi. On the other side, the effects of deviator stress level on the plastic strain relationship was observed specially at higher number of loading cycles. However, the differences in slope was insignificant at 50-psi in

comparison with 30-psi deviator stress. Therefore, the NCHRP 9-30A team recommended confining pressure of 10 psi and deviator stress of 50-psi for the test. The major observation from this study is that the slope of plastic strain relationship ranges from 0.17 to 0.35 which is same to the field derived value of N -term exponent given as in NCHRP report 719, Table 8 and 9 (refer to Table A-1 and A-2 in the Appendix of the thesis). NCHRP 9-30A team further observed slight but systematic difference between the repeated-load triaxial and shear strain in the primary stage of rutting, however, the slope of the secondary stage almost remains within the range of 0.15 to 0.40 as reported in NCHRP report 719, Tables 24 and 25 (refer to Table A-3).

2.5.3.2 Effects of Temperature

Similarly, the study characterized the overall temperature effect by power law trend lines. The value of trend line coefficients was around 1.0 and was the image of the temperature exponent value which is substantially less than its corresponding globally calibrated value of 1.5606, although it was dependent on the volumetric properties of the mixtures. On the other side, a contradictory result is observed for temperature exponent through repeated-load triaxial and shear tests as reported in NCHRP report 719, Tables 24 and 25 which is significantly high with respect to its global value of 1.5606. Under this scenario, the team observed accurate simulate the AC layer rutting with global value of temperature exponent by simply adjusting the intercept value with field conditions. Thus, their study found that all the models incorporated in the MEPDG software Version NCHRP 9-30A accurately simulate the evolution of AC layer rutting with proper calibration using repeated-load plastic deformation tests (shear and triaxial) that allows the user to enter the layer-specific permanent deformation parameters and provide a choice of transfer functions for predicting the rutting behaviour of the AC layer.

2.5.4 Remarks

Based on the discussions in this section, it is clear that the model coefficients differ in each global calibration exercise and they are influenced by the properties of the pavement materials. However, the global calibration studies continuously put their efforts to upgrade the prediction performance of the models by taking account of the material properties in both field and laboratory environment. The latest effort on NCHRP Project 9-30A is taken as the basis for this research.

2.6 Efforts on Local Calibration

Many highway agencies in North America have prepared plans to implement the AASHTO MEPDG in the practice of design and rehabilitation of the pavements. However, due to the difference in input parameters for different jurisdictional regions, the global rutting models result in significantly biased prediction. Therefore, transportation agencies throughout North America started partial or full local calibration studies of the empirical distress models to use it in local level. The previous local calibration studies in U.S. and Canada are summarized below.

2.6.1 The Local Calibration Guide

To facilitate and somehow unite the local calibration studies that many transportation agencies need to do, AASHTO (2010) developed a Guide for the Local Calibration of the Mechanical-Empirical Pavement Design Guide (or “Local Calibration Guide” hereafter for brevity). This guide elaborates the step-by-step procedure of local calibration. The basic steps are summarized in the form of a flow chart in Figure 2.8.

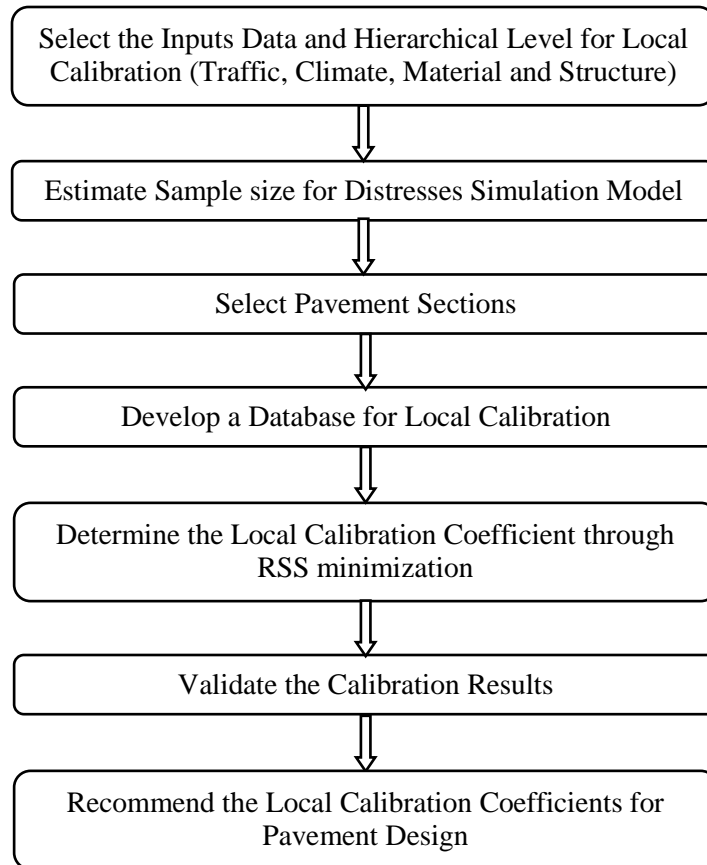


Figure 2.8: Generalized basic steps of local calibration methodology

According to the guide, the local calibration process starts by selecting the accuracy level for each input parameter. The selection of input accuracy is influenced by agencies because of their policy differences but it is better to use the highest level of inputs available at the time of design to improve the standard error of the prediction model. The guide also specifies a minimum number of pavement sections for local calibration studies. For the rutting study, it recommended a minimum number of 20 pavement sections at a significance level of 90%. The guide further suggests a fractional balance factorial of the key factors such as climatic zone (geographical regions), pavement types (new and rehabilitated sections), truck traffic application (highway type), etc. when selecting the roadway sections for the study. These recommendations are considered in this research study.

The next major step of local calibration stated by the guide is the extraction of project specific data such as location parameters, traffic loading, material properties, design structure and performance observation. This study developed a local calibration database for selected, typical pavement sections from MTO-PMS including all these features.

Before optimization of the models, the guide recommended for the validation test of the global models by comparing the predicted versus observed performance data in terms of bias and standard error. Based on the findings, local calibration coefficients are adjusted to eliminate the bias and reduce the standard error by optimization process. Finally, the optimized models are compared with global models, and calibration results are validated for general use.

2.6.2 Local Calibration Efforts in USA

Many states in the USA have completed their local calibration studies. For Montana State, VonQuintus and Moulthrop (2007) focused on implementation of MEPDG distress models in local conditions using 102 new, reconstructed and rehabilitated AC pavement test sections: 34 LTPP and 13 non-LTPP pavements sections from Montana and 55 LTPP sections from adjacent US States and Canadian provinces. The analysis using material test data, historical traffic data with input level 1 and level 3 showed that the global models significantly over-predict rutting, which is similar to what Jannat (2012) and Waseem (2013) have observed recently for Ontario's roads. Also, the model resulted in significant erroneous predictions to AC rutting. Similarly, the field investigation showed that most of the rutting occurred in the AC layer. Based on these findings, Von Quintus and Moulthrop proposed a new method for local adjustment factor of AC

layer ($\beta_{r1}, \beta_{r2}, \beta_{r3}$) as described in NCHRP Project 1-40 and a value of 0.20 for both base (β_{GB}) and sub-grade (β_{SG}) material.

For Texas, Banerjee et al. (2009) calibrated MEPDG distress transfer functions for flexible pavements using eighteen Specific Pavement Studies (SPS) 1 and 3 sections from LTPP database of 5 different geographical regions. They established the overall default calibration coefficient of Texas for input Level 3 using the average of Level 2 calibration coefficients of these regions. Trial runs were conducted for all regions separately with multiple combinations of the calibration coefficients to minimize the RSS between predicted and measured values. During this study, β_{r2} for AC rutting model was fixed to one by assuming that the temperature dependency of the specific material depends upon its mix properties and should be determined in the laboratory. Similarly, the calibration coefficient for unbound sub-grade material (β_{SG}) was set to the regional default value on the basis of average moisture content of the sub-grade soil. Although, the proposed calibration parameters can be safely used for the regions and location undertaken in the study, it pointed out the possibility of further updates on these calibration parameters by calibrating all the sections jointly with additional data sets.

For Washington State, Li et al. (2009) conducted local calibrated of MEPDG rutting models for flexible pavements using level 2 inputs from WSDOT default value. Five basic steps including: (a) bench testing (b) model analysis (c) calibration (d) validation, and (e) iteration are followed during the calibration process. The sensitivity study of various input parameters showed that the global models under-predict rutting for Washington State pavements, which is opposite to what Jannat (2012) and Waseem (2013) have observed for Ontario's roads. Also the model was found less sensitive to layer thickness and resilient strain which helps to conclude that the corresponding rutting model calibration factor (β_{r1}) should be very near to its global value. Meanwhile, the observation of historical pavement performance data from WSPMS showed very small rutting in sub-grade of Washington State pavements. So, Li et al. (2009) preset zero for the local calibration coefficient for sub-grade (β_{SG}). Among the 18 possible subgroups categorized based on 3 traffic level with different AADTT, 2 sub-grade soil types with different resilient modulus and 3 different climates, only eight subgroups having section information were used for calibration. The calibration process involved an iterative method with a set of calibration parameters to obtain least value of RMSE between the MEPDG prediction and WSPMS measures.

For Ohio State, Glover and Mallela (2009) performed validation and recalibration of MEPDG rutting models for new and reconstructed AC pavements using 13 LTPP projects with sufficient amount of distress data. The statistical and non-statistical analysis was performed to determine overall adequacy of MEPDG model in terms of prediction capability, accuracy, and bias under Ohio conditions. Considering the biased predictions and poor correlation as a result on findings, Glover and Mallela (2009) purposed modification to the local calibration coefficients β_{r_1} , β_{GB} and β_{SG} only which significantly improved the model accuracy but not the bias. So, they further purposed recalibration to β_{r_2} and β_{r_3} of the AC rutting model by laboratory investigation of accumulation of permanent deformation with repeated loadings.

Darter et al. (2009) presented a final report on "Implementation of MEPDG in Utah: validation, calibration and development of the UDOT MEPDG user's guide" for Flexible Pavement Design to the Utah Department of Transportation Research Division. The study focused on the validation and calibration of the MEPDG distress prediction models for new, reconstructed and overlaid AC pavements using data from both LTPP and UDOT's pavement management system. The statistical and non-statistical analysis showed biased and poor correlation between the measured and predicted rutting specially for new Superpave pavement under Utah conditions. So, Darter et al. (2009) purposed optimization of model's local calibration coefficients using SAS statistical software maintaining the proportion of the contribution of each layers to rutting. A sensitivity analysis showed that the locally calibrated model significantly improve the goodness of fit and removed all significant bias.

For Arkansas, Hall et al. (2010) presented a study of MEPDG local calibration and validation for flexible pavement models using 26 sections (20 for calibration and 6 for validation) from LTPP and PMS database. Depending upon the information available for traffic, climate and structure, they used all three input level for Iterative runs of the MEPDG using discrete calibration coefficients to minimize the RSS between predicted and measured values. But, the calibration coefficient for granular base was set as one assuming that the rutting mostly occur in AC and sub-grade layers. It is found that the local calibration improve the prediction performance of the rutting models. Thus, it sets up a basic outline for MEPDG local calibration procedure, however the paper strongly recommended to collect more rutting data in the PMS database before implementation of the MEPDG in Arkansas.

For Arizona, Souliman et al. (2010) performed the calibration of the MEPDG predictive models for flexible pavement using 39 Arizona pavement sections included in LTPP database. The study focused on the development of ADOT database for MEPDG input parameters related to asphalt binders, asphalt mixtures, base and sub-grade materials, climate, and traffic characteristics. The data obtained from LTPP and ADOT databases were used for optimum calibration coefficients producing least sum of squared error and zero sum of standard error between measured and predicted values by trial and error method.

Momin (2011) in his dissertation study completed local calibration for north eastern United States including General Pavement Section (GPS) 1 and 2 experiments. The calibration parameters for flexible pavements were found through a mathematical process using 17 GPS sections from LTPP database. The process involved estimating the measured rut depth in each layer by finding the layer contribution to rutting using globally calibrated model ($\beta_{r_1}=1.0$, $\beta_{GB}=1.0$ and $\beta_{SG}=1.0$). The measured and predicted values of rutting in each layer were used simultaneously to obtain the local calibration parameters by performing a simple linear regression with no intercept, taking the measured value as the independent variable. The study didn't say anything about other two calibration parameters (β_{r_2} and β_{r_3}). An analysis suggested that the local calibration coefficients give a better fit between measured and predicted permanent deformation in all layers.

Kim et al. (2011) compiled a report on Local Calibration of the MEPDG for Flexible Pavement Design to the North Carolina Department of Transportation. The study was performed with 46 sections among which 22 LTPP sections, 6 SPS and 16 GPS were used for calibration and 24 NCDOT PMS sections for validation. Two approaches, i.e., a generalized reduced gradient (GRG) approach and a genetic algorithm optimization (GAO) approach have been used to calibrate the rutting models for local conditions and materials. The GRG approach used 110 combinations of β_{r_2} and β_{r_3} to optimize β_{r_1} , β_{GB} and β_{SG} for smallest RSS between the predicted and measured distresses using Microsoft Excel Solver. The GAO approach used the MATLAB® environment to optimize for a single set of all five model coefficients β_{r_1} , β_{r_2} , β_{r_3} , β_{GB} and β_{SG} simultaneously. The study suggested the results of GAO approach as local calibration coefficients for North Carolina because of its better validation statistics.

Tareder et al. (2013) finished the local calibration for New Mexico using a flexible pavement database of New Mexico Department of Transportation. The project was based on the study of model's performance prediction to local condition using a total of 24 sections: 11 from LTPP pavement sections and 13 from PMS database. The calibration involved finding a set of calibration coefficients (β_{r_1} , β_{r_2} , β_{r_3} , β_{GB} and β_{SG}) that minimizes the sum of squared error. The analysis observed that the non-linear calibration coefficients β_{r_2} and β_{r_3} (exponents to T and N) are highly sensitive to rutting. So, Tareder et al. (2013) proposed two step iterative process for calibration of rutting model. The first step is minimizing the RSS with different set of β_{r_2} and β_{r_3} taking all other betas constant to 1, whereas, the second step utilizes the obtained β_{r_2} and β_{r_3} values for further reduction of RSS by changing β_{r_1} , β_{GB} and β_{SG} .

For Oregon, Williams and Shaidur (2013) calibrated rutting distress model using 44 rehabilitated pavements integrating from 3 regions, 5 pavement types, 2 traffic level and 3 level of pavement performance. The field condition distress surveys showed that most of the rutting is from the AC layers only. So, Williams and Shaidur (2013) proposed zero for calibration parameters of granular base and sub-grade layer. However, they proposed two steps iterative calibration approach for AC layer because of highly sensitivity nature of rutting to overlay properties. The first step concerned with finding the value of β_{r_2} and β_{r_3} whereas the second step involved for estimation of β_{r_1} by minimizing the RSS using Excel Solver.

For Colorado, Mallela et al. (2013) performed a study of MEPDG model for calibration and validation to local Colorado conditions. This was accomplished by using collectively 72 LTPP and 55 CDOT PMS database for new and rehabilitated pavement projects located throughout Colorado. The analysis showed that the globally calibrated models have significant bias in prediction of total rutting. So, Mallela et al. (2013) proposed an adjustment in rutting models by considering the information obtained through laboratory testing (RLPD test and HWT tests) and trench analysis. The calibration involved the use of non-linear model optimization function of SAS statistical software using laboratory-derived AC rutting model coefficients k_{r_1} , k_{r_2} and k_{r_3} as seed values and simultaneously ensuring the contribution of each layers to rutting without compromising goodness of fit and bias.

Beside these, Donahue (2008) performed a study of local calibration of AC pavements by using MoDOT and LTPP database for Missouri. For New Jersey, verification of distress and

roughness of MEPDG was done by Siraj et al. (2008) with combination of LTPP and non-LTPP pavement sections. Hoegh et al. (2010) published an article about the local calibration of rutting model using historical rutting performance data of 12 test sections for MnDOT full-scale pavement sections. Schram and Abdelrahman (2010) used PMS database of Nebraska for calibration and validation of distress models at the local project level. Similarly, Ahammed et al. (2011) worked for sensitivity of MEPDG with variation of truck traffic distributions, AADTT and axle load spectra using regional data on Manitoba pavement section.

Calibration parameters of rutting model obtained from past local calibration studies in the USA are present in Table 2.10. Clearly, the previous calibration studies did not follow a same optimization procedure on local calibration practices. Some of these studies proposed a preset value for calibration parameter(s) from global calibration or/and regional default or/and pilot study, specifically 1.0, the global value for temperature exponent (β_{r2}) whereas some calibrated all the coefficients simultaneously. However, The final value of temperature exponent (β_{r2}) and traffic exponent (β_{r3}) in most of these studies are nearly equal to 1.0 and less than 1.0. The other calibration parameters largely fluctuate in each study.

Table 2.10: Proposed calibration parameters from past local calibration studies

S.N.	Reference	Location	Recommended Calibrated Values				
			β_{r1}	β_{r2}	β_{r3}	β_{GB}	β_{SG}
1	VonQuintus and Moulthrop (2007)	Montana	Proposed new method as described in NCHRP 1-40.			0.2	0.2
2	Banerjee et al. (2009)	Texas	2.39	1.00	0.86	1.00	0.50
3	Li et al. (2009)	Washington	1.05	1.11	1.10	1.00	0.00
4	Glover and Mallela (2009)	Ohio	0.51	1.00	1.00	0.32	0.33
5	Darter et al. (2009)	Utah	0.56	1.00	1.00	0.604	0.40
6	Hall et al. (2010)	Arkansas	1.20	1.00	0.80	1.00	0.50
7	Souliman et al. (2010)	Arizona	3.63	1.10	0.70	0.11	1.38
8	Momin (2011)	Northeastern USA	1.308	1.00	1.00	2.065	1.48
9	Kim et al. (2011)	North Carolina	0.95	0.86	1.35	0.54	1.50
10	Tarefder et al. (2013)	New Mexico	1.1	1.1	0.8	0.8	1.2
11	Williams and Shaidur (2013)	Oregon	1.48	1.00	0.90	0.00	0.00
12	Mallela et al. (2013)	Colorado	1.34	1.00	1.00	0.40	0.84

2.6.3 Local Calibration Efforts in Canada

Although, numerous studies were performed for calibration and validation of distress model in the USA, Canadian studies have been very few. The Ryerson group has been the major research group of local calibration in Canada.

For Alberta, He et al. (2011) evaluated Darwin-ME pavement rutting prediction models using automatically collected pavement inventory and performance data from Alberta's PMS database. A unique network level approach was adopted to handle the rutting issue where the average rut depths of inventory sections are organized in 14 pavement groups within three category: five under the new construction category, four under the rehabilitation with milling category and five under the straight overlay category. These rut depths were compared with predicted rut depths against the pavement age for each group at the network level. The study found that DARWin-ME global rutting model over predict the total rutting for newly constructed flexible pavements, under predict for treated milling overlay pavements and closely predict for treated straight overlays pavements against the Alberta's local conditions. The findings from the study provide a general sense about the sensitivity of input parameter for future calibration of the rutting models in DARWin-ME for Canadian studies.

Boone (2013) performed a comparative study of Ontario pavement designs using AASHTO 1993 method and MEPDG method. A two-stage procedure was used to evaluate a total of 140 Ontario's historical pavements designed by AASHTO 1993 method. The first stage was the pavements performance prediction using globally calibrated MEPDG distress models to determine the prediction consistency of the methods under local design conditions whereas the next step was comparison between methods based on the thickness of AC layers required to satisfy their respective design criteria. The analysis found that the MEPDG method generally under-predict pavement performance of flexible pavements w.r.t. AASHTO 1993 method and increase the cost of the design by increasing the AC layer thickness. So, Boone (2013) recommended recalibration and validation of the MEPDG models for Ontario conditions.

Jannat (2012) was the first investigator who started a systematic study for Ontario's roads. Funded by an Highway Infrastructure Innovation Fund Program (HIIFP) project entitled *Database Development for Ontario's local calibration of Mechanistic Empirical Pavement Design Guide (MEPDG) distress models*, Jannat's MASc dissertation research started with 5,555 pavement section cycles from Ontario's PMS-2 considering geographical regions, highway

types, facility types, number of lanes, lengths of section, rehabilitation type, and quality of performance to develop a unified high quality pavement database for local calibration. She introduced the term “section cycle” to define the life of a section from its construction or reconstruction or rehabilitation year to the next major rehabilitation year. In the end, she developed a database composing of 101 section cycles integrated with high quality section specific material, pavement performance and traffic data. While the project specific information (construction dates, locations, and site data) was retrieved from the MTO’s contract documents, the pavement performance data (rutting and IRI) were developed from the Ministry’s Pavement Management System (PMS) database. Because pavement cracking damage was qualitatively evaluated in the MTO until 2012 when the new ARAN system was deployed, the local calibration database did not include useful crack data. Meanwhile, the Ministry had also developed a MEPDG Default Input Parameters Guide (MTO 2012). Missing traffic, climate and environmental data, and material properties have been collected from that Guide as a Level 3 inputs. On the other hand, all of these sections, including both reconstructed and rehabilitated sections, are flexible pavements with asphalt concrete of Marshall mix. These all represent the limitations of the first local calibration database that was developed by the Ryerson Group.

Based on the database developed, Jannat (2012) evaluated the MEPDG rutting models using 77 section cycles and concluded that the globally calibrated models generally over predict rutting for Ontario’s roads. Some preliminary regression analyses based on road section, highway functional class, geographical region, AC layer properties and sub-grade modulus were carried out. It was suggested that highway functional class be the best clustering parameter for local calibration of rutting to Ontario’s highways.

Using the same database, Waseem (2013) performed a more rigorous local calibration study of the rutting models for the Ontario’s flexible pavements. In his study, he selected 29 flexible pavement sections (10 reconstructed and 19 rehabilitated). The calibration process expected a unique optimum point for the calibration parameters by RSS minimization process; however, he found multiple local optima. This triggered his first attempt to determine the layer contribution of rutting in pavement structural layers. Hence, based on previous studies, Waseem (2013) proposed a set of layers contributions (for new/reconstructed pavement sections: 32% from AC, 59% from granular base and 9% from sub-grade soil and for rehabilitated pavement sections: 50% from AC layer and granular layer each) to the total rutting.

Further, he utilized preset layer contribution from different structural layers and used a two-stage layer-by-layer, section-by-section longitudinal local calibration methodology for the calibration of permanent deformation models to both reconstructed as well as rehabilitated pavement sections by using DARWin ME software. The first stage utilized a linear optimization to calibrate β_{r_1} , β_{GB} and β_{SG} with exponential calibration parameters (β_{r_2} and β_{r_3}) at default value of 1 while the second stage used a MATLAB environment for non linear optimization of only AC layer rutting parameters (β_{r_1} , β_{r_2} and β_{r_3}), by minimizing the RSS of each individual structural layer. The final result of the layer-by-layer, section-by-section longitudinal local calibration parameters obtained by Waseem (2013) are presented in the Table 2.11 and 2.12 below.

The Section-by-Section longitudinal calibration provided large variation in the optimized local calibration coefficients. The average values of the five calibration parameters (for reconstructed sections: 0.290, 1.209, 0.810, 1.455 and 0.034 and for rehabilitated sections: 0.632, 1.203, 0.869, 1.152 and 0.000) were found to be inapplicable for future pavement design. Moreover, the cross-sectional calibration coefficients (for reconstructed sections: 0.30, 1.00, 1.00, 0.80 and 0.03 and for rehabilitated sections: 0.90, 1.23, 0.77, 0.985 and 0.00) were found to be very different than the averaged value of the longitudinal calibration results. Thus, several areas of further study were recommended in the end to enhance the local calibration of the rutting models for Ontario's flexible pavements.

Table 2.11: Local calibration results for new/reconstructed pavements by Waseem (2013)

S. No.	Section ID.	Local Calibration Coefficients for Rutting Models				
		β_{r_1}	β_{r_2}	β_{r_3}	β_{GB}	β_{SG}
1	9	0.144	1.738	0.229	3.060	0.033
2	43	0.162	1.091	0.920	3.170	0.033
3	191	0.290	0.975	1.105	1.570	0.039
4	376	0.310	1.200	0.835	0.410	0.025
5	1049	0.196	0.991	0.985	0.960	0.037
6	1053	0.256	1.262	0.719	0.630	0.016
7	1188	0.370	1.040	0.970	1.110	0.040
8	1189	0.470	1.130	0.870	1.270	0.041
9	1200	0.368	1.480	0.580	1.610	0.050
10	1311	0.336	1.182	0.892	0.660	0.022

Table 2.12: Local calibration results for rehabilitated pavements by Waseem (2013)

S. No.	Section ID.	Local Calibration Coefficients for Rutting Models				
		β_{r_1}	β_{r_2}	β_{r_3}	β_{GB}	β_{SG}
1	139	1.010	1.230	0.770	1.090	0
2	217	0.900	1.230	0.770	1.274	
3	347	1.010	1.230	0.770	1.860	
4	348	0.276	1.601	0.581	1.124	
5	349	1.050	1.255	0.745	1.297	
6	350	1.100	1.155	0.850	1.308	
7	353	0.490	1.235	0.865	1.303	
8	356	0.270	0.935	1.185	0.713	
9	357	0.980	1.055	0.945	1.337	
10	358	0.225	1.447	0.774	0.726	
11	361	0.366	1.408	0.721	0.614	
12	377	0.440	1.175	0.925	0.853	
13	378	0.300	1.080	1.130	0.985	
14	379	1.010	1.230	0.770	1.336	
15	386	0.295	1.166	0.989	0.804	
16	803	0.356	1.115	0.935	1.140	
17	811	0.400	1.000	1.000	2.245	
18	951	0.287	1.157	0.983	1.237	
19	981	1.250	1.170	0.820	0.641	

2.6.4 Existing Local Calibration Methodologies

Most of the previous calibration studies took the cross-sectional calibration, or pooled calibration approach in which all sections under the study area were analyzed jointly to propose a set of calibration parameters with a minimized RSS. The RSS is calculated by comparing the observed total rutting and the AASHTOWare predicted total rutting. Such approach suggested a set of regional average value of local calibration. In contrast, Waseem (2013) proposed site specific calibration parameters by a section-by-section calibration approach for Ontario’s roads. However, the accuracy of the model depends on the approach of optimization to selection of final calibrated coefficient.

The previous studies are summarized into the following four categories based on the approaches they used for optimization:

- i) Studies used regional default values or historical performance data or laboratory findings to preset one or two local calibration parameters, whereas, the studies suggested to use their global default value in case of lack of information. Trial runs are conducted with multiple combinations of remaining calibration coefficients and a set of calibration coefficients are selected corresponding to minimum RSS (Banerjee et al. 2009).
- ii) Studies focused on finding a single set of all five model coefficients β_{r_1} , β_{r_2} , β_{r_3} , β_{GB} and β_{SG} simultaneously through iteration process. Multiple combinations of calibration coefficients are used as seed value for the analysis and final calibration coefficients are determined by using numerical optimization process such as MATLAB® or SAS statistical software (Darter et al. 2009).
- iii) Studies focused on two steps iterative process for calibration of rutting model. The first step is minimizing the RSS with different set of β_{r_2} and β_{r_3} taking all other betas constant to 1, whereas, the second step utilizes the obtained β_{r_2} and β_{r_3} values for further reduction of RSS by changing β_{r_1} , β_{GB} and β_{SG} using Microsoft Excel Solver (Tareder et al. 2013).
- iv) Studies utilized a preset value of layer contribution to rutting during two steps iterative process for calibration of rutting model. The first step is finding the calibration parameters of β_{GB} and β_{SG} by minimizing the RSS with different set of β_{r_1} , β_{GB} and β_{SG} , whereas, the second step utilizes the MATLAB® environment for numerical optimization of β_{r_1} , β_{r_2} and β_{r_3} in AC layer rutting model (Waseem 2013).

2.7 Concluding Remarks

Standing out as an emerging mainstream pavement design method throughout the North America, the MEPDG is still considered as unsuitable in predicting the performance of pavement for all locations. To implement the method in Ontario's conditions, local calibration is unavoidable. Waseem (2013) recently worked toward the local calibration of rutting models for Marshal mix pavements. Although, Superpave mix has since 2001 been almost exclusively used in Ontario's roads, it is still unknown whether a separate set of calibration parameters are required for Superpave pavements or not. This research contributes to calibrate the rutting model for Ontario's Superpave pavements.

The AASHTO local calibration guidelines and experiences of numerous transportation agencies throughout North America provide guidance for this study. Their calibration approaches serve for better understanding of adopted process and methodology. The knowledge from these calibration effort will be utilized during the calibration process of rutting models under this research.

However, the literature review has clearly indicated that there has been no universally accepted local calibration method. Two major categories of approaches emerge from the divergent local calibration practice. The first approach leaves the optimization process to determine their values, while the other would prefix some of the local calibration parameters to a certain value before optimization and ask the RSS minimization to determine the others. Because of indeterminacy and interdependency between the models, the first approach blurs the nature of the problem that without layer contribution to rutting there would exist multiple optimum solutions. Indirect pilot studies have been attempted to determine the layer contribution, but in the absence of sample trench studies for Ontario's roads, the results were hard to validate. Meanwhile, the recent NCHRP 9-30A project published some reliable calibration results based on field performance and laboratory test data. These studies and data thereof may form a solid ground to prefix some of the local calibration parameters before the RSS minimization process. The next Chapter deals with the determination of the traffic and temperature exponents of the AC rutting model by studying the results from the NCHRP 9-30A project.

CHAPTER 3 TRAFFIC AND TEMPERATURE EXPONENTS

3.1 Introduction

As one can see in Chapter 2, different calibration procedures have been tried out in previous global and local calibration studies, resulting in very dissimilar optimal values of the local calibration parameters. Some researchers chose to prefix a certain local calibration parameters before the RSS minimization for probably two reasons: (1) The fewer optimization variables would reduce the numerical burden of the optimization iterations; (2) Some engineering experience may indicate a certain local calibration parameter to be a particular value. For example, Waseem (2013) prefixed $\beta_{SG} = 0$ for rehabilitated pavement sections on the ground that subgrade soils in those sections have been sufficiently consolidated and no further significant permanent deformation will occur in relatively deep depth. This Chapter reports the result of a similar effort of determining a prior value of the temperature and traffic exponents (β_{r2} and β_{r3}) by reviewing the calibration results in NCHRP Report 719.

Report 719 (Von Quintus et al. 2012) summarizes the major research findings of NCHRP Project 9-30A. The project team focused on recalibration of the MEPDG AC rutting model by measuring its rutting property in both field and laboratory. The field test were performed through forensic investigations (e.g., trenches cutting, cores excavation, falling weight deflectometer deflection), whereas, repeated-load triaxial test and shear test were performed for laboratory test protocols. A total number of 60 field sections and 46 laboratory specimens were used in their calibration. For each of those sections, longitudinal calibration was performed and the plastic deformation coefficients of temperature and traffic terms, known as temperature exponent ($n = k_{r2}\beta_{r2}$) and traffic exponent ($m = k_{r3}\beta_{r3}$), respectively, were determined. The results of field derived coefficients for new and rehabilitated pavement sections are replicated in Tables A-1 and A-2. Similarly, the results of laboratory derived coefficient are replicated in Table A-3. In the following, a few simple statistical analyses and sensitivity analyses were performed to determine a proper value for the subsequent local calibration study for Ontario's roads.

3.2 The Traffic Exponent

In order to determine a proper prefixed traffic exponent ($m = k_{r3}\beta_{r3}$) value, three hypotheses have to be tested at first:

- (1) H1: The new and rehabilitated pavement sections share the same traffic exponent value.
- (2) H2: The field- and laboratory-derived traffic exponents are the same.
- (3) H3: Material testing protocols do not affect the traffic exponent.

To test these hypotheses, t-tests are performed.

Table 3.1: Test statistics between observed traffic exponents under NCHRP Project 9-30A

Hypothesis	Test data	Statistic and degrees of freedom	p value
H1	Table A1 vs. A2	0.322 (n = 39)	0.374
H2	Table (A1+A2) vs. A3 (TT)	4.744 (n = 52)	8.36E-0.6
	Table (A1+A2) vs. A3 (ST)	0.187 (n = 37)	0.426
H3	Table A3 (TT and ST)	3.323 (n = 39)	0.001

The number of t-tests analysis are done during this research by using the field and laboratory derived traffic exponent under NCHRP Project 9-30A. For the first test, it was hypothesized that there is no significant difference between derived mean value for new and rehabilitated sections. The calculated t-value for field derived traffic exponent between new and rehabilitated sections is 0.322 which accepts the null hypothesis. Hence, there is no need to separate the traffic exponent for new and rehabilitated sections as mentioned by Waseem (2013).

Similarly, *t*-test analysis is performed to identify the feasibility of direct use of repeated-load triaxial and shear test for calibration of AC layer rutting model. It is observed that there is no difference in traffic exponent from field derived and repeated-load shear test (t value = 0.187), whereas significant difference from repeated-load triaxial test (t value = 4.744). Further, a large difference is observed in traffic exponent between data collected by repeated-load triaxial test (TT) and shear test (ST). Due to such observation, further *t*-test analysis is performed to identify the difference between mean value of traffic exponent from these test protocols. The test verifies that there is a significant difference (t value = 3.323) in traffic exponent by material testing

protocols. These test results guided that the mean traffic exponent value from repeated-load plastic deformation shear tests can be directly used as a level-2 input for the calibration of rutting model. But, repeated-load plastic deformation shear tests are usually not performed not only because of time limitation, but also of the test apparatus and protocol limitations.

A further sensitivity analysis was carried out to check the overall impact of the traffic exponent (m) on rutting prediction. For this purpose, the total rutting of 12 Ontario Superpave sections are predicted at different value of m ranging from 0.11 to 0.57, with the local calibration coefficient β_{r3} correspondingly being 0.2296 to 1.1897. The comparison between the predicted rutting with different value of m for these typical Superpave pavement sections are shown in Figure 3.1. An ANOVA analysis as presented in Table 3.2 and 3.3 found that the value of traffic exponent is insensitive within its global value of 0.48, but highly sensitive beyond this value. The reason for such a variation is indistinct and need further intensive study.

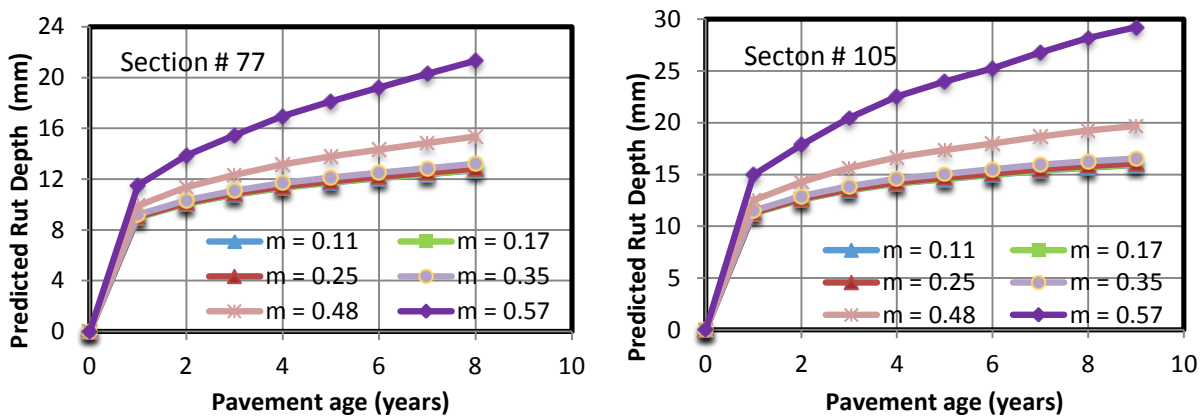


Figure 3.1: Comparison between the predicted rutting with different value of m

Table 3.2: Statistical results for total predicted rut within the global value of traffic exponent

Groups	Counts	Sum	Average	Std. Deviation
Rutting with $m = 0.11$	98	1203.794	12.284	5.699
Rutting with $m = 0.17$	98	1205.899	12.305	5.709
Rutting with $m = 0.25$	98	1213.125	12.379	5.747
Rutting with $m = 0.35$	98	1240.652	12.660	5.901
Rutting with $m = 0.48$	98	1396.076	14.246	6.875

ANOVA

Source of Variation	SS	df	MS	F	P - value	F critical
Between Groups	273.949	4	68.487	1.901	0.109	2.390
Within Groups	17477.249	485	36.036			
Total	17751.198	489				

Table 3.3: Statistical results for total predicted rut beyond the global value of traffic exponent

Groups	Counts	Sum	Average	Std. Deviation
Rutting with $m = 0.11$	98	1203.794	12.284	5.699
Rutting with $m = 0.17$	98	1205.899	12.305	5.709
Rutting with $m = 0.25$	98	1213.125	12.379	5.747
Rutting with $m = 0.35$	98	1240.652	12.660	5.901
Rutting with $m = 0.48$	98	1396.076	14.246	6.875
Rutting with $m = 0.57$	98	1827.220	18.645	9.987

ANOVA

Source of Variation	SS	df	MS	F	P - value	F critical
Between Groups	3088.426	5	617.685	13.240	0.000	2.230
Within Groups	27151.499	582	46.652			
Total	30239.925	587				

On the other hand, some models (e.g., the modified Leahy model and the Verstraeten model) used m -value of 0.25. Also, a histogram plotted from the results of field and laboratory derived traffic exponent concentrated to an average value of 0.30 with standard deviation of 0.08 as presented in Figure 3.2. Further, NCHRP Report 719 demonstrated no significant evidence for different m for new and rehabilitated sections and concluded that the current global coefficient for traffic exponent seems to be too large. Thus, under these circumstances, the traffic exponent is fixed to a value of 0.30 as level 3 input for this research.

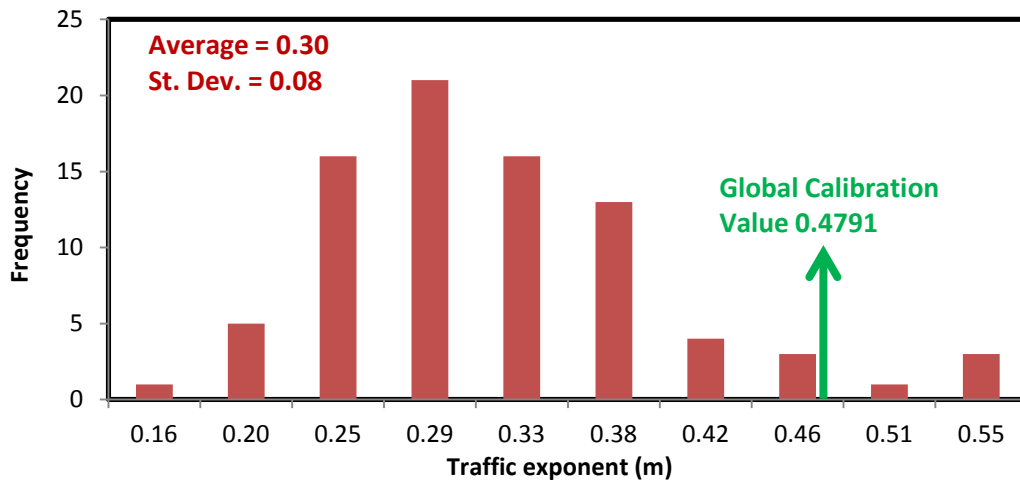


Figure 3.2: Frequency evaluation for traffic exponent under NCHRP Project 9-30A (Data source: Table A-1, A-2 and A-3)

3.3 Temperature Exponent

Among the alternative rutting models, only the MEPDG model and the Asphalt Institute (AI) model include a temperature term. The AI model used a temperature exponent (n) of 2.767 whereas the value is 1.5606 for MEPDG model. Report 719 concludes that the laboratory-derived temperature exponent (Refer to Table A.3 for the replicated data) are highly dependent upon the material testing methods. The histograms of the triaxial and shear loading test data are depicted in Figure 3.3. While the mean exponent of the triaxial test is 2.665, that of the repeated load shear test is 7.720, more than doubled. Moreover, most of the past local calibration studies as reviewed in Section 2.6 simply used its global value. For these reasons, this study also chose to fix the temperature exponent at its global value of 1.5606. That is, the local calibration coefficient β_{r2} is preset to 1.0 in this local calibration study.

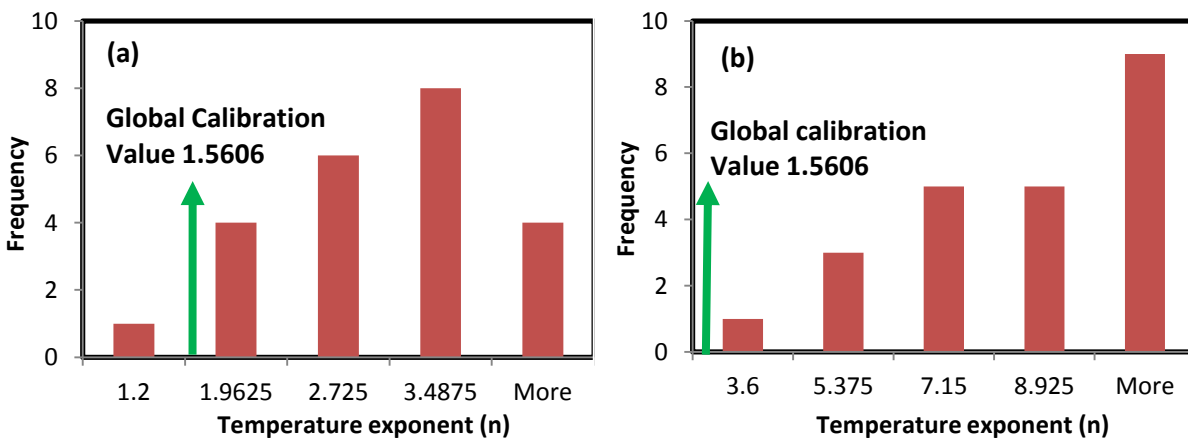


Figure 3.3: Frequency evaluation for temperature exponent under NCHRP Project 9-30A (a) repeated load triaxial test and (b) repeated load shear test (Data source: Table A-3)

3.4 Concluding Remarks

The global value of temperature exponent (n) of the AC rutting model in the MEPDG based on the NCHRP 1-40D is 1.5606. A recent research by Waseem (2013) found this value ranging from 1.459 to 2.712 for Ontario's Marshall mix design, whereas NCHRP Project 9-30A found its laboratory derived values to lie between 1.200 to 4.25. Also, the study of the effect of temperature on plastic deformation coefficients by NCHRP Project 9-30A team found this value around 1.0 and slightly less for high quality of material. This large variation and contradictory observations of temperature exponent blurs the issue and the solution becomes vague. The author

believes that an intensive study of temperature exponent be required to settle down this issue. For this study, the coefficient is pragmatically fixed to 1.5606 . That is, β_{r2} is preset to 1.0.

On the contrary, the traffic exponent has shown much smaller variation in the global and local calibration studies. The global value of traffic exponent (m) for MEPDG rutting model based on the NCHRP 1-40D is 0.4791. Waseem (2013) found this value ranging from 0.11 to 0.57 for Ontario's Marshall mix design, whereas NCHRP Project 9-30A team found this value between 0.16 to 0.55 with an average of 0.30 and standard deviation of 0.08. This statistical result showed that the current global coefficient for traffic exponent seems to be too large. The statistical analysis of the Project 9-30A data also confirmed that the field- and laboratory-derived traffic exponents for new and rehabilitated sections can be considered to come from the same population and thus there is no need to separately treat the new and rehabilitated sections in local calibration. Moreover, a pilot sensitivity study shows that the m value has little effects on rutting prediction if the range is confined to be within 0.11 – 0.35. Therefore, this study chose to preset the m value at 0.30 (or $\beta_{r3} = 0.6262$) for the local calibration, while using 0.11 to 0.57 for sensitivity studies.

CHAPTER 4 LOCAL CALIBRATION METHODS

4.1 Guiding Principle

This chapter discusses the two local calibration methods that are used in this study. As discussed in Chapter 2, the MEPDG method includes three empirical rutting models (c.f., equations 2.7 and 2.8) for asphalt concrete, granular base/sub-base materials, and sub-grade soils, respectively. These models altogether contain five calibration coefficients ($\beta_{r1}, \beta_{r2}, \beta_{r3}$ for AC, β_{GB} for granular base/sub-base, and β_{SG} for sub-grade soils). As discussed in Chapter 3, to reduce the indeterminacy of the optimization process, the two exponent coefficients (β_{r2} and β_{r3}) have been prefixed to some specific values. Therefore, the local calibration optimization aims to determine the three scale coefficients ($\beta_{r1}, \beta_{GB}, \beta_{SG}$) with the following two objectives: (1) minimize bias and (2) minimize the Residual Sum of Squares (RSS). These two objectives are usually compatible because any additional bias will increase the RSS. In ideal case, the RSS is minimized only if the bias is eliminated. However, the natural constraint that the three scale coefficients must be nonnegative sometimes cannot ensure that the bias be eliminated when the RSS is minimized.

The residual in the term RSS is defined as the difference between the observed or measured rut depth that is available from the PMS database (Details are explained in Chapter 5) and the MEPDG-predicted total rut depth at the same measurement or inspection time. The RSS and bias are expressed as, respectively,

$$\text{RSS} = \sum_{i=1}^n (D_i - d_i)^2 \quad (4-1a)$$

$$\text{Bias} = \sum_{i=1}^n (D_i - d_i) \quad (4-2b)$$

where: n = total number of rut depth measurements in the calibration set;

d_i = observed total rut depth;

D_i = calculated total rut depth as given in equation (4-2), which is a function of the five local calibration parameters;

$$D_i = D_{ACi} + D_{GBi} + D_{SGi} \quad (4-3)$$

D_{ACi} = calculated total rut depth of AC layer, which is a function of the three local calibration parameters $\beta_{r1}, \beta_{r2}, \beta_{r3}$.

D_{GBi} = calculated total rut depth of granular base layer, a function of β_{GB} .

D_{SGi} = calculated total rut depth of sub-grade layer, a function of β_{SG} .

Based on the previous discussion on Chapter 3, a preset value for temperature exponent (n) and traffic exponent (m) are suggested as 1.5606 and 0.30, respectively, in the following study. This fixes the local calibration parameters β_{r2} and β_{r3} as 1.0 and 0.6262 respectively. Since the calibration parameters β_{r1}, β_{GB} and β_{SG} all are direct multipliers of the rutting models, one can estimate the rut depth for each structural layer by using the rutting models with $\beta_{r1}=1, \beta_{GB}=1$ and $\beta_{SG}=1, \beta_{r2} = 1.0$ and $\beta_{r3} = 0.6262$. Denote so estimated rut depths by $D_{ACi,g}, D_{GBi,g}$ and $D_{SGi,g}$ for the AC, granular base/sub-base, and sub-grade soil layers, respectively. Then Eq. (4-2) can be rewritten as

$$D_i = \beta_{r1}D_{ACi,g} + \beta_{GB}D_{GBi,g} + \beta_{SG}D_{SGi,g} \quad (4-3)$$

If RSS is the only objective function of the local calibration, then it can be readily shown that the three scale parameters can be solved from the following simultaneous linear equations, which are derived from the simple least square principle:

$$\sum D_{ACi,g}d_i = \beta_{r1} \left(\sum D_{ACi,g}^2 \right) + \beta_{GB} \left(\sum D_{ACi,g}D_{GBi,g} \right) + \beta_{SG} \left(\sum D_{ACi,g}D_{SGi,g} \right) \quad (4-4)$$

$$\sum D_{GBi,g}d_i = \beta_{r1} \left(\sum D_{ACi,g}D_{GBi,g} \right) + \beta_{GB} \left(\sum D_{GBi,g}^2 \right) + \beta_{SG} \left(\sum D_{GBi,g}D_{SGi,g} \right) \quad (4-5)$$

$$\sum D_{SGi,g}d_i = \beta_{r1} \left(\sum D_{ACi,g}D_{SGi,g} \right) + \beta_{GB} \left(\sum D_{GBi,g}D_{SGi,g} \right) + \beta_{SG} \left(\sum D_{SGi,g}^2 \right) \quad (4-6)$$

Unfortunately, some testing calibrations suggested that this simple least square solution sometimes led to negative values for the three parameters. Therefore, additional constraints should be added to the minimization process and the other objective: minimization of the absolute value of the bias has to be introduced. In the end, the local calibration problem is formulated as the following two-objective constrained optimization problem:

$$\begin{aligned} \min \quad & \text{RSS and Bias} \\ \text{s.t.} \quad & \beta_{r1}, \beta_{GB}, \beta_{SG} \geq 0 \end{aligned}$$

To solve this problem, the author realize that the best feasible solution is the trial and error method to reach a minimum RSS value. A number of trial run are conducted with multiple combination of calibration coefficients β_{r_1} , β_{GB} and β_{SG} using the semi-automated local calibration procedure developed by Waseem (2013) in Excel Macros. A set of calibration coefficients are selected corresponding to minimum RSS. Some random spot checks are done to confirm the optimization before selecting optimal solution by varying β_{r_1} , β_{GB} and β_{SG} with few neighbouring values. Finally, the results from this method are validated and compared with global calibration efforts.

4.2 Cross-sectional Calibration and Longitudinal Calibration

This study proposes two different local calibration methods: the cross-sectional calibration and longitudinal calibration. In the first type of model calibration, the rut depth measurements from the calibration sections are pooled together for the local calibration. An advantage of the cross-section calibration, or pooled calibration as Waseem (2013) named it, is that it allows to use as many sections as possible in the minimization process to obtain a single set of local calibration parameters. Therefore, The cross-sectional study does not require long-time rut records for any specific sections. However, the data quality requirement is not less constrained. To avoid the high fluctuation on the observed rut depth along the service life of the pavement and for the consistency consideration, only the last rut depth measurements of the calibration sections in the year 2012 are used for cross-sectional calibration.

In the longitudinal calibration, each calibration section is treated as a calibration object for which the minimization process is performed to obtain a section-specific set of local calibration coefficients. Therefore, only those sections with a relatively long series of rut records (say, at least 3 years) were calibrated. Unfortunately, the magnitude of field observed rut depth data retrieved from the MTO's PMS database fluctuate with high variability along the service life of the pavement. This has greatly limited the number of pavement sections that can be used in the longitudinal study.

It is important to understand that the equal weight is given for each observed rut depth during the both type of model calibration. On the other side, the predicted rut data are estimated using rutting models within the AASHTOWare pavement design software environment. This

requires the detailed input and level of accuracy of the sections as described in Chapter 5. Input and its level significantly contributes towards total standard error. However, this research completely relied on the already available database and no additional tests were performed to upgrade the input level. Figure 4.2 is presented here to elaborate the example of longitudinal calibration methodology.

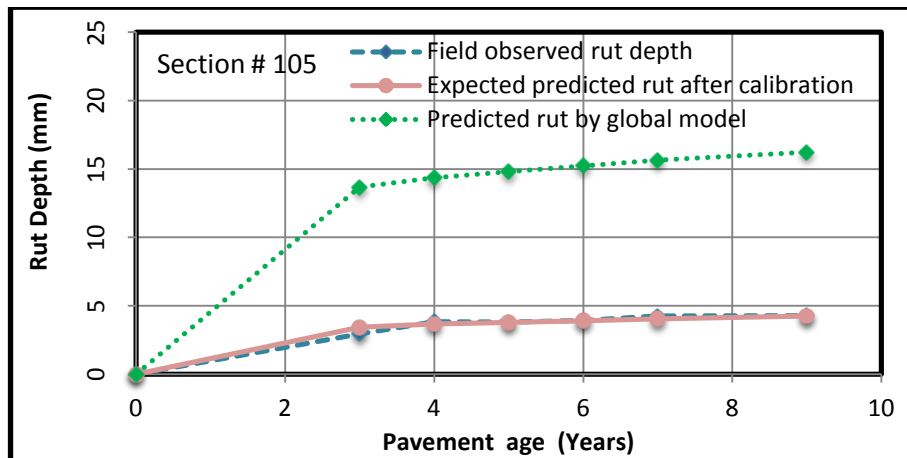


Figure 4.1: Typical example for longitudinal calibration methodology

The cross-sectional calibration approach is easy for data management, analysis and adaptation for further pavement design, in contrast to the longitudinal calibration approach. However, the results are less precise. In the longitudinal calibration, model development for precise estimation of calibration parameters for specific pavement section is always the challenging part during design and maintenance practices.

4.3 Validation Methods

The calibration results from cross-sectional and longitudinal calibration methods are verified separately. For the cross-sectional validation, the optimized calibration parameters are used on 35% of selected pavement sections to predict the total rut depth. Finally, the statistical analysis is performed to test the variance of the residual error between the calibration and validation sets at a significant level of 5%. For longitudinal approach, each calibrated sections are individually verified with the latest rut depth measurements.

CHAPTER 5 CALIBRATION DATABASE

5.1 Data Requirement for Local Calibration

Basically, two types of data are required for local calibration to rutting models: observed rut depth data and pavement analysis input data for the prediction of rut depth of selected pavement sections. The observed data are retrieved from the MTO's database and integrated into the calibration database through screening and selection process. The predicted rut data are estimated using rutting models that are to be locally calibrated by simulating the existing field pavement condition within the AASHTOWare pavement design software. This requires the detailed input and level of accuracy of selected road sections. The major inputs for the evaluation of pavement rutting in the AASHTOWare include:

- i) General project information
- ii) Traffic data
- iii) Climate data
- iv) Pavement material and structural data

The details of the data are discussed in details in the following. But before this, the pavement sections selected for the calibration study is described at first.

5.2 Accuracy of Input Data

Based on the availability of resources, input data for traffic and materials are classified in three levels of accuracy as described below. AASHTOWare pavement design software provides flexibility to make a choice of level of accuracy of input data depending on the importance of the project. This research utilizes the highest level of inputs as far as available.

Level 1:

This level of inputs represents highest level of accuracy and obtained directly from specific site measurements, laboratory observations and actual field testing results. However, these inputs require expensive experimentation and, hence, used for the projects having high economical risks. Generally, dynamic modulus, resilient modulus, AADTT, lane number, growth factor, etc. are used for this level.

Level 2:

This level of inputs represents intermediate level of accuracy and obtained from mathematical correlations or regression equations. Regional default values established by local authority also represent level 2 input. Some examples of level 2 data are resilient modulus estimated from CBR values, axle configuration, truck vehicle classification, etc. and are used whenever project or site specific values are not available.

Level 3:

This level of inputs represents lowest level of accuracy and estimated based on the experiences. Regional and global default values also represent level 3 input. As far, this level of inputs are avoided for the design practices, however, can be used for low volume roads.

5.3 Sample Selection

The Province of Ontario has more than 16,500 lane-km paved roads segmented into about 1,800 pavement sections under the jurisdiction of the Ministry of Transportation of Ontario (MTO) (Li et al. 2008). Among them, the majority are flexible pavements. Studying all of the flexible sections for the rutting model calibration is neither possible (because of time and cost limitation) nor necessary. However, there is a minimum number of pavement sections (sample size) that a local calibration study needs so that the results can be statistically generalized without biasing the findings. The Guide for the Local Calibration of the Mechanical-Empirical Pavement Design Guide (AASHTO 2010) recommends a minimum number of 20 pavement sections for total rutting study at a significance level of 90%. The guide further suggests a fractional balance factorial of the key factors such as climatic zone (geographical regions), pavement types (new and rehabilitated sections), truck traffic application (highway type), etc. when selecting the roadway sections for the study. This recommendations are considered in this research study.

MTO started to introduce Superpave in the year of 2001. As of 2012, there have been in total 87 projects that used Superpave mix in the top asphalt layer(s), which amounts to 140 sections. These projects have different pavement structures and highway types, spreading over all of the five climatic zone of Ontario as shown in Figure 5.1. Preliminarily, 133 pavement sections are selected excluding the secondary highway because of its small sample size. A total of 31 SMA and widening sections are also removed. The remaining 102 sections are further processed

for the cross-sectional calibration. However, only 84 sections are viable for cross-sectional calibration because of lack of trustable structural and/or material information.

For longitudinal calibration purpose, further screening of the 84 sections are performed based on the quality of the observed rut depth data. In this regard, the pavement sections with service life of more than 3 years are selected to ensure that a realistic trend of rut progression can be established and observed. Finally 33 sections from 22 roadway segments are selected for the longitudinal local calibration purpose as shown in Figure 5.2.

For these selected pavement sections, the input data are collected, verified and combined with assistance from MTO staff to create a unified database for the use of local calibration. The details of the selected sections are presented in Table B-1 to B-5.

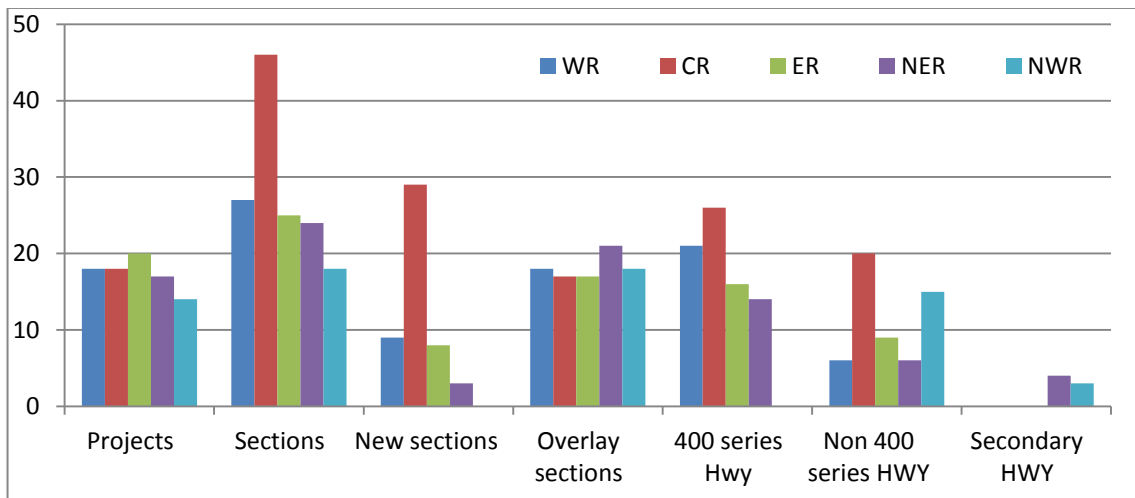


Figure 5.1: Distribution of number of available sections by climatic zone

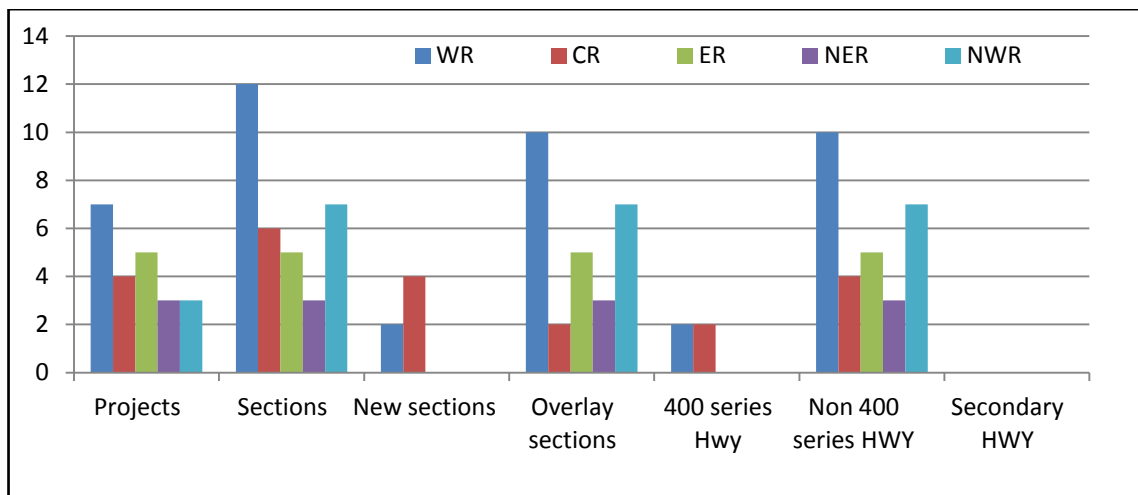


Figure 5.2: Distribution of number of selected sections by climatic zone

Similarly, the same calibration methodology was applied to the Ontario’s Marshall mix sections calibrated by Waseem (2013). The details of the sections are presented in Table B-6.

5.4 Major Input Variables for MEPDG

A typical design in MEPDG required numerous inputs related to material, traffic and climate for the AASHTOWare pavement design analysis. The input requirements during local calibration of new, reconstructed and rehabilitated flexible pavement sections are discussed below.

5.4.1 General Project Information

In AASHTOWare pavement design software, project related inputs regarding some general information, design criteria and project identifiers are required as in Table 5.1. The general information includes the life, type and history of the pavement section where as project identifiers represents the identity of the pavement section under consideration. These information are collected from MTO database for each pavement sections. However, limiting value of predicted distress corresponding to 50 % reliability recommended in Ontario’s default parameters for AASHTOWare pavement ME design interim report 2012 are taken as input data under design criteria for local calibration.

Table 5.1: Summary of general project input used for AASHTOWare in this study

Item Name	Input Requirement	Value	Input level	Source
General Information	• Design type	Project specific	1	This study
	• Pavement type			
	• Base construction (month, year)			
	• Pavement construction date (month, year)			
	• Pavement overlay construction (month, year)			
	• Traffic opening (month, year)			
	• Design life			
Design Criteria	• Initial IRI (m/km)	Project specific	2	MTO (2012)
	• Terminal IRI	2.7		
	• AC top-down fatigue cracking (m/km)	378.8		
	• AC bottom-up fatigue cracking (m/km)	25		
	• AC thermal fracture (m/km)	189.4		
	• Permanent deformation – total (mm)	19		
	• Permanent deformation – AC only (mm)	6		

5.4.2 Traffic Data

The AASHTOWare incorporate traffic inputs under 6 main groups as presented in Table 5.2. The site specific traffic data are mostly preferred for the analysis. However, site-related, regional or agency-wide or AASHTOWare default traffic parameters can be used in some specific cases. For this study, MTO database, Ontario’s default parameters for AASHTOWare pavement ME design interim report 2012, AASHTOWare default values are taken as key sources for traffic input for each pavement sections during local calibration. Traffic information for selected pavement sections are presented in Tables C-15 to C-20.

Table 5.2: Summary of traffic input requirements and the accuracy level used in this study

Item Name	Input Requirement	Value	Input level	Source
Annual Average Daily Truck Traffic (AADTT)	• Two way AADT	Project specific	1	This study
	• Number of lanes in the design direction			
	• Percent of trucks in design direction	50%	3	Local Calibration Guide
	• Percent of trucks in design lane	Table C-1	2	MTO (2012)
	• Operational speed	Table C-2		
Traffic Volume Adjustment Factors	• Vehicle class distribution	Table C-3	2	This study
	• Traffic Growth rate	Project specific	1	
	• Growth function	Compound		
	• Monthly adjustment factor	1.0	3	MTO (2012)
	• Hourly adjustment factor	Default		
Axle Per Truck	• Single axial per truck	Tables C-4 & 5	2	MTO (2012)
	• Tandem axial per truck			
	• Tridem axial per truck			
	• Quad axial per truck			
Axle Load Distribution	• Single Axle Distribution	Tables C-6 to 13	2	MTO (2012)
	• Tandem Axle Distribution			
	• Tridem Axle Distribution			
	• Quad axles Axle Distribution			
Axial Configuration	• Average axle width (m)	2.59	3	AASHTO MOP
	• Dual tire spacing (mm)	305		
	• Tire pressure (kPa)	827.4		
	• Number of Axles per Truck	-	2	MTO (2012)
	• Tandem axle spacing (m)	1.45		
	• Tridem axle spacing (m)	1.68		
	• Quad axle spacing (m)	1.32		

Lateral Traffic Wander	• Mean wheel location (mm)	460	3	AASHTO MOP
	• Traffic wander standard deviation (mm)	254		
	• Design lane width (m)	Project specific	1	MTO (2012)
Wheel Base	• Average spacing of short axles (m)	5.1	2	MTO (2012)
	• Average spacing of medium axles (m)	4.6		
	• Average spacing of long axles (m)	4.7		
	• Percent of trucks with short axles (%)	33	3	AASHTO MOP
	• Percent of trucks with medium axles (%)	33		
	• Percent of trucks with long axles (%)	34		
Note: MOP - Manual of Practice				

5.4.3 Climatic Data

Local weather conditions such as temperature, precipitation, season and depth of water table acts as a phenomenon of producing extreme long term distresses that significantly affect the pavement performance. As a result, estimation of local climate conditions are essential to predict the distribution of temperature and moisture in the pavement structure that are highly sensitive to AC and unbound material stiffness respectively. The AASHTOWare uses the observed location parameters in the Integrated Climatic Model (ICM) to obtain the local climatic data (mean annual air temperature, mean annual precipitation, mean monthly temperatures, number of wet days, freezing index and average number of freeze/thaw cycles) from a library of more than 800 weather stations throughout USA and Canada. Table D-1 presents the Ontario's 34 weather stations that are included in AASHTOWare pavement design software.

In AASHTOWare, location parameters and ground water related information are required for climatic data inputs as shown in Table 5.3. The location parameters include the latitude, longitude and elevation of the pavement sections under consideration as shown in Table D-2 to D-7, for which the site specific information are collected from Google maps. However, a regional default value of 6.1 m is used for the depth of ground water table (GWT).

Table 5.3: Climate input requirement used for AASHTOWare in this study

Item Name	Input Requirement	Value	Input level	Source
Location Parameters	• Latitude	Project specific	1	Google maps
	• Longitude			
	• Elevation			
Ground Water Parameter	• Ground water table (GWT)	6.1	3	MTO (2012)

5.4.4 Pavement Material and Structural Data

A typical flexible pavement is designed in two types of structural layers, known as AC layer and unbound (granular and fine) layer by using different types of material. AC layer mainly uses Superpave, stone matrix asphalt (SMA), Marshall mix and asphalt stabilized material, whereas, Granular materials, chemically stabilized base materials and fine sub-grade soil are used for unbound layer in Ontario’s roads, which are presented in Tables E-7 to E-11.

The AASHTOWare needs material properties of the pavement layers for mechanistic analysis to obtain the pavement responses and distresses under local condition. The material inputs are categorized into 5 main groups for AC layer and 3 groups for unbound layer, as presented in Tables 5.4 and 5.5, respectively. In terms of the accuracy level, the Level 1 (project specific) material properties are preferred. However, many properties such as aggregate gradation, air voids, binder content are difficult, but not impossible to obtain or retrieve. For this reason and to facilitate the local calibration, the MTO has developed a guide document that specifies the default values for those parameters that are not easy to obtain their project-specific values (MTO 2012).

Table 5.4: AC layer material input requirements and the accuracy level used in the study

Item Name	Input Requirement	Value	Input level	Source
Asphalt Layers	<ul style="list-style-type: none"> Type of material Thickness (mm) 	Project specific	1	This Study
Mixture Volumetric Properties	<ul style="list-style-type: none"> Unit weight (Kg/m³) 	Tables E-1, 2 & 3	2	MTO (2012)
	<ul style="list-style-type: none"> Effective binder content (%) 			
	<ul style="list-style-type: none"> Air voids (%) 			
Poisson's Ratio	<ul style="list-style-type: none"> Is Poisson’s ratio calculated? 	No	-	-
	<ul style="list-style-type: none"> Poisson’s ratio 	0.35	3	AASHTO MOP
Mechanical Properties	<ul style="list-style-type: none"> Dynamic modulus 	Default model	3	AASHTO MOP
	<ul style="list-style-type: none"> Aggregate gradation 	Tables E-1, 2 & 3	2	MTO (2012)
	<ul style="list-style-type: none"> Asphalt binder 			
	<ul style="list-style-type: none"> G* predictive model 	Default model	3	AASHTO MOP
	<ul style="list-style-type: none"> Creep compliance (1/GPa) 			
	<ul style="list-style-type: none"> Indirect tensile strength at -10 °C (MPa) 			
	<ul style="list-style-type: none"> Reference temperature (C_o) 	21.1		

Thermal Properties	• Thermal conductivity (W/m·K)	1.16	3	AASHTO MOP
	• Heat capacity (J/kg.K)	963		
	• Thermal Contraction	Default model		

Table 5.5: Unbound layer material input requirements and the accuracy level used in the study

Item Name	Input Requirement	Value	Input level	Source
Unbound Layers	• Type of material • Thickness (mm)	Project specific	1	This study
	• Poison's Ratio	0.35	3	AASHTO MOP
	• Coefficient of lateral earth pressure	0.50		
Modulus	• Resilient modulus (MPa)	Tables E-1, 2 & 3	1	This study
Sieve	• Gradation and other engineering properties		2	MTO (2012)

5.5 Calibration Database

In Canada, Jannat (2012) was the first person who worked on development of calibration database during her MASc requirement. She used 5555 pavement section cycles (the life of a section from its construction or reconstruction or rehabilitation year to the next major rehabilitation year) from Ontario's PMS-2 considering geographical regions, highway types, facility types, number of lanes, lengths of section, rehabilitation type and quality of performance and finally, she developed a unified high quality pavement database of 101 section cycles for local calibration. The developed database was further used by Waseem (2013), a member of Ryerson group led by Professor Yuan, during local calibration study to the Ontario's Marshall mix sections.

This study differ from the study of Waseem (2013) in terms of AC layer(s) material and methodology. The study mainly focus on the local calibration of MEPDG rutting models for Ontario's Superpave sections and the required database is developed during the study. However, the database developed by Jannat (2012) and used by Waseem (2013) are also used in this study to see the reliability of developed new methodology to the Marshall mix sections.

5.6 Summary

This chapter discussed the details of three major categories of input data (i.e., traffic, climate and materials) requirement and their hierarchical level used for local calibration of pavement sections in Ontario. Pavement sections for local calibration were selected by screening based on the quality of historical pavement performance data retrieved from the MTO database.

For all the selected sections, performance data including section name, route name, route direction, station beginning mile, station end mile, facility type, functional class, AADTT, sub-grade modulus, axle configuration, vehicle class, materials properties etc. were collected and compiled to the proper format for the use of local calibration. Latitude, longitude and elevation for specific section are collected from google map and complied accordingly in to the data file. Finally, these integrated data will be used for pavement analysis as discussed in the following local calibration studies.

CHAPTER 6 CROSS-SECTIONAL CALIBRATION

6.1 Calibration and Validation Results

6.1.1 Results for Superpave Sections

The rutting models for Superpave sections are calibrated by using local calibration methodology as described in Chapter 4. The cross-sectional calibrations was performed on fifty three Ontario’s Superpave pavement sections by comparing the observed and predicted rut depth in the year 2012. The total RSS was minimized at $\beta_{r_1} = 2.692$, $\beta_{GB} = 0.000$ and $\beta_{SG} = 0.185$ with standard error of 1.200 mm and a bias of 0.086 mm, yielding an average layer contribution of 31.21%, 0.00% and 68.79% for AC, base and sub-grade layer respectively.

Meanwhile, the observed total pavement rutting is plotted against the corresponding predicted values as shown in Figure 6.1a which showed a poor correlation (0.350) between them. However, the obtained calibration parameters are further used to the 31 Superpave sections (refer Figure 6.2b) that results in a standard error of 1.193 mm and a bias of 0.151 mm. An F-test for the residual error was performed among these calibration and validation sets. The test result is presented in Table 6.1, where the ratio of variance (F=1.02) is less than F critical (F critical=1.76) at a significance level of 5%. Thus, the null hypothesis of no significant difference between the residual error of calibration and validation sets is accepted.

Table 6.1: Statistical results between calibration and validation sets of Superpave sections

Parameters	Calibration Sets	Validation Sets	F	P	F Critical
Mean residual error	0.086	0.151	1.02	0.42	1.76
Standard deviation	1.197	1.183			
Observation	53	31			
Degree of freedom (df)	52	30			

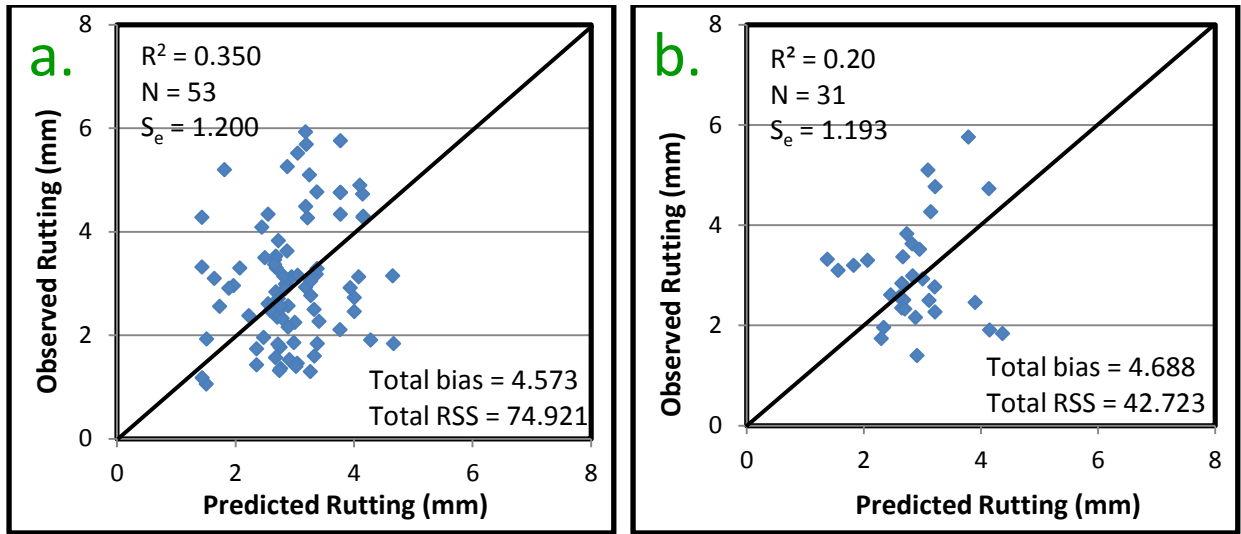


Figure 6.1: Predicted versus observed plots for (a) calibration (b) validation

A plot of residual errors (Figure 6.2) for total predicted rut depth showed that the residuals errors for cross-sectional calibration are widely but equally scattered on both sides of zero line with under prediction for total rut less than 3 mm and over prediction for total rut greater than 3 mm. Although it shows extremely poor correlation (0.350), the overall standard error of 1.200 mm (refer to Figure 6.1a) is better than the result from the global calibration. However, the observation of small R^2 value pointed toward a need to consider the weighted on the observed rutting with the age of the pavement during the calibration.

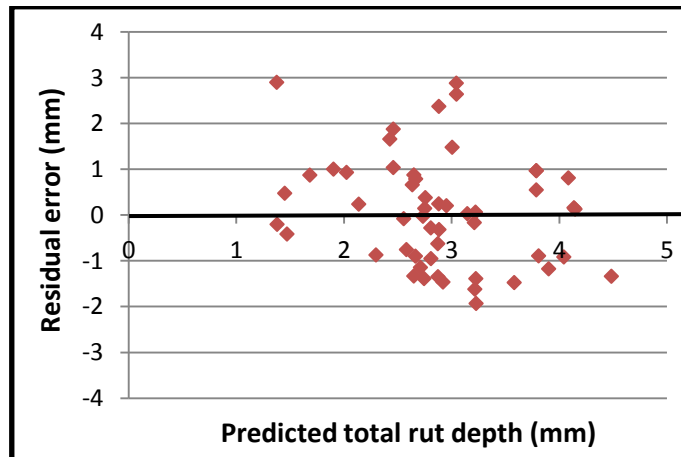


Figure 6.2: Residual error for Superpave sections

6.1.2 Results for Marshall Mix Sections

The cross-sectional calibration methodology was applied to Ontario’s Marshall mix pavement sections taken by the Waseem (2013) considering the rut depth measured in the year 2009 and 2010 using preset value of local calibration parameters for temperature exponent (β_{r_2}) and traffic exponent (β_{r_3}). Most of these Marshall mix sections under gone for the rehabilitated process after year 2010 and have no information about the structural layer. Thus, the latest rut observation in the year 2012 could not be used for the analysis as done in Superpave sections.

The analysis was performed on 19 Marshall mix pavement sections with a preset value of 1.000 and 0.6262 for local calibration parameters of temperature exponent (β_{r_2}) and traffic exponent (β_{r_3}) respectively. The total RSS was minimized at $\beta_{r_1} = 3.449$, $\beta_{GB} = 1.207$ and $\beta_{SG} = 0.058$ resulting an average layer contribution of 21.53%, 68.98% and 9.49% for AC, base and sub-grade layer respectively. Meanwhile, the observed total pavement rutting is plotted against the corresponding predicted values as shown in Figure 6.3a which showed a poor correlation (0.521) between them with a standard error of 2.208 and a bias of 0.202 mm.

However, the obtained calibration parameters are further used to 10 Marshall mix sections that results in a standard error of 2.495 mm and a bias of 0.329 mm (refer to Figure 6.3b). A F-test for the residual error was performed among these calibration and validation sets. The test result is presented in Table 6.2, where the ratio of variance (F = 1.26) is less than F critical (F critical = 2.46). Thus, the null hypothesis of no significant difference between residual error of calibration and validation sets is accepted.

Table 6.2: Statistical results between calibration and validation sets of Marshall mix sections

Parameters	Validation Sets	Calibration Sets	F	P	F Critical
Mean residual error	0.329	0.202	1.26	0.32	2.46
Standard deviation	2.471	2.199			
Observation	10	19			
Degree of freedom (df)	9	18			

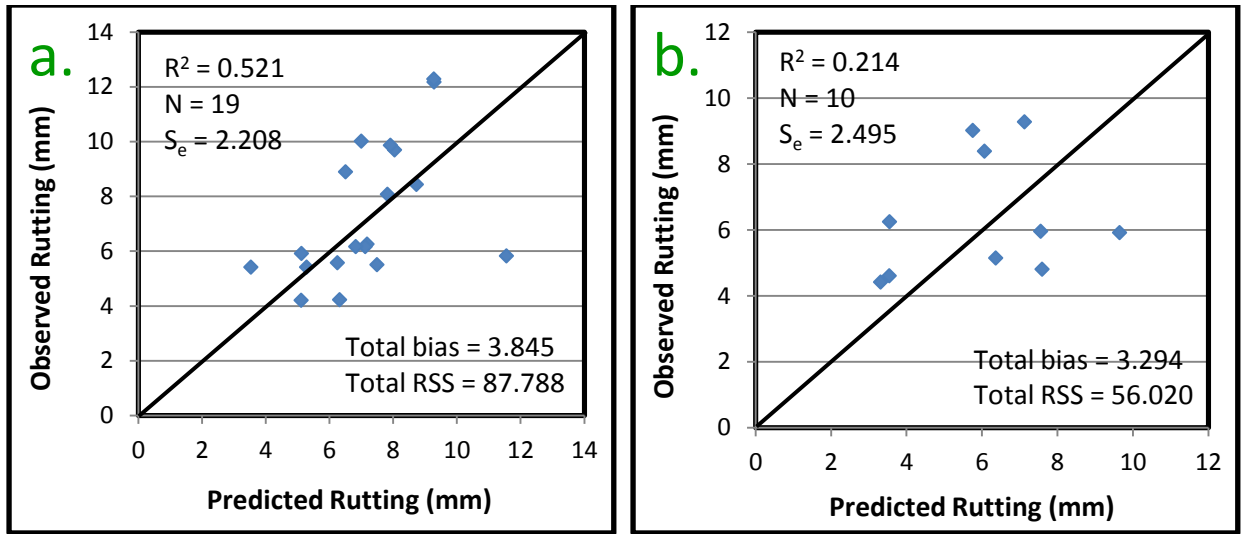


Figure 6.3: Predicted versus observed plots for (a) calibration (b) validation

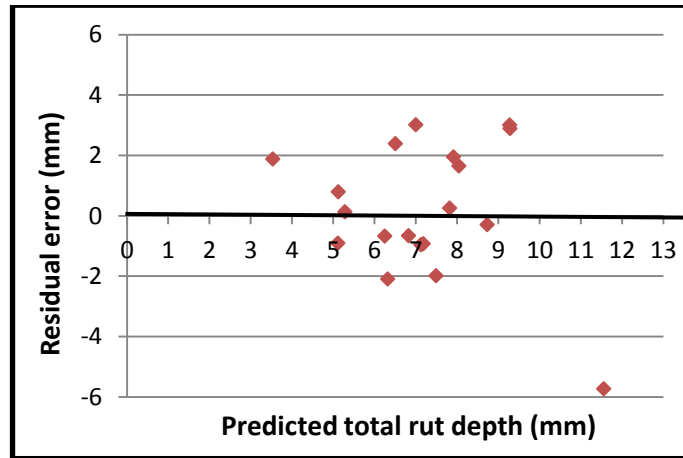


Figure 6.4: Residual error for Marshall mix sections

A plot of residual errors (Figure 6.4) for total predicted rut depth showed that the residuals errors are closely and equally scattered on both sides of zero line for rut depth less than 6 mm, whereas they are widely scattered and mostly under predicted thereafter. On the other side, it shows poor correlation (0.521) that is expected to improve by considering the weighted on the observed rutting with the age of the pavement during the calibration. However, the standard error of 2.208 (refer to Figure 6.3a) is better than the result from the global calibration.

6.1.3 Discussions

The local calibration coefficients for Superpave sections $\beta_{r_1} = 2.692$, $\beta_{GB} = 0.000$ and $\beta_{SG} = 0.185$ with corresponding average layer contribution of 31.21%, 0.00% and 68.79% and Marshall mix sections $\beta_{r_1} = 3.449$, $\beta_{GB} = 1.207$ and $\beta_{SG} = 0.058$ with corresponding average layer contribution of 21.53%, 68.98% and 9.42% shows a great variation between these two mix type, which is expected because of difference in the performance behavior to rutting by the pavement materials. The superior performance of the Superpave section provides a long term protection to the underneath granular base/ sub-base layer which is relatively poor in Marshall mix type.

Despite of these large variation in calibration coefficient and layer contribution, all Superpave and Marshall sections are collectively recalibrated to see the possibility of use of a single model for these two materials. The total RSS was minimized at $\beta_{r_1} = 2.701$, $\beta_{GB} = 0.198$ and $\beta_{SG} = 0.215$, yielding corresponding average layer contribution of 23.76%, 18.02% and 58.21% and a standard error of 2.396 mm and a bias of 0.078 mm. The recalibration results are almost similar to the result of Superpave sections because of its large sample size in compare to Marshall mix sections. But on the other side, the standard error is increased.

Meanwhile, the cross-sectional calibration results obtained for Ontario's Superpave and Marshall mix pavement sections are also compared with the global calibration results in terms of the standard error as shown in Table 6.3. Although the cross-sectional calibration bear very poor correlation between the predicted and observed rutting, the resulting overall standard error is lower than that from the global calibration which indicates the improvement in the performance of the models. It is noted that all three models have a bias of almost zero and a standard error of lower than from global calibration, all these models can be used for Ontario's pavement design. However, the use of separate models for Superpave and Marshall mix sections are considered as efficient and precise model for Ontario's condition.

Table 6.3: Comparison of statistics of Global and Local calibration

Parameters	Global calibration		Cross-sectional calibration			Cross-sectional validation		
	NCHRP 2004	AASHTO 2008	Superpave	Marshall	Combined	Superpave	Marshall	Combined
Number of data points	387	334	53	19	72	31	10	41
Standard error (mm)	3.07	2.72	1.200	2.270	2.396	1.396	2.454	2.188
R ²	0.399	0.577	0.350	0.484	0.354	0.148	0.515	0.039

As the observed rut trend along the pavement age is different for different mix type including Superpave and Marshall type (refer to chapter 1.1), it is important to see whether cross-sectional calibration can capture this longitudinal trend of rutting or not. Thus, the model coefficients from cross-sectional calibration results are further used on typical selected Superpave and Marshall sections to predict the longitudinal rutting trend. The comparison of observed and predicted rutting is shown in the Figure 6.5 and 6.6. The two major conclusions are made from this study. One is that the cross-sectional calibration fails to capture the longitudinal trend of evolution of rutting and the bias increases with pavement age. The next is that the separate model coefficients clustering by pavement mix type are more precise than the combined model coefficients for estimate of the longitudinal trend. This issue can be addressed either by considering the weighted value of observed rut depth along the pavement age or/and by longitudinal calibration. In this research, longitudinal approach of model calibration is discussed in the later chapter.

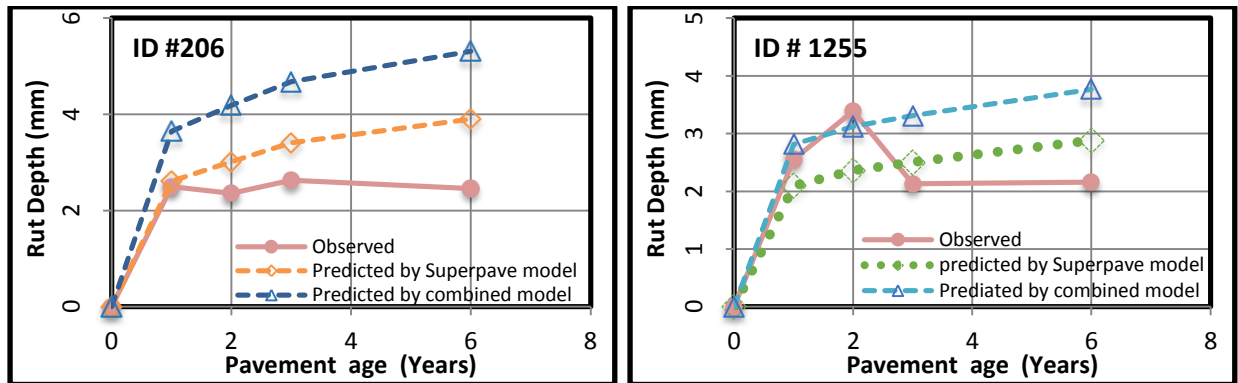


Figure 6.5: Comparison of longitudinal trend of rutting for Superpave pavements

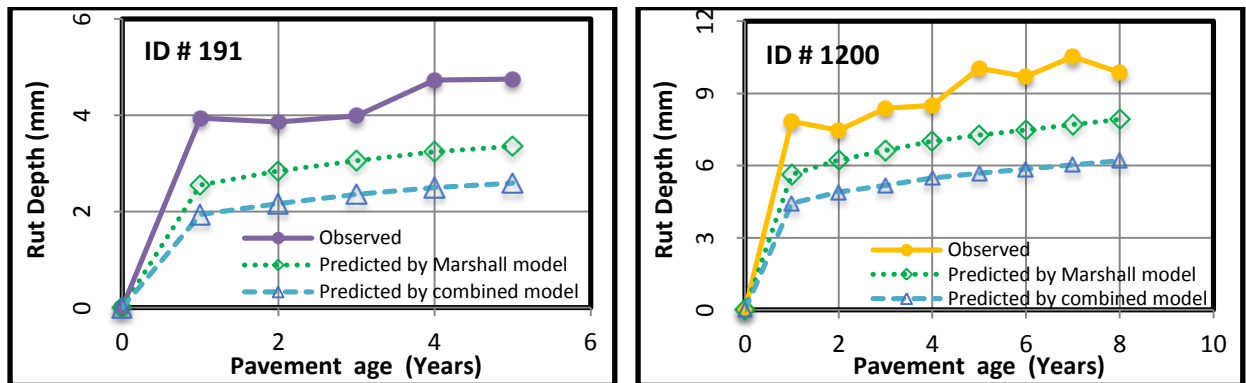


Figure 6.6: Comparison of longitudinal trend of rutting for Marshall mix pavements

6.2 Clustering Analysis

As discussed in section 6.1.3, the cluster analysis by pavement mix type may improve the performance of the model. Thus, the author of this research is interested for further cluster analysis in order to improve the standard error and goodness of fit. The cross-sectional calibration methodology was applied to Ontario's flexible pavements in different cluster groups to evaluate the prediction performance of the models in terms of standard error. All the sections used for cross-sectional calibration as in section 6.1.1 and section 6.1.2 are sub-grouped in the following criteria and analyzed to adjust the three permanent deformation models using preset value of local calibration parameters for temperature exponent (β_{r_2}) and traffic exponent (β_{r_3}).

1. Ontario zone
2. Highway functional class
3. Sub-grade modulus
4. Top layer material
5. Top layer performance grade

6.2.1 Cluster Analysis for Superpave Sections

As described above, the cross-sectional calibration methodology was used on fifty three Ontario's Superpave pavement sections in different cluster groups for recalibration by comparing the observed and predicted rut depth in the year 2012 for three rutting models. The summary of the results are presented in the Table 6.4, which shows that there is no significant improvement in the prediction performance of the rutting models in Ontario's Superpave highways. However, the layer contribution remains almost same as obtained in non-cluster calibration, with major contribution by sub-grade layer.

Table 6.4: Cluster analysis results for Superpave Sections

Cluster Groups		Local Calibration Parameters			Layer Contribution			Statistical Parameters			
		β_{r_1}	β_{GB}	β_{SG}	AC	Base	Sub-grade	R ²	N	Bias	S _e
Ontario zone	SO	2.671	0.000	0.182	30.82	0.00	69.18	0.29	33	0.048	1.214
	NO	2.365	0.100	0.155	27.46	16.11	56.43	0.46	20	0.245	1.211

Highway class	400	3.292	0.000	0.178	36.73	0.00	63.27	0.51	28	0.421	1.217
	Non 400	1.286	0.000	0.209	16.11	0.00	83.89	0.19	25	0.147	1.294
Sub-grade modulus	> 35	1.014	0.191	0.178	12.23	23.51	64.27	0.22	15	0.211	1.309
	= 35	1.013	0.118	0.214	11.13	13.21	75.66	0.49	17	0.005	1.113
	< 35	0.896	0.006	0.231	9.99	1.23	88.78	0.54	21	0.008	1.253
Top layer material	SP12.5	1.008	0.036	0.239	13.16	6.98	79.86	0.51	19	0.076	1.109
	SP12.5FC1	1.008	0.137	0.119	14.06	19.77	66.17	0.48	11	-0.01	0.643
	SP12.5FC2	1.445	0.000	0.261	13.73	0.00	86.27	0.34	23	0.064	1.234
Top layer Performance grade	58-28	1.447	0.079	0.144	20.85	13.21	65.93	0.24	13	0.119	0.905
	58-34	1.447	0.118	0.146	21.22	14.71	64.06	0.54	19	0.050	0.951
	64-28	1.451	0.144	0.283	19.24	13.49	67.28	0.67	13	-0.07	0.992
	64-34	3.192	0.383	0.090	17.14	10.90	71.96	0.21	8	0.151	1.191

6.2.2 Cluster Analysis for Marshall Mix Sections

As described above, the cross-sectional calibration methodology was used on 19 Ontario's Marshall mix pavement sections in different cluster groups for recalibration by comparing the observed and predicted rut depth in the year 2009 and 2010. The summary of the results are presented in the Table 6.5, which shows a significant improvement in the prediction performance of the rutting models in Ontario's highway. However, we observed a large variation on the layer contribution to the rutting specially by Ontario zone, but the base layer remains as the major contributor as obtained in non-cluster calibration.

Table 6.5: Cluster analysis results for Marshall mix Sections

Cluster Groups		Local Calibration Parameters			Layer Contribution			Statistical Parameters			
		β_{r1}	β_{GB}	β_{SG}	AC	Base	Sub-grade	R ²	N	Bias	S _e
Ontario zone	SO	3.727	1.405	0.000	23.30	76.70	0.00	0.70	14	0.32	1.88
	NO	3.514	0.499	0.140	25.47	44.75	29.78	0.23	5	0.41	1.59

Highway class	400	1.383	1.271	0.071	10.96	74.55	14.49	0.39	9	0.41	2.06
	Non 400	4.178	1.185	0.000	22.94	77.06	0.000	0.51	10	0.35	2.67
Subgrade Modulus	> 35	2.099	1.578	0.000	11.26	88.74	0.00	0.84	6	-0.09	1.89
	= 35	3.403	0.819	0.285	19.54	40.94	39.52	0.66	8	-0.02	1.82
	< 35	3.200	0.613	0.106	23.55	47.69	28.75	0.24	5	0.12	1.59
Top layer material	DFC	3.439	1.158	0.062	30.15	58.12	11.74	0.79	4	0.21	1.25
	HL1	3.997	1.213	0.000	22.30	77.70	0.00	0.30	12	0.47	2.69
	HL3	3.436	1.140	0.000	22.93	77.07	0.00	0.10	3	0.06	1.38

6.3 Concluding Remarks

A separate cluster, non-cluster and combined cross-calibration to both Superpave and Marshall mix sections give some concrete results about the performance efficiency of the model. One of the important finding is that it is unrealistic to use a single model for both materials for Ontario's condition. Secondly, cluster calibration based on top layer material and its performance grade improves the Superpave rutting models whereas the models for Marshall mix are improved by Ontario zone and sub-grade modulus. Thus, it establishes the need of more sophisticated cluster analysis. Further, the simple cross-sectional calibration is not sufficient to capture the longitudinal trend of rutting and the nature of the residual error consistently changes from a certain value of total rut depth. To address this issue, the model need to be recalibrated by considering the weighted on the observed rutting with the age of the pavement.

A summary of the cross-sectional results for Marshall mix sections by Waseem (2013) is presented in the Table 6.6 for the purpose of comparison with cluster and non-cluster calibration. A large variation in the calibration parameters is observed that is believed to cause due to specific issues (c.f. layer contribution to rutting, temperature and traffic exponent) involved in local calibration method which are still unknown to the Ontario's roads. Despite of this large variation, the model developed by non-cluster calibration has almost same precision as developed

by Waseem for Ontario condition. However, the models developed by cluster analysis in this research are more precise among all these models. Thus, this observation also confirms a need of more sophisticated cluster analysis in the local calibration practices.

The most optimal cluster analysis in the local calibration study are calibrating the individual pavement section having a relatively long series of rut records, thus the study is a section-by-section longitudinal calibration. The following chapter discuss the details of longitudinal calibration methodology.

Table 6.6: Comparison of cross-sectional calibration results for Marshall mix sections

		Local Calibration Parameters					% Layer Contribution			Statistical Parameters		
		β_{r1}	β_{r2}	β_{r3}	β_{GB}	β_{SG}	AC	Base	Sub-grade	R ²	N	S _e
This research		3.449	1.000	0.626	1.207	0.058	21.53	68.98	9.42	0.521	19	2.21
Waseem (2013)	Reconstructed	0.300	1.000	1.000	0.800	0.030	32.0	59.0	9.0	0.016	68	2.22
	Rehabilitated	0.900	1.230	0.770	0.985	0.000	50.0	50.0	0.0	0.339	150	1.76

CHAPTER 7 LONGITUDINAL CALIBRATION

7.1 Characterization of Rut Depth

Local calibration compares the predicted rut depth against the observed rut depth. In this study, the field observed rut depth data are retrieved from the MTO's database. The database consists of a series of ARAN rut depth data for each pavements measured by MTO staff. However, the magnitude of these data randomly fluctuate with high variability. On the other side, the quality of observed rut depth affects the overall accuracy of the design. Hence, the author realized the need of screening the pavement sections before selecting and integrating into the calibration database.

The observed rutting data for each pavement section included in the study were reviewed through visual inspections. Screening was done based on the quality of pavement performance and observed number of rutting data points as explained in section 5.3. Any zeros in the observed rut in between the pavement service life was removed and deemed to be no observation at that point. Measurements on rehabilitation year were carefully considered as either the first reading of the next cycle or the last reading of the ongoing cycle.

The observed rutting data were used in two ways during previous local calibration studies. Some researchers suggested to use smoothed observed rutting data to minimize the magnitude of residual error. In contrast, other researchers emphasized the use of unmodified observed rutting data to simplify the local calibration procedure from variance associated with smoothed data. A study conducted by Waseem (2013) also found smaller RSS value for smoothed rut data as compared to the original rut data. However, his study found no effect in final selection of local calibration parameters. Considering that the smoothing of the observed rutting data would distort the estimation of the standard error in the local calibration, this study used the original observed rut data for the calibration purpose.

The predicted rut data are estimated using rutting models within the AASHTOWare pavement design software version 2.1. This requires the detailed input and level of accuracy of selected road sections as described in chapter 5.

7.2 Results for Superpave Sections

7.2.1 Calibration Results

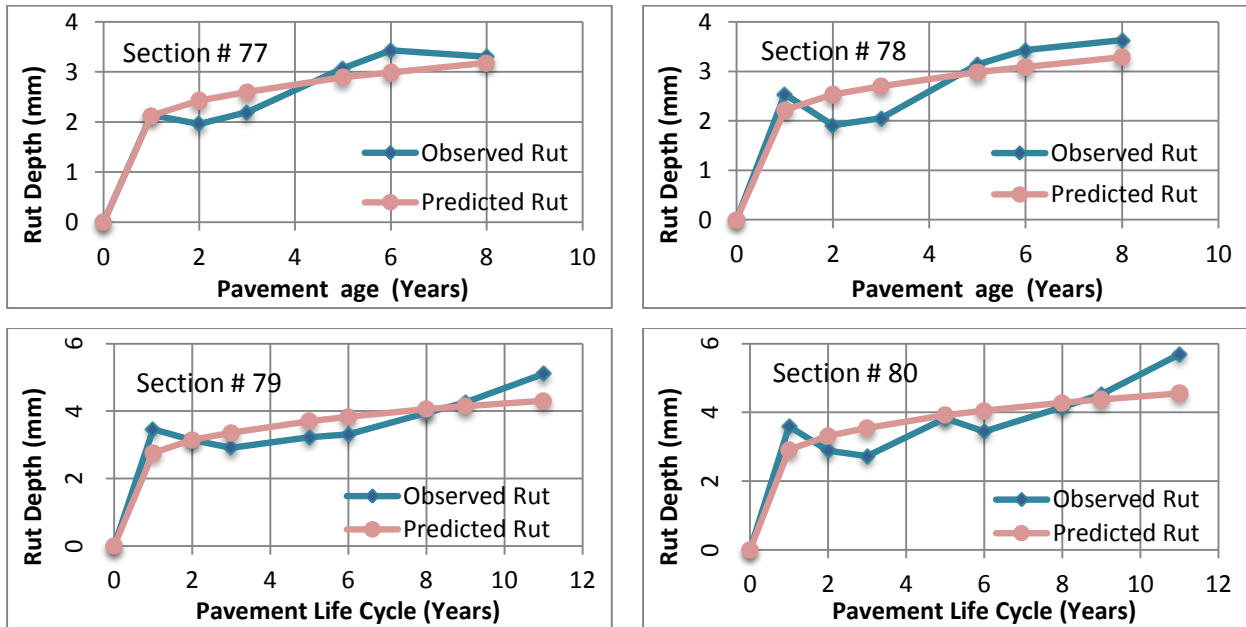
The section-by-section, longitudinal local calibration methodology as described in Chapter 4 was employed for the 33 flexible pavement sections to calibrate the five local calibration parameters in the three rutting models. As discussed in Chapters 3 and 4, a preset value of 1.0 and 0.6262 were used for the temperature exponent (β_{r_2}) and traffic exponent (β_{r_3}), respectively. The RSS minimization process is followed to obtain the other three parameters. The obtained optimum values of β_{r_1} , β_{GB} and β_{SG} for the 33 sections are listed together with the corresponding RSS, bias and percentage of layer contribution in Table 7.1.

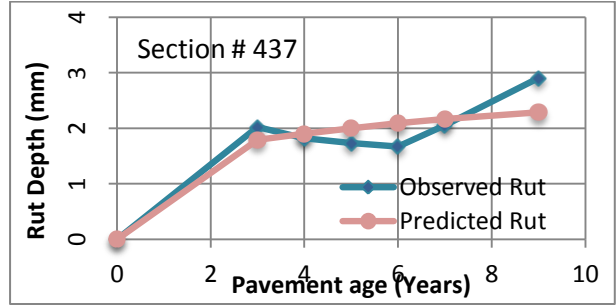
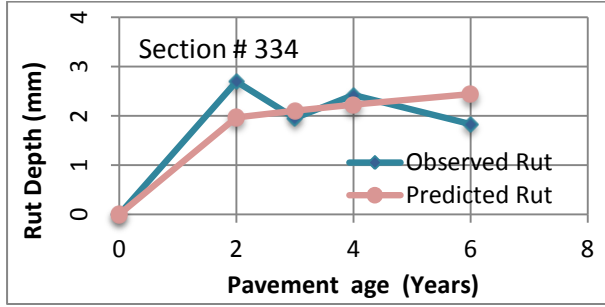
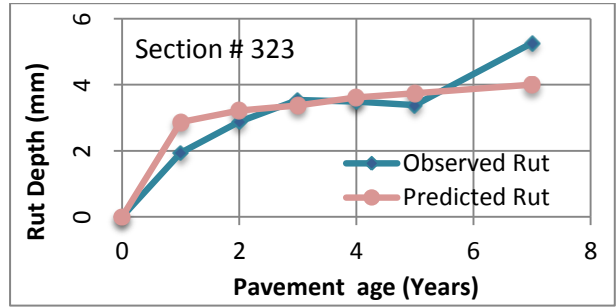
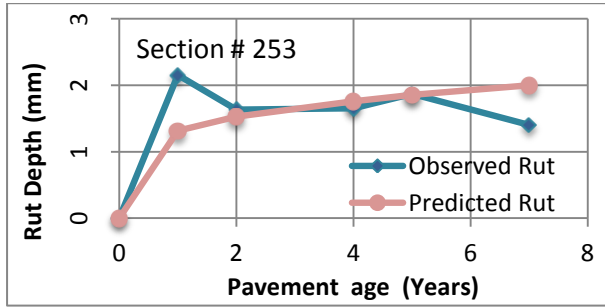
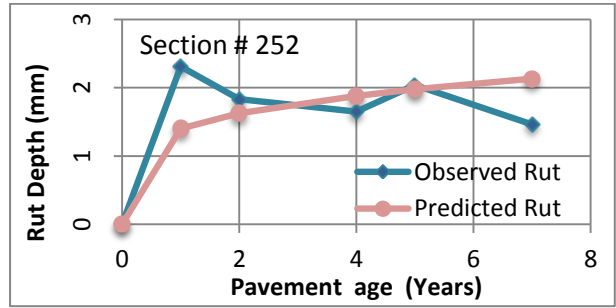
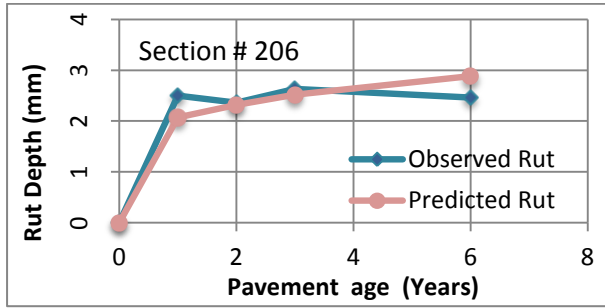
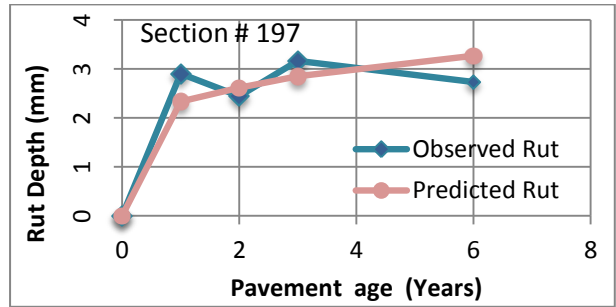
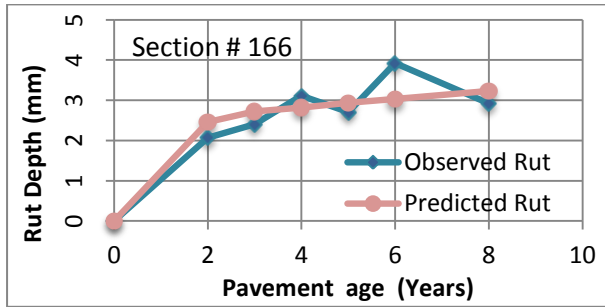
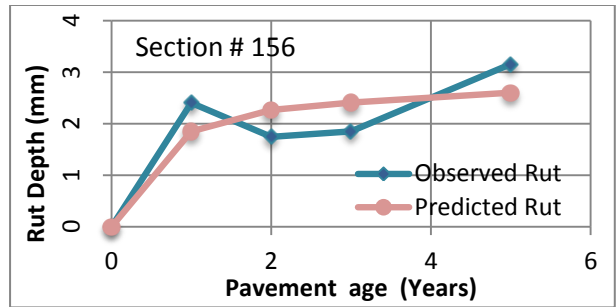
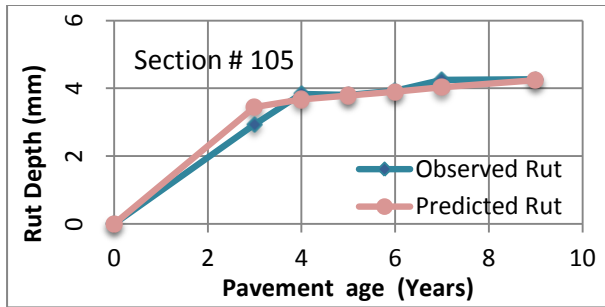
*Table 7.1: Longitudinal calibration results for the Superpave sections
(with $\beta_{r_2} = 1.0$ and $\beta_{r_3} = 0.6262$)*

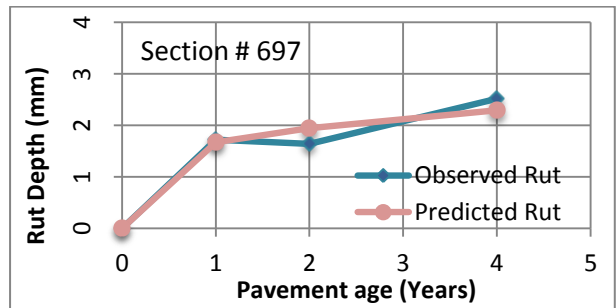
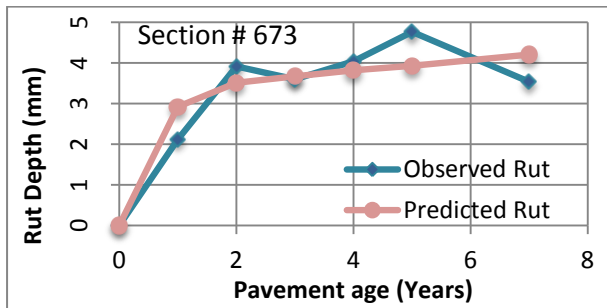
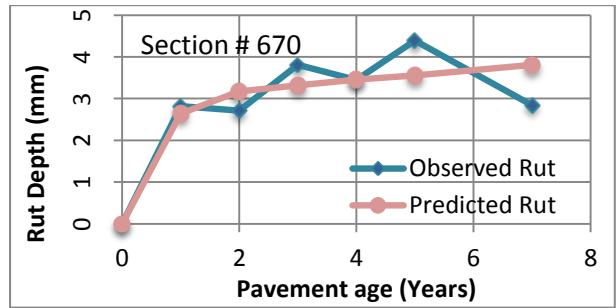
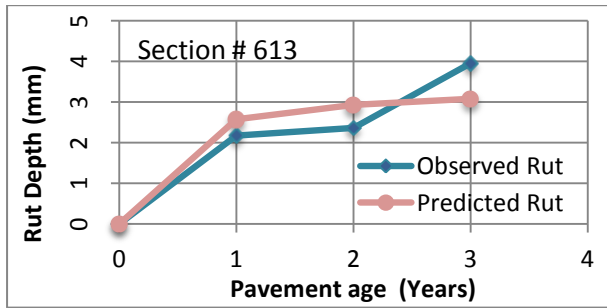
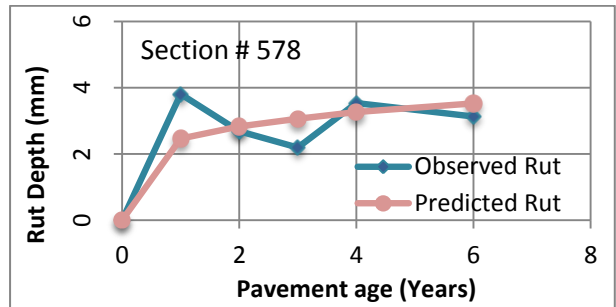
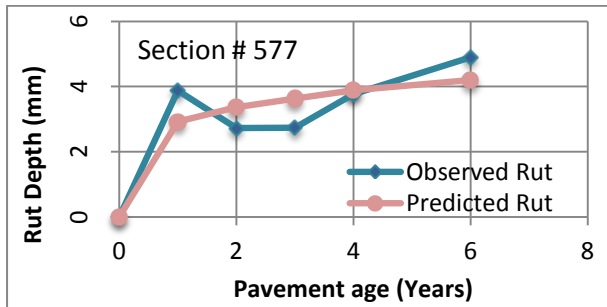
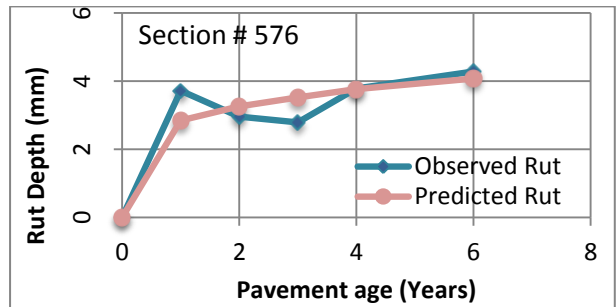
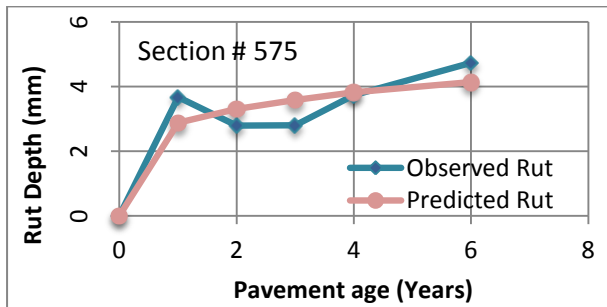
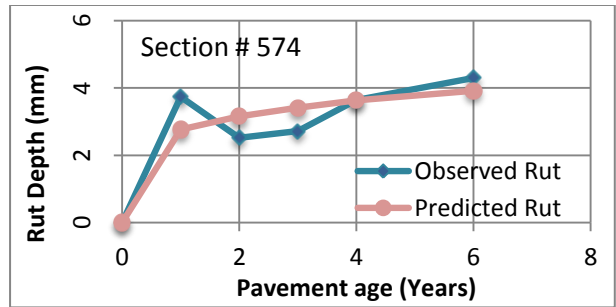
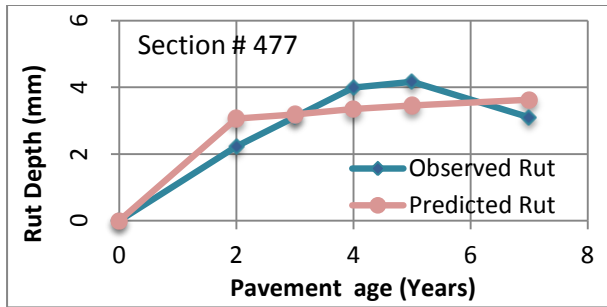
No.	Section ID	Calibration Parameters			Total Bias	Total RSS	Average Layer Contribution (%) After Calibration		
		β_{r_1}	β_{GB}	β_{SG}			AC	Granular	Sub-grade
1	77	4.100	0.402	0.085	-0.106	0.555	38.84	35.38	25.78
2	78	4.051	0.391	0.078	-0.082	1.078	40.98	34.86	24.16
3	79	4.270	1.549	0.085	0.041	1.843	24.64	49.51	25.85
4	80	4.300	1.401	0.125	-0.107	3.005	23.01	41.46	35.53
5	105	3.375	0.510	0.075	-0.048	0.323	29.08	50.20	20.72
6	156	1.987	0.452	0.021	0.016	1.174	32.32	53.29	14.39
7	166	3.283	0.644	0.052	-0.068	1.261	37.17	38.38	24.45
8	197	2.200	0.416	0.019	0.171	0.716	29.57	62.01	8.42
9	206	1.900	0.383	0.013	0.152	0.367	28.87	64.54	6.60
10	252	1.856	0.337	0.031	0.268	1.308	24.92	58.24	16.83
11	253	1.801	0.314	0.027	0.235	1.023	26.48	57.71	15.81
12	323	2.547	0.322	0.049	-0.313	2.713	28.76	60.15	11.10
13	334	1.940	0.484	0.017	0.152	0.941	18.43	74.02	7.55
14	437	2.217	0.264	0.033	-0.036	0.698	30.05	54.96	14.99
15	477	4.109	1.211	0.137	-0.081	1.839	15.24	60.42	24.34
16	574	2.001	0.189	0.081	0.031	1.932	30.48	41.00	28.52
17	575	2.600	0.185	0.074	0.004	1.822	37.97	37.73	24.30
18	576	2.661	0.194	0.061	0.065	1.410	39.49	40.17	20.34
19	577	2.830	0.201	0.063	0.009	2.565	39.73	39.99	20.29
20	578	2.860	0.193	0.069	0.198	2.762	35.62	40.54	23.84

21	613	3.468	0.411	0.121	-0.100	1.195	22.17	32.17	45.66
22	670	2.600	0.715	0.090	0.067	2.102	22.56	54.94	22.50
23	673	2.803	0.812	0.095	-0.083	2.038	22.04	56.43	21.54
24	697	2.581	0.368	0.038	-0.028	0.144	43.58	41.47	14.95
25	698	2.813	0.258	0.050	-0.073	0.192	39.54	49.67	10.79
26	719	2.150	0.961	0.037	0.055	0.513	19.25	69.31	11.44
27	835	2.057	0.325	0.041	-0.127	1.649	20.47	57.51	22.02
28	951	2.895	0.507	0.062	-0.083	0.726	28.45	52.29	19.27
29	952	3.101	0.682	0.088	-0.123	0.610	25.20	55.68	19.12
30	1240	2.002	0.543	0.102	0.201	2.210	22.76	47.06	30.18
31	1255	1.910	0.526	0.063	0.164	1.831	25.26	53.02	21.72
32	1297	2.303	2.137	0.047	0.063	0.737	18.57	71.48	9.95
33	1301	2.100	1.657	0.042	0.100	1.432	20.87	68.31	10.82

The calibration results from section-by-section longitudinal calibration methodology are further used on each pavement to compare the predicted rut depth against its measured value along the service life of the pavement. These longitudinal plots for all the calibrated sections are presented here in Figure 7.1.







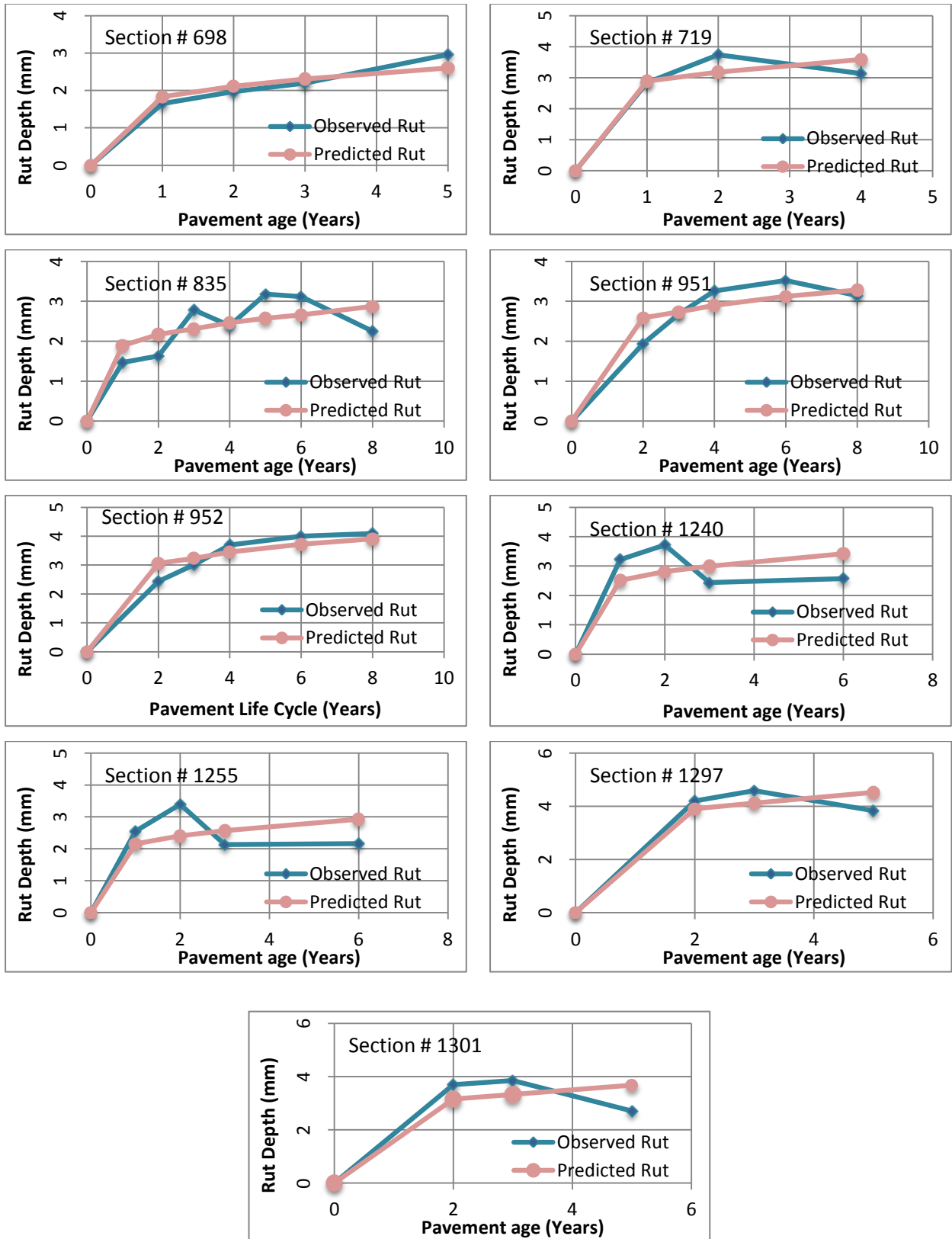


Figure 7.1: Longitudinal plots for predicted and observed rut

7.2.2 Discussions

The optimized calibration parameters are consistently varying from one section to the other; in specific, the AC scaling parameter (β_{r_1}) varies from 1.801 to 4.300, the granular base parameter (β_{GB}) from 0.185 to 2.137 and the fine soil parameters (β_{SG}) varied from 0.013 to 0.137. The layer contribution by AC layer, granular base layer and fine soil layer after calibration also seems to be consistent with small variation resulting an average value of about 28.56%, 51.63% and 19.81% respectively.

However, the fine soil scaling parameters (β_{SG}) of section 80, 477 and 613 is relatively in higher range whereas this value goes to the lower range for sections 197, 206 and 334 in compare to other sections. The reason for such a variation in the value of fine soil scaling parameters (β_{SG}) is indistinct and need further study. Similarly, granular base scaling parameters (β_{GB}) for sections 1297 and 1301 are 2.137 and 1.657 respectively representing high value as compared to other sections. This higher end values for these sections are due to a layer of 100 mm cement treated OGD (Open graded drainage layer), which provides a long term protection to the underneath granular layer. Also, this value is 1.549 and 1.401 to the sections 78 and 79 respectively because of the presence of 150 mm old asphalt layer. The section 477 also has a higher end value of 1.211 as a result 75 mm asphalt stabilized CIR (cold in-place recycling) material. On the other side, due to the influence of thin AC layer, sections 574, 575, 576, 577 and 578 has the lowest values for granular base scaling parameters (β_{GB}) ranging in between 0.185 to 0.201 as shown in Table 7.1.

Further, these sections are grouped together by projects. Despite of large variation in the calibration coefficients from one section to another, the calibration coefficients of the sections within a project are almost similar.

Meanwhile, the observed total pavement rutting is plotted against the corresponding predicted values as shown in Figure 7.2 which showed a good correlation (0.804) between them with a standard error of 0.524 mm. The local calibration results small RSS for all the sections except sections 80, 323, 577, 578 and 1240. This large RSS is contributed due to a large fluctuation of observed rut depth in between the service life of the pavement sections.

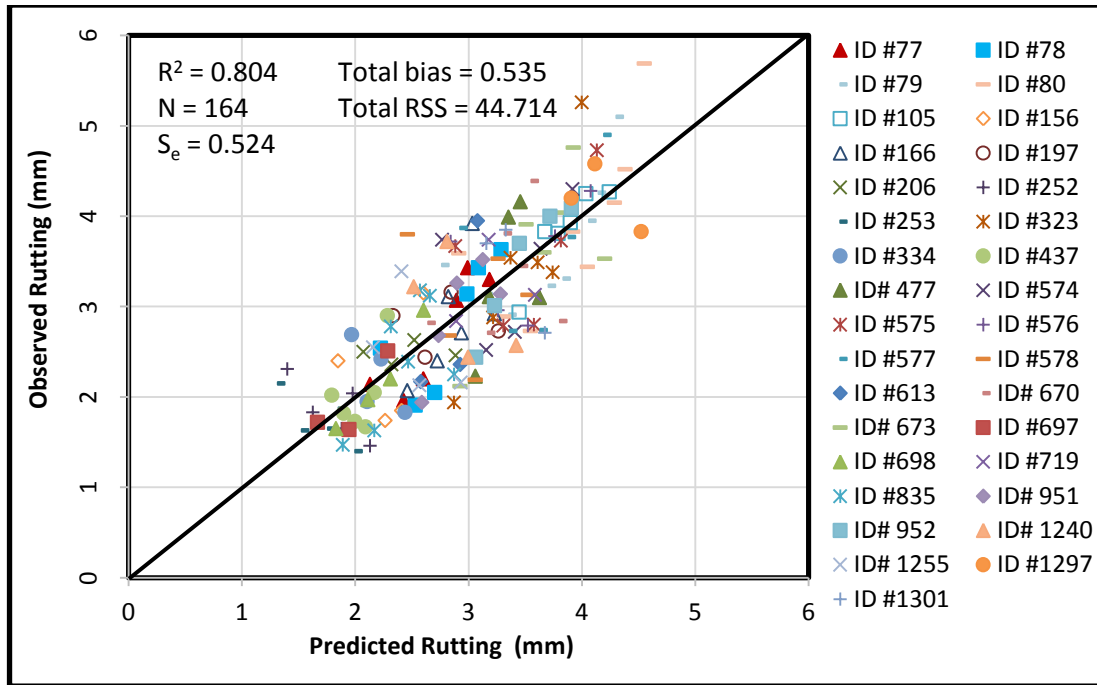


Figure 7.2: Predicted versus observed plots (with $\beta_{r_2} = 1.0$ and $\beta_{r_3} = 0.6262$)

Next, the optimum average values for the three calibration parameters of all 33 sections are 2.717, 0.604 and 0.063. The reason for variation in local calibration parameters is not clear and need further intensive study. However, the changes are project specific and governed by pavement material properties and structure. The use of an average values of these three calibration parameters results a standard error of 1.761 which is as good as to the result from the global calibration. However, it shows a very poor correlation ($R^2 = 0.122$) with a bias of -0.613 . Hence, these average values will be appropriate as level 3 input for Ontario.

7.2.3 Validation

Ontario's thirty three Superpave pavement sections were calibrated by section-by-section longitudinal local calibrations methodology with a preset value of 1.000 and 0.6262 for local calibration parameters of temperature exponent (β_{r_2}) and traffic exponent (β_{r_3}) respectively and the results was presented in Table 7.1. The calibration process utilized the field observed rut depth data from MTO's database that consist of a series of rut depth data for each pavements by the end of year 2012. But after calibration, MTO staff provide the rut depth data for the year 2013 and 2014. Hence, the author decided to apply the most recent data of all 33 sections for validation purposes during this study.

Sections having no observation in the year 2013 or/and 2014 are carefully removed from the analysis. Thus, sections 156, 613 and 835 are removed from validation process because of lack of rut data in the database. Finally, the calibration results presented in Table 7.1 are utilized on all 30 sections to compare the predicted rut depth against its measured value during the year 2013 and 2014. Meanwhile, a plot between the observed total pavement rutting and the corresponding predicted values (refer to Figure 7.3) bears relatively low correlation (0.731) between them with a standard error of 0.958 mm, the resulting overall standard error is actually as good as to the result from the global calibration, as shown in Table 7.8.

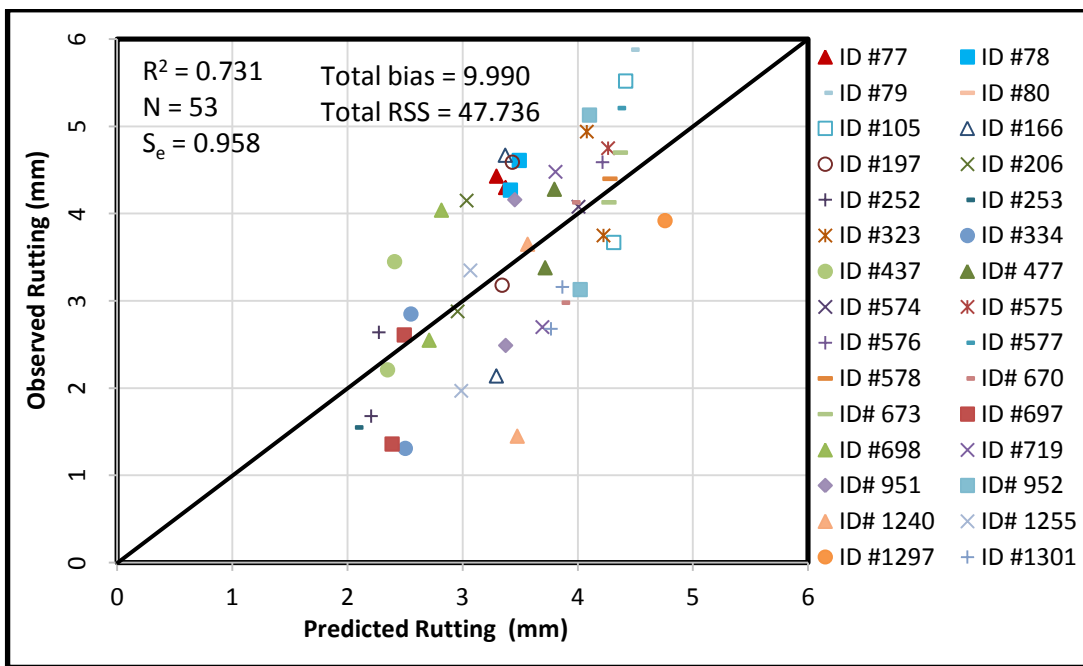


Figure 7.3: Predicted versus observed plots for validation (with $\beta_{r_2} = 1.0$ and $\beta_{r_3} = 0.6262$)

7.3 Sensitivity Analysis for Local Calibration Results

The preceding longitudinal local calibration was performed on the premise that $m = 0.30$ or $\beta_{r_3} = 0.6262$. For prudence, a set of sensitivity analyses were also carried out to test the robustness of the local calibration results at different values of m or β_{r_3} . For all of the following analyses, the temperature exponent is kept to be 1.0, with reasons already explained in Chapter 3.

7.3.1 Local Calibration Parameters for $m=0.25$

At $m = 0.25$ or $\beta_{r_3} = 0.5218$, the optimum values of β_{r_1} , β_{GB} and β_{SG} through the RSS minimization process are presented in Table 7.2 with the corresponding RSS, bias and percentage of layer contribution. The observed total pavement rutting is plotted against the corresponding predicted values as shown in Figure 7.4 which showed a good correlation (0.798) between them with a standard error of 0.531 mm. The average values of the three optimum calibration parameters of the 33 sections are 2.853, 0.661 and 0.076, respectively.

*Table 7.2: Longitudinal calibration results for the Superpave section
(with $\beta_{r_2} = 1.0$ and $\beta_{r_3} = 0.5218$)*

No.	Section ID	Calibration Parameters			Total Bias	Total RSS	Average Layer Contribution (%) After Calibration		
		β_{r_1}	β_{GB}	β_{SG}			AC	Granular	Sub-grade
1	77	4.250	0.499	0.101	-0.146	0.697	23.63	44.87	31.50
2	78	4.200	0.433	0.112	-0.124	1.222	24.65	39.61	35.74
3	79	4.300	1.703	0.099	-0.010	1.901	14.16	55.27	30.56
4	80	4.350	1.603	0.135	-0.164	3.180	13.08	48.18	38.74
5	105	3.474	0.597	0.085	-0.061	0.389	16.45	59.77	23.78
6	156	2.296	0.473	0.031	0.004	1.166	21.19	56.67	22.14
7	166	3.383	0.775	0.065	-0.085	1.336	21.67	47.17	31.16
8	197	2.285	0.423	0.042	0.156	0.639	16.82	64.06	19.12
9	206	2.205	0.388	0.029	0.139	0.312	18.33	66.35	15.32
10	252	2.005	0.359	0.037	0.258	1.224	16.58	62.75	20.67
11	253	1.850	0.335	0.036	0.225	0.950	16.79	62.39	20.82
12	323	2.747	0.376	0.060	-0.373	2.961	16.37	62.58	21.05
13	334	2.100	0.513	0.020	0.148	0.910	12.33	78.92	8.74
14	437	2.316	0.298	0.040	-0.046	0.725	18.50	62.83	18.67
15	477	4.009	1.405	0.115	-0.089	1.855	8.46	70.79	20.75
16	574	2.115	0.245	0.076	0.011	1.937	17.95	54.42	27.63
17	575	2.318	0.233	0.094	-0.027	1.887	18.99	49.02	31.99
18	576	2.460	0.253	0.074	0.033	1.353	20.53	53.98	25.49
19	577	2.800	0.257	0.077	-0.022	2.620	22.15	52.41	25.44
20	578	2.560	0.257	0.078	0.223	3.596	18.52	54.29	27.19
21	613	3.500	0.515	0.122	-0.104	1.250	12.97	40.59	46.44
22	670	2.795	0.763	0.105	0.046	2.027	13.79	59.48	26.73

23	673	3.200	0.903	0.096	-0.104	2.107	14.30	63.64	22.07
24	697	2.782	0.401	0.062	-0.038	0.169	29.06	46.13	24.80
25	698	2.952	0.277	0.089	-0.088	0.260	25.94	54.38	19.68
26	719	2.841	0.964	0.050	0.049	0.490	14.65	69.99	15.36
27	835	2.374	0.347	0.045	-0.145	1.669	13.72	62.05	24.23
28	951	2.595	0.573	0.079	-0.093	0.762	15.41	59.73	24.85
29	952	3.001	0.787	0.093	-0.133	0.681	14.77	64.77	20.46
30	1240	1.911	0.533	0.137	0.188	2.022	11.57	47.07	41.36
31	1255	2.091	0.515	0.092	0.153	1.700	14.73	52.84	32.43
32	1297	3.154	2.140	0.067	0.063	0.684	13.81	72.01	14.18
33	1301	2.917	1.659	0.059	0.098	1.364	15.75	68.85	15.40

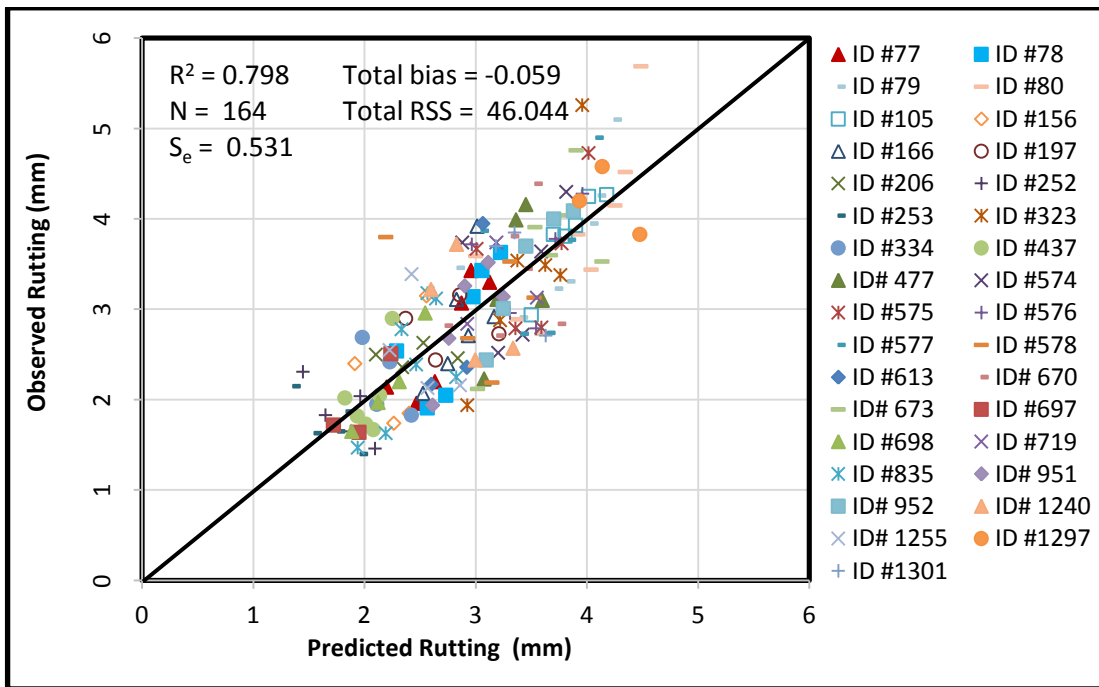


Figure 7.4: Predicted versus observed plots (with $\beta_{r_2} = 1.0$ and $\beta_{r_3} = 0.5218$)

7.3.2 Local Calibration Parameters for $m=0.479$

Similarly, At $m = 0.479$ or $\beta_{r_3} = 1.0$, the optimum values of β_{r_1} , β_{GB} and β_{SG} through the RSS minimization process are presented in Table 7.3. The observed total pavement rutting is plotted against the corresponding predicted values as shown in Figure 7.5 which showed a good correlation (0.798) between them with a standard error of 0.542 mm. The average values of the three optimum calibration parameters of the 33 sections are 0.522, 0.485 and 0.054, respectively.

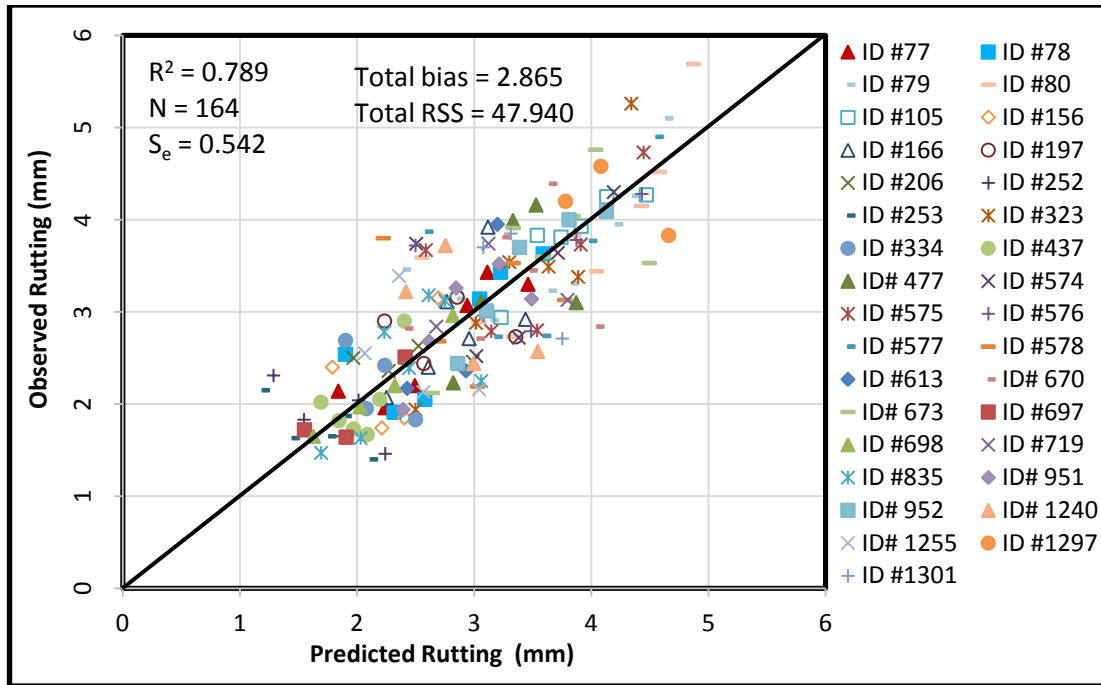


Figure 7.5: Predicted versus observed plots (with $\beta_{r_2} = 1.0$ and $\beta_{r_3} = 1.0$)

Table 7.3: Longitudinal calibration results for the Superpave section (with $\beta_{r_2} = 1.0$ and $\beta_{r_3} = 1.0$)

No.	Section ID	Calibration Parameters			Total Bias	Total RSS	Average Layer Contribution (%) After Calibration		
		β_{r_1}	β_{GB}	β_{SG}			AC	Granular	Sub-grade
1	77	0.673	0.354	0.066	0.010	0.397	52.41	28.96	18.63
2	78	0.627	0.343	0.062	0.038	0.904	53.57	28.47	17.96
3	79	0.864	1.197	0.069	0.271	1.996	44.86	35.58	19.56
4	80	0.869	1.098	0.104	0.116	2.581	42.03	30.38	27.58
5	105	0.563	0.364	0.069	-0.001	0.227	48.01	34.05	17.95
6	156	0.233	0.301	0.046	0.039	1.112	34.55	34.22	31.23
7	166	0.524	0.549	0.034	-0.015	1.166	53.99	30.78	15.24
8	197	0.199	0.390	0.035	0.212	0.943	28.14	56.39	15.47
9	206	0.198	0.352	0.023	0.196	0.580	31.46	57.13	11.41
10	252	0.471	0.248	0.033	0.322	1.788	42.30	40.45	17.25
11	253	0.468	0.237	0.025	0.290	1.474	45.78	40.86	13.36
12	323	0.436	0.236	0.047	-0.193	1.511	49.08	35.86	15.07
13	334	0.403	0.338	0.057	0.170	1.119	25.61	50.34	24.04
14	437	0.452	0.197	0.029	-0.007	0.607	48.44	38.89	12.66

15	477	1.478	0.782	0.104	-0.026	1.781	45.96	36.65	17.38
16	574	0.338	0.178	0.045	0.106	2.225	49.42	35.80	14.78
17	575	0.383	0.159	0.053	0.087	1.955	53.63	30.11	16.26
18	576	0.411	0.169	0.032	0.156	2.019	58.12	32.05	9.83
19	577	0.425	0.174	0.038	0.101	2.740	56.91	31.93	11.17
20	578	0.509	0.179	0.047	0.269	3.643	49.56	35.19	15.26
21	613	0.759	0.511	0.059	-0.078	0.957	39.65	38.67	21.68
22	670	0.518	0.605	0.067	0.149	2.591	40.68	43.66	15.66
23	673	0.611	0.636	0.074	0.017	2.099	43.11	41.27	15.62
24	697	0.433	0.263	0.057	-0.001	0.109	50.69	28.15	21.17
25	698	0.647	0.159	0.064	-0.015	0.039	59.02	28.30	12.68
26	719	0.607	0.705	0.021	0.112	0.854	46.17	47.83	6.00
27	835	0.538	0.207	0.045	-0.012	1.629	43.30	34.21	22.49
28	951	0.699	0.421	0.033	-0.022	0.598	49.56	40.89	9.55
29	952	0.762	0.523	0.071	-0.056	0.320	44.95	40.40	14.65
30	1240	0.246	0.490	0.095	0.237	2.832	32.79	40.52	26.69
31	1255	0.216	0.444	0.072	0.194	2.267	33.59	42.71	23.70
32	1297	0.381	1.701	0.055	0.086	1.114	33.90	54.95	11.15
33	1301	0.272	1.485	0.041	0.113	1.762	30.04	59.59	10.38

7.3.3 Discussions

The summary statistics of the three scenarios are summarized in Table 7.4. It is clear that in terms of R^2 and standard error, the case of $m = 0.3$, or $\beta_{r3} = 0.6262$ is the best, although the improvement from the other two scenarios are limited. However, there is significantly greater bias for the case of the default β_{r3} .

Table 7.4: Comparison of statistical analysis with different value of traffic exponent

Parameters	m = 0.25	m = 0.30	m = 0.479
Number of data points	164	164	164
Standard error (mm)	0.531	0.524	0.542
R^2	0.798	0.804	0.798
Average bias	0.000	0.003	0.017
Total RSS	46.044	44.714	47.940

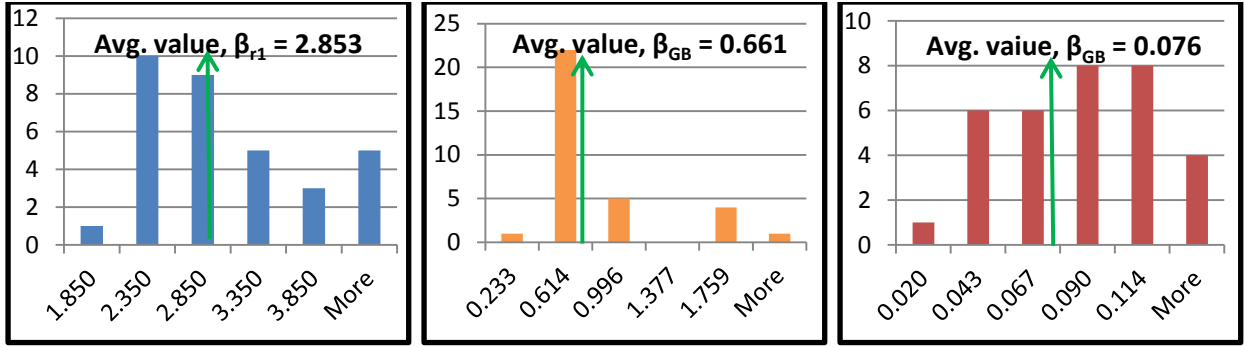


Figure 7.6: Histograms of local calibration coefficients for $m = 0.25$ (or $\beta_{r3} = 0.5218$)

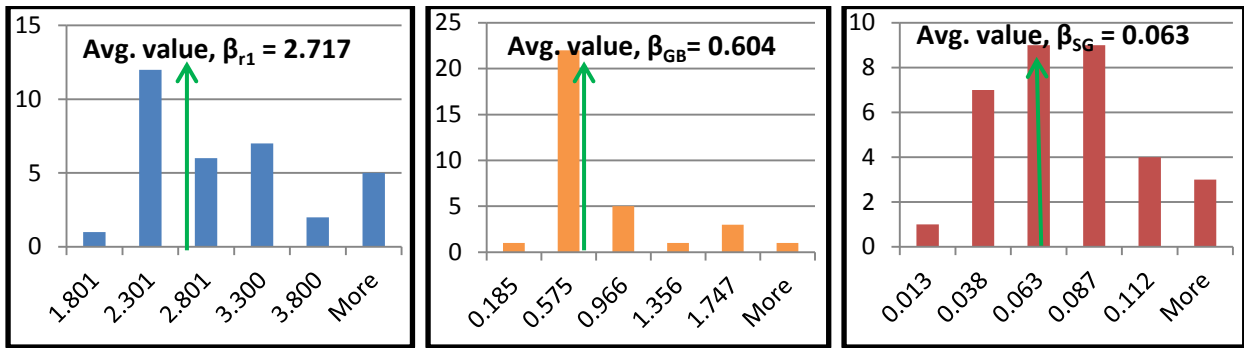


Figure 7.7: Histograms of local calibration coefficients for $m = 0.30$ (or $\beta_{r3} = 0.6262$)

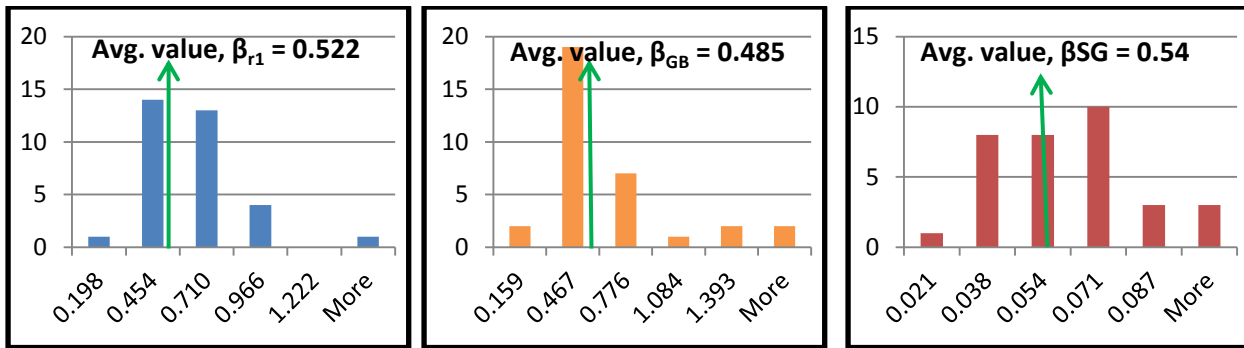


Figure 7.8: Histograms of local calibration coefficients for $m = 0.479$ (or $\beta_{r3} = 1.0$)

The histogram for the local calibration coefficients for all three scenarios are presented in the Figure 7.6, 7.7 and 7.8. It is clear that the value of local calibration coefficient for AC layer, base layer and sub-grade layer decreases with increase in traffic exponent value (refer to Figure 7.9). However, the average layer contribution of AC layer increases with the increase in the traffic exponent value, but the contribution decreases for base and sub-grade layer (refer to Figure 7.10).

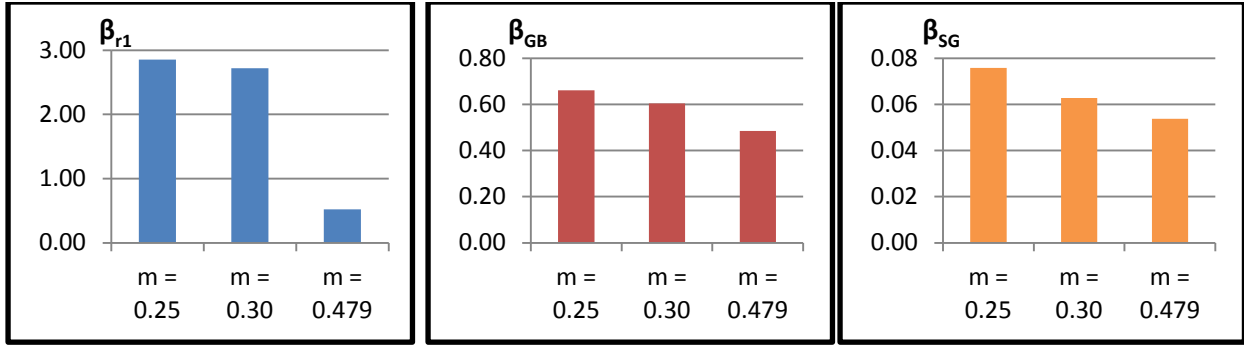


Figure 7.9: Histogram for average calibration coefficients

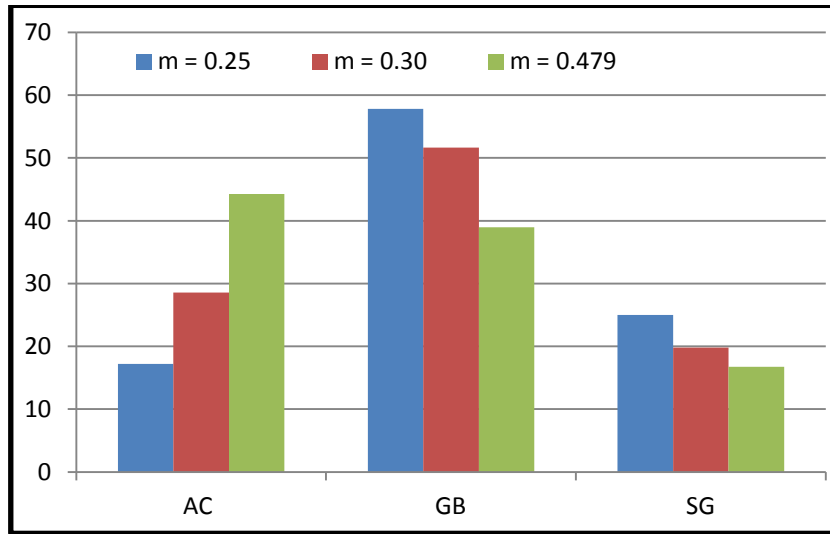


Figure 7.10: Variation of layer contribution with section specific calibration coefficients

7.4 Results of Marshall Mix Sections

Similar longitudinal calibration is done to the 29 Marshall mix sections selected by Waseem (2013). Waseem (2013) already did a longitudinal calibration. But his methodology was slightly different than this. In this study, the traffic and temperature exponents are pre-fixed, as explained earlier, whereas in Waseem's study all of the five parameters are determined under a pre-assumed layer contribution distribution. A set of sensitivity analysis was also carried out to test the robustness of the local calibration results at different values of m or β_{r3} . For all of the following analyses, the temperature exponent is kept to be 1.0, with reasons already explained in Chapter 3.

7.4.1 Local Calibration Parameters for m=0.30

At $m = 0.30$ or $\beta_{r_3} = 0.6262$, the optimum values of β_{r_1} , β_{GB} and β_{SG} through the RSS minimization process are presented in Table 7.5 with the corresponding RSS, bias and percentage of layer contribution. The observed total pavement rutting is plotted against the corresponding predicted values as shown in Figure 7.11 which showed a good correlation (0.975) between them with a standard error of 0.436 mm.

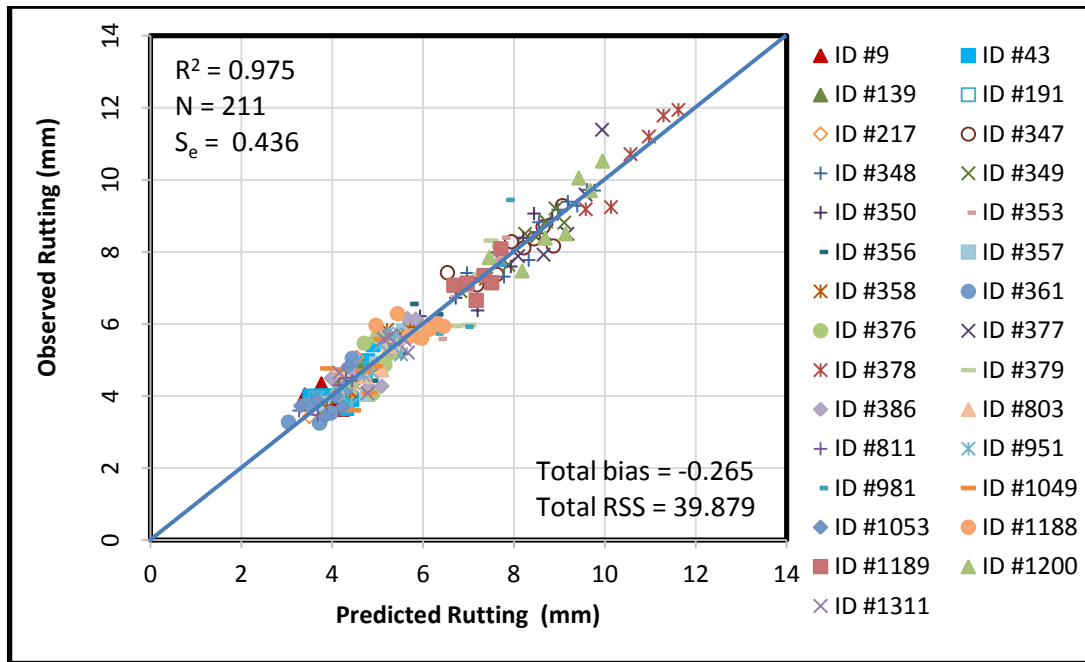


Figure 7.11: Predicted versus observed plots for marshal mix sections with $m = 0.30$ (or $\beta_{r_3} = 0.6262$)

Table 7.5: Longitudinal calibration results for the Marshall mix section (with $\beta_{r_2} = 1.0$ and $\beta_{r_3} = 0.6262$)

S. No.	Section ID	Rutting Model			Total Bias	Total RSS	Average Layer Contribution (%) After Calibration		
		β_{r_1}	β_{GB}	β_{SG}			AC	Granular	Sub-grade
1	9	1.567	2.497	0.060	-0.002	1.334	13.27	75.41	11.32
2	43	2.709	2.570	0.061	0.034	1.330	25.39	64.94	9.67
3	139	1.429	1.227	0.075	0.009	0.825	7.39	79.27	13.34
4	191	2.019	1.899	0.096	0.025	0.250	7.73	75.74	16.53
5	217	1.492	1.213	0.090	-0.012	0.696	10.83	73.80	15.37
6	347	1.518	1.842	0.066	0.210	1.534	7.10	86.05	6.86

7	348	1.811	1.723	0.062	0.004	0.909	8.86	84.30	6.84
8	349	1.828	1.791	0.116	-0.005	0.340	8.41	78.94	12.65
9	350	4.221	0.373	0.621	-0.010	1.522	18.04	16.28	65.68
10	353	3.345	0.390	0.639	-0.290	1.352	15.43	18.14	66.44
11	356	2.747	0.249	0.409	-0.020	1.007	17.96	17.00	65.04
12	357	4.001	0.523	0.349	-0.135	0.806	22.84	25.81	51.35
13	358	4.108	0.267	0.378	-0.125	0.659	24.98	22.11	52.91
14	361	4.002	0.031	0.382	0.010	0.950	29.09	3.25	67.67
15	376	1.607	0.502	0.056	0.036	1.757	9.82	70.76	19.42
16	377	5.001	0.066	0.748	-0.161	1.138	20.67	3.71	75.62
17	378	5.006	0.022	0.899	-0.126	1.378	18.69	1.11	80.20
18	379	3.933	0.469	0.598	-0.013	2.797	19.68	19.56	60.76
19	386	3.899	0.559	0.262	-0.002	1.590	21.02	35.85	43.13
20	803	1.201	1.005	0.089	0.054	0.408	8.87	70.19	20.94
21	811	3.896	2.996	0.006	0.010	0.370	30.97	67.01	2.02
22	951	3.999	0.618	0.206	-0.035	1.249	27.97	42.40	29.63
23	981	4.027	0.155	0.510	-0.163	4.061	18.36	11.23	70.42
24	1049	1.601	0.834	0.145	0.102	2.557	16.31	51.81	31.88
25	1053	2.022	0.603	0.048	0.048	0.903	19.92	54.37	25.72
26	1188	0.990	1.182	0.128	0.274	2.284	7.09	62.88	30.03
27	1189	0.962	1.690	0.026	0.016	0.722	7.32	86.68	6.00
28	1200	2.997	1.879	0.051	-0.073	1.868	17.44	73.72	8.84
29	1311	1.026	0.883	0.006	0.078	1.282	6.57	91.38	2.05

Next, the average values of the three optimum calibration parameters of the 29 sections are 2.723, 1.036 and 0.248, respectively. The reason for variation in local calibration parameters is not clear and need further intensive study. However, using an average values of these three calibration parameters results a standard error of 2.392 mm, an average bias of -0.993 and $R^2 = 0.732$ which is as good as to the result from the global calibration. Hence, these average values will be appropriate as level 3 input for Ontario.

7.4.2 Local Calibration Parameters for $m=0.479$

Similarly, At $m = 0.479$ or $\beta_{r3} = 1.0$, the optimum values of β_{r1} , β_{GB} and β_{SG} through the RSS minimization process are presented in Table 7.6. The observed total pavement rutting is plotted against the corresponding predicted values as shown in Figure 7.12 which showed a good

correlation (0.970) between them with a standard error of 0.437 mm. The average values of the three optimum calibration parameters of the 29 sections are 0.259, 1.458 and 0.060, respectively.

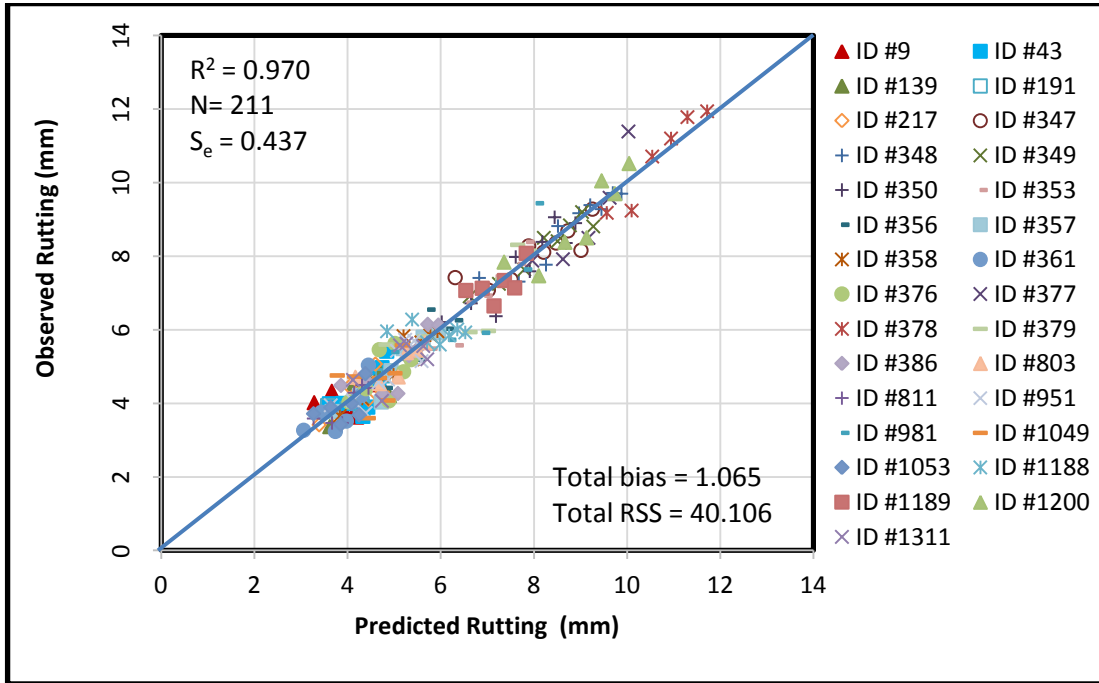


Figure 7.12: Predicted versus observed plots for marshal mix sections with $m = 0.479$ (or $\beta_{r3} = 1.0$)

Table 7.6: Longitudinal calibration results for the Marshall mix sections (with $\beta_{r2} = 1.0$ and $\beta_{r3} = 1.0$)

S. No.	Section ID	Rutting Model			Total Bias	Total RSS	Average Layer Contribution (%) After Calibration		
		β_{r1}	β_{GB}	β_{SG}			AC	Granular	Sub-grade
1	9	0.157	2.600	0.029	0.226	1.528	17.25	77.24	5.51
2	43	0.065	2.903	0.137	-0.007	1.332	8.57	74.36	17.07
3	139	0.275	1.174	0.061	0.038	0.902	14.76	74.50	10.74
4	191	0.283	1.990	0.059	0.045	0.273	11.58	78.44	9.98
5	217	0.184	1.271	0.046	0.030	0.726	16.60	75.78	7.62
6	347	0.238	1.78	0.045	0.332	2.158	13.92	81.49	4.59
7	348	0.183	1.768	0.030	-0.083	0.942	11.18	85.52	3.30
8	349	0.248	1.788	0.082	0.088	0.447	13.82	77.40	8.77
9	350	0.375	1.764	0.048	-0.014	1.477	18.37	76.55	5.07
10	353	0.397	1.541	0.088	-0.239	1.104	20.03	70.91	9.06

11	356	0.250	1.151	0.028	-0.017	0.977	17.35	78.16	4.49
12	357	0.441	1.381	0.046	-0.056	0.645	26.69	66.75	6.56
13	358	0.326	0.819	0.082	-0.088	0.569	21.03	67.58	11.39
14	361	0.262	0.714	0.033	0.008	0.965	20.09	74.12	5.79
15	376	0.204	0.565	0.023	0.066	1.798	13.70	78.45	7.85
16	377	0.466	1.206	0.100	-0.138	2.805	22.89	67.08	10.03
17	378	0.370	1.198	0.271	-0.116	1.261	17.03	58.98	23.99
18	379	0.589	1.476	0.090	0.130	2.700	31.37	59.77	8.87
19	386	0.390	1.034	0.079	0.057	1.560	22.04	65.14	12.82
20	803	0.133	1.185	0.023	0.083	0.465	12.86	81.83	5.31
21	811	0.183	2.998	0.042	0.012	0.369	18.58	66.89	14.53
22	951	0.238	1.027	0.057	-0.003	1.222	22.31	69.60	8.09
23	981	0.505	0.888	0.089	-0.053	3.469	25.35	62.66	11.99
24	1049	0.122	1.294	0.015	0.135	2.833	17.95	78.88	3.18
25	1053	0.103	0.697	0.044	0.057	0.945	14.04	62.47	23.48
26	1188	0.103	1.605	0.024	0.305	2.766	10.03	84.36	5.61
27	1189	0.134	1.596	0.018	0.040	0.842	15.41	80.59	4.00
28	1200	0.170	1.996	0.048	-0.042	1.694	14.30	77.56	8.14
29	1311	0.105	0.887	0.003	0.101	1.329	7.82	91.09	1.10

7.4.3 Discussions

The summary statistics of the two scenarios are summarized in Table 7.7. It is clear that in terms of R^2 , bias and standard error, the case of $m = 0.3$, or $\beta_{r3} = 0.6262$ is the best, although the improvement from the other scenario is limited. However, there is significantly greater bias for the case of the default β_{r3} .

Table 7.7: Comparison of statistical analysis with different value of traffic exponent

Parameters	$m = 0.30$	$m = 0.479$
Number of data points	211	211
Standard error (mm)	0.436	0.437
R^2	0.975	0.970
Average bias (mm)	-0.001	0.005
Total RSS	39.879	40.106

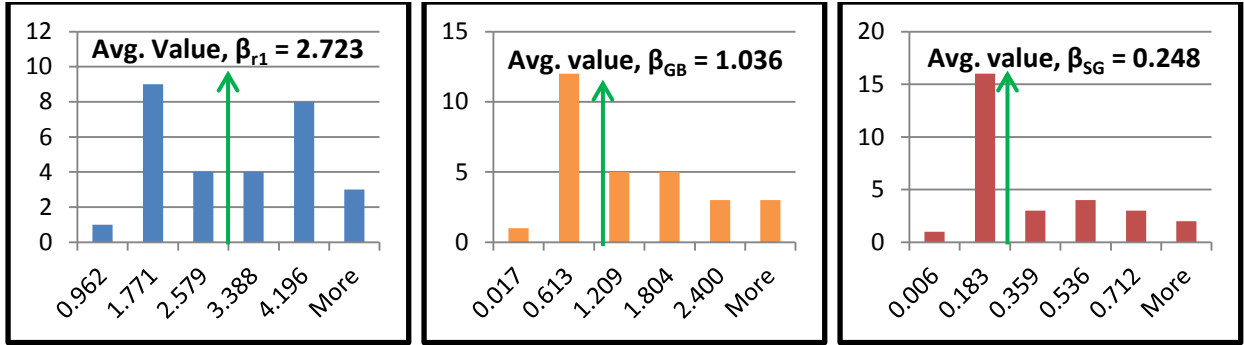


Figure 7.13: Histograms of local calibration coefficients for $m = 0.30$ (or $\beta_{r3} = 0.6262$)

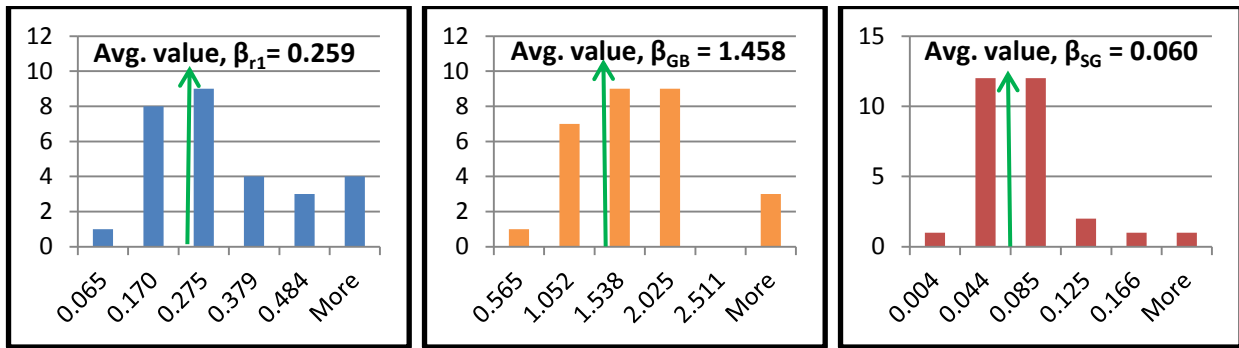


Figure 7.14: Histograms of local calibration coefficients for $m = 0.479$ (or $\beta_{r3} = 1.0$)

The histogram of the local calibration coefficients for two different scenarios are presented in the Figure 7.13, and 7.14. It is clear that the value of local calibration coefficient for AC layer and the sub-grade layer decreases with increase in traffic exponent value whereas it increases with increase in traffic exponent for the base layer (refer to Figure 7.15). However, the average layer contribution of AC and base layer increases with the increase in the traffic exponent value, but the contribution of sub-grade layer decreases (refer to Figure 7.16).

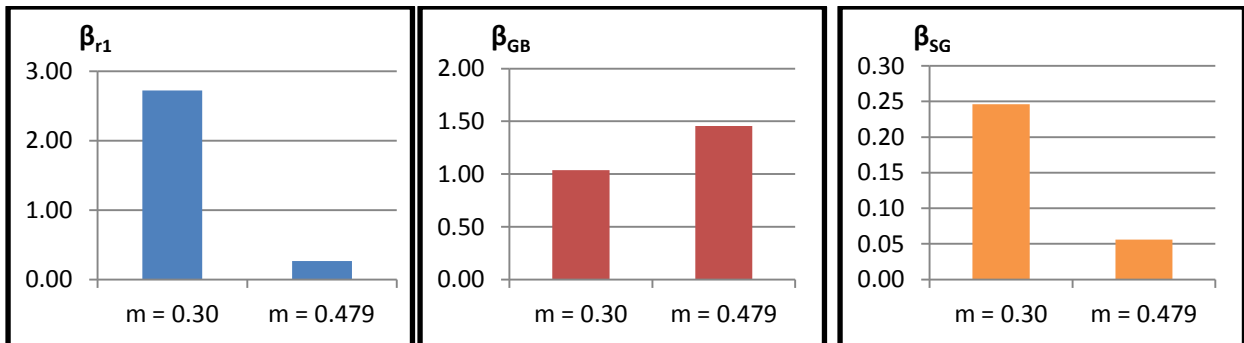


Figure 7.15: Histogram for average calibration coefficients

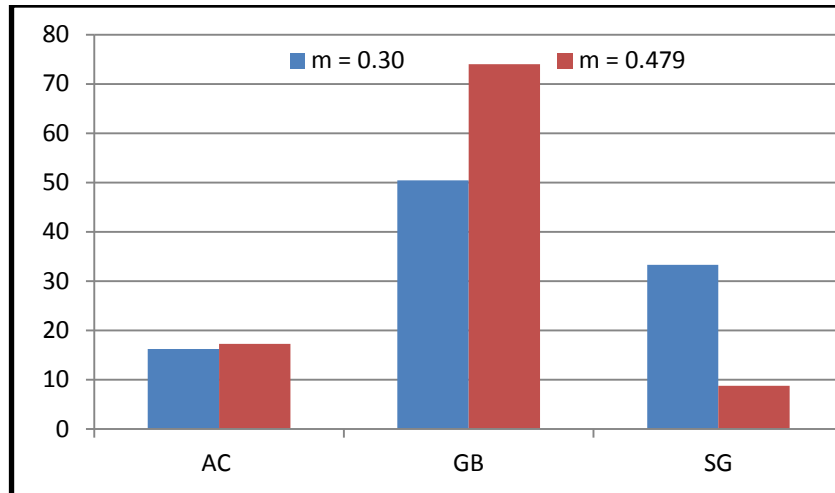


Figure 7.16: Variation of layer contribution with section specific calibration coefficients

7.4.4 Validation for Local Calibration Results

Ontario's twenty nine Marshall mix pavement sections were calibrated by section-by-section longitudinal local calibrations methodology with a preset value of 1.0 and 0.6262 for local calibration parameters of temperature exponent (β_{r_2}) and traffic exponent (β_{r_3}) respectively and the results was presented in Table 7.5. The most of these Marshall mix sections under gone for the rehabilitated process by the year 2010 and 2011 and thus Waseem (2013) used a series of the field observed rut depth data for each pavements from MTO's database by the end of year 2010 for the calibration. Because of the lack of structural layer information as well as insufficient number of rut depth observation after rehabilitated process, this research failed to use the most recent rut depth observation by the year 2012, 2013 and 2014. However, the calibration and validation process under this research used the field observed rut depth data for each pavements from MTO's database by the end of year 2010 as used by Waseem (2013) for the calibration. Keeping on the mind for the validation of the results, the author decided to split the rut depth observation of all 29 sections till the year 2009 for calibration and at year 2010 for validation purposes during this study.

However, the sections 356, 1189 and 1200 having poor quality of rut observation in the year 2010 are carefully removed from the analysis through screening process. Similarly, sections 139, 811, 1053 and 1188 are removed from validation process because of lack of observed rut data in the database. Finally, the calibration results presented in Table 7.5 are used on all 22 sections to compare the predicted rut depth against its measured value. Meanwhile, a plot

between the observed total pavement rutting and the corresponding predicted values (refer to Figure 7.17) bare very good correlation (0.948) between them with a standard error of 0.879 mm. The resulting overall standard deviation is actually as good as to the result from the global calibration, as shown in Table 7.8.

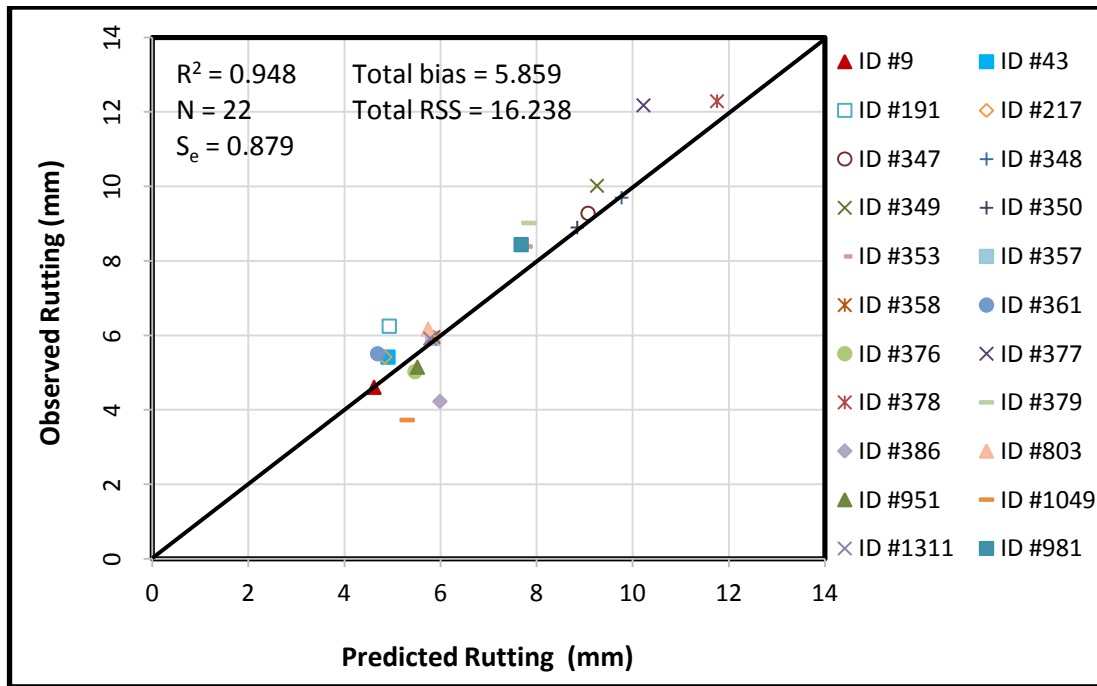


Figure 7.17: Validation - predicted versus observed plots with $m = 0.30$ (or $\beta_{r3} = 0.6262$)

7.5 Comparison with Global Calibration Results

These section-by-section longitudinal calibration and validation results obtained for Ontario's Superpave and Marshall mix pavement sections are also compared with the global calibration results in terms of the standard deviation. The calibration and validation bare good correlation between the predicted and observed rutting and the resulting overall standard error is also actually as good as to the result from the global calibration, as shown in Table 7.8.

Table 7.8: Comparison of statistics of Global and Local calibration

Parameters	Global calibration		Longitudinal calibration		Longitudinal Validation	
	NCHRP 2004	AASHTO 2008	Superpave	Marshall mix	Superpave	Marshall mix
Number of data points	387	334	164	248	53	22
Standard error (mm)	3.07	2.72	0.524	0.436	0.958	0.904
R ²	0.399	0.577	0.804	0.975	0.731	0.947

7.6 Second-Stage Factor Analysis

Despite of difficulties for data management, analysis and result adaptation, the longitudinal calibration is performed to address the limitations of cross-sectional calibration. Due to a number of sets of calibration parameters, it is not possible to apply the results of longitudinal calibration directly for design and maintenance practices. Therefore, it is essential to develop a model that can best estimate the value of calibration parameters. Factor analysis is aimed to identify the causes behind the variation of calibration parameters for individual section so that a regression equation can be developed through multiple regression analysis

7.6.1 Superpave versus Marshall mix

After obtaining a different sets of calibration coefficients, this study was concerned to find out whether a separate set of calibration parameters are required for Superpave and Marshall mix sections or not. A t-test was performed by setting a hypothesis that there is no significant difference between mean value of calibration coefficients for Superpave and Marshall mix sections. The summary of the test is presented in Table 7.9 which rejects the null hypothesis for β_{GB} and β_{SG} and hence, it indicates a need of separate models for them. But on the other side, the null hypothesis is accepted for β_{r1} and indicates that there is no need to separate the AC layer rutting model for both mix type. The stiffness of Superpave mix is much greater than Marshall mix type and provide a strong protection to the underneath pavement layer. This difference in the mix properties cause a change in the calibration coefficients for base and sub-grade layer. Further, the better stiffness of Superpave mix enhance the load resistance and cause an increase in AC layer contribution to rutting in compare to Marshall mix type. The similar behavior on AC layer contribution is observed in the cross-sectional calibration.

However, there is large variation in the calibration coefficients. The use of average value of calibration coefficient increases the standard error and reduces the R^2 value as explained in Section 7.2.2 and 7.4.1. Although it is better than the results from global calibration, this is not only the enough evident to generalize the calibration coefficients for the rutting models. A comparison of total rutting in Superpave and Marshall mix pavement also shows a great variation in the rutting behavior by project group but it is almost similar to a project (refer to section 1.1). The similar conclusion is drawn during the local calibration (refer to section 7.2.2). Hence, a comprehensive study of the rutting behavior for different mix type is required to explain the AC rutting model.

Table 7.9: Summary of the t-test statistics for calibration parameters

Calibration coefficients	Pavement type	Observation	Mean	Standard deviation	t-value	t-critical at 95%	Status of Null Hypothesis
β_{r1}	Superpave	33	2.717	0.772	-0.020	2.015	Accepted
	Marshall mix	29	2.723	1.313			
β_{GB}	Superpave	33	0.604	0.477	-2.458	2.017	Rejected
	Marshall mix	29	0.693	0.832			
β_{SG}	Superpave	33	0.063	0.032	-3.909	2.045	Rejected
	Marshall mix	29	0.246	0.250			

7.6.2 Single factor analysis

Further, the calibration coefficients obtained for each sections differ from another. This adds difficulties in the application of the model for design and maintenance practices. To overcome from such a situation, the effects of the local parameters such as environment, highway type, top AC layer thickness (T_{ACtop}), total AC layer thickness (T_{AC}), total granular base layer thickness (T_{GB}), sub-grade modulus (M_{SG}), and AADTT on the obtained calibration coefficients were observed.

7.6.2.1 Environment

A t-test was performed by setting a hypothesis that there is no environmental effect on calibration coefficients. The statistics also shows that there is no effect of environment on the sub-grade layer. This is because there is least effect of environment at low level. Similarly, the effect is insignificant for AC layer. From this observation, we can simply say that the model for dynamic

modulus included in AASHTOWare is sufficient to reflect the environmental effects. However, the test statistics for base layer rejects the null hypothesis. The possible reasons may be that the resilience modulus itself is either inadequate or does not reflect the environmental effect in the base layer.

Table 7.10: Test statistics of calibration parameters of Superpave mix for effect of environment

Calibration coefficients	Zone	Observation	Mean	Standard deviation	t-value	t-critical at 95%	Status of Null Hypothesis
β_{r_1}	SO	22	2.723	0.859	0.069	2.051	Accepted
	NO	11	2.706	0.597			
β_{GB}	SO	22	0.705	0.517	2.076	2.042	Rejected
	NO	11	0.403	0.316			
β_{SG}	SO	22	0.061	0.033	-0.508	2.080	Accepted
	NO	11	0.067	0.031			

Table 7.11: Test statistics of calibration parameters of Marshall mix for effects of environment

Calibration coefficients	Zone	Observation	Mean	Standard deviation	t-value	t-critical at 95%	Status of Null Hypothesis
β_{r_1}	SO	23	2.548	1.344	-1.696	2.228	Accepted
	NO	6	3.394	1.011			
β_{GB}	SO	23	1.213	0.844	4.392	2.052	Rejected
	NO	6	0.355	0.208			
β_{SG}	SO	23	0.230	0.273	-0.967	2.110	Accepted
	NO	6	0.306	0.133			

7.6.2.2 Highway types

A t-test was performed by setting a hypothesis that there is no effect of highway type on calibration coefficients. The statistics accepts the null hypothesis and concludes no effect of highway type on calibration coefficients. This further concludes that the traffic load component is adequately considered in MEPDG rutting models and the estimation of its exponent is also reasonable. However, a effect is observed in the AC layer for Superpave sections which is not trustable because of very few number of Superpave sections from 400 series.

Table 7.12: Test statistics of calibration parameters of Superpave mix for effects of highway type

Calibration coefficients	HWY type	Observation	Mean	Standard deviation	t-value	t-critical at 95%	Status of Null Hypothesis
β_{r_1}	Non-400 series	29	2.805	0.782	4.329	2.064	Rejected
	400 series	4	2.079	0.168			
β_{GB}	Non-400 series	29	0.520	0.358	-1.694	3.182	Accepted
	400 series	4	1.216	0.811			
β_{SG}	Non-400 series	29	0.063	0.033	-0.057	2.776	Accepted
	400 series	4	0.064	0.027			

Table 7.13: Test statistics of calibration parameters of Marshall mix for effects of highway type

Calibration coefficients	HWY type	Observation	Mean	Standard deviation	t-value	t-critical at 95%	Status of Null Hypothesis
β_{r_1}	Non-400 series	21	2.921	1.290	1.326	2.160	Accepted
	400 series	8	2.203	1.308			
β_{GB}	Non-400 series	21	1.057	0.922	0.270	2.086	Accepted
	400 series	8	0.979	0.579			
β_{SG}	Non-400 series	21	0.287	0.269	1.836	2.080	Accepted
	400 series	8	0.137	0.160			

7.6.2.3 Top AC layer thickness

A regression analysis, as shown in Table 7.14, was performed by setting a hypothesis that there is no effect of top AC layer thickness on calibration coefficients. The relationship of top AC layer thickness with calibration coefficients are presented in Figures 7.18 and 7.19. A negative relationship is established by general observation but the effect is significant only for base layer. This is because the base layer is protected from thick top layer. The observation for Marshall mix are not trustable because of same thickness for almost all sections.

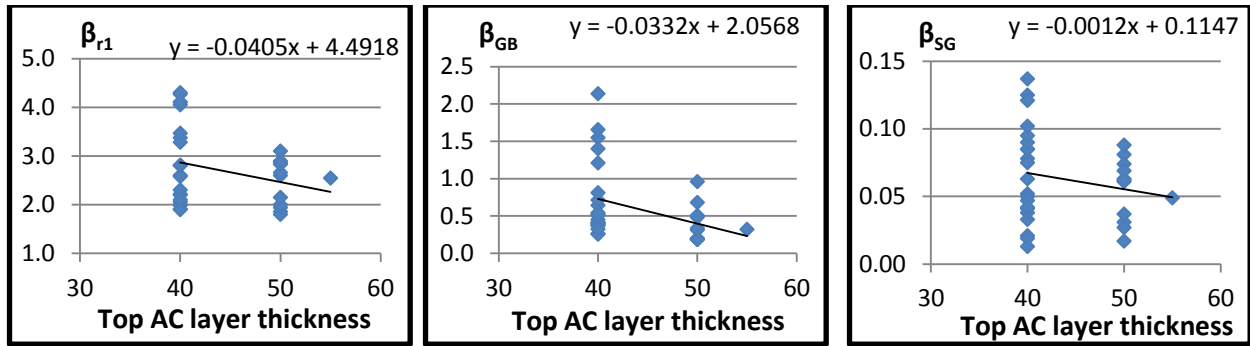


Figure 7.18: Effects of top AC layer thickness on calibration coefficients for Superpave mix

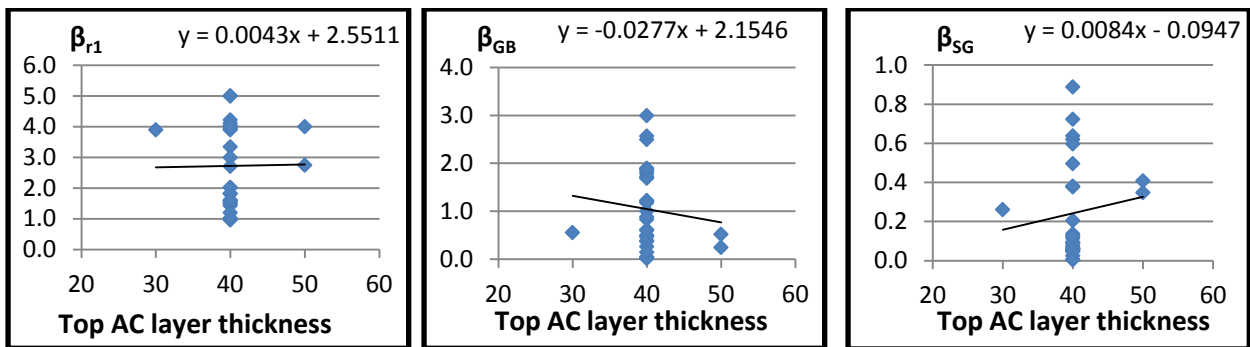


Figure 7.19: Effects of top AC layer thickness on calibration coefficients for Marshall mix

Table 7.14: Summary of the regression analysis for effect of top AC layer thickness

Pavement type	N	Calibration coefficients	R^2	S_e	t-value	t-critical at 95%	P-value	Status of Null Hypothesis
Superpave	33	β_{r1}	0.271	0.755	-1.567	2.037	0.127	Accepted
		β_{GB}	0.359	0.452	-2.141		0.040	Rejected
		β_{SG}	0.191	0.032	-1.082		0.288	Accepted
Marshall	29	β_{r1}	0.010	1.337	0.055	2.048	0.957	Accepted
		β_{GB}	0.108	0.842	-0.567		0.575	Accepted
		β_{SG}	0.109	0.253	0.573		0.571	Accepted

7.6.2.4 Total AC layer thickness

A regression analysis (refer to Table 7.15) was performed by setting a hypothesis that there is no effect of total AC layer thickness on calibration coefficients. The relationship of total AC layer thickness with calibration coefficients are presented in Figures 7.20 and 7.21. By general observation, a positive relationship is established for Superpave mix. But for Marshall type, a negative relationship is seen to AC and sub-grade layer where as a positive for base layer. On the

other side, the effect is significant only for base and sub-grade layer. The reason is not clear and hence this relationship is not trustable. However, an intensive investigation with precise material properties and layer specific coefficient is required to establish the relationship.

Table 7.15: Summary of the regression analysis for effect of total AC layer thickness

Pavement type	N	Calibration coefficients	R ²	S _e	t-value	t-critical at 95%	P-value	Status of Null Hypothesis
Superpave	33	β_{r_1}	0.212	0.766	1.210	2.039	0.236	Accepted
		β_{GB}	0.807	0.286	7.608		1.41E-08	Rejected
		β_{SG}	0.348	0.031	2.064		0.047	Rejected
Marshall	29	β_{r_1}	0.334	1.260	-1.840	2.048	0.077	Accepted
		β_{GB}	0.582	0.689	3.722		0.0009	Rejected
		β_{SG}	0.412	0.232	-2.347		0.026	Rejected

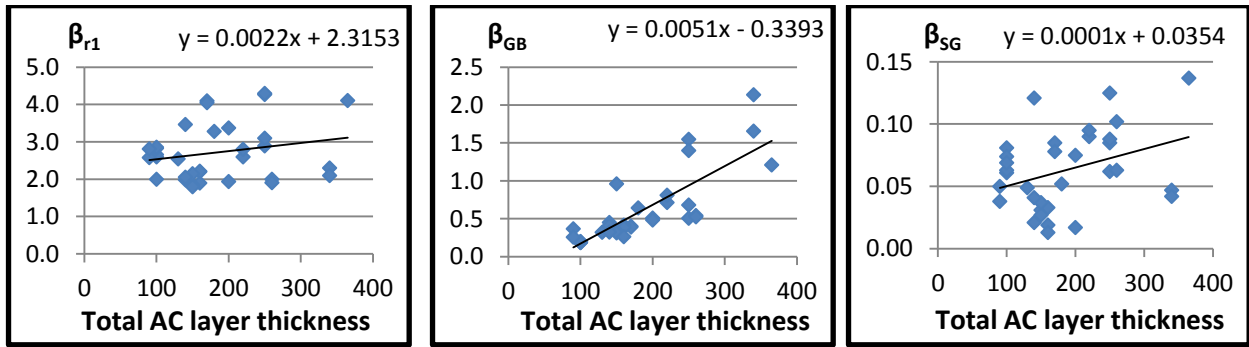


Figure 7.20: Effects of total AC layer thickness on calibration coefficients for Superpave mix

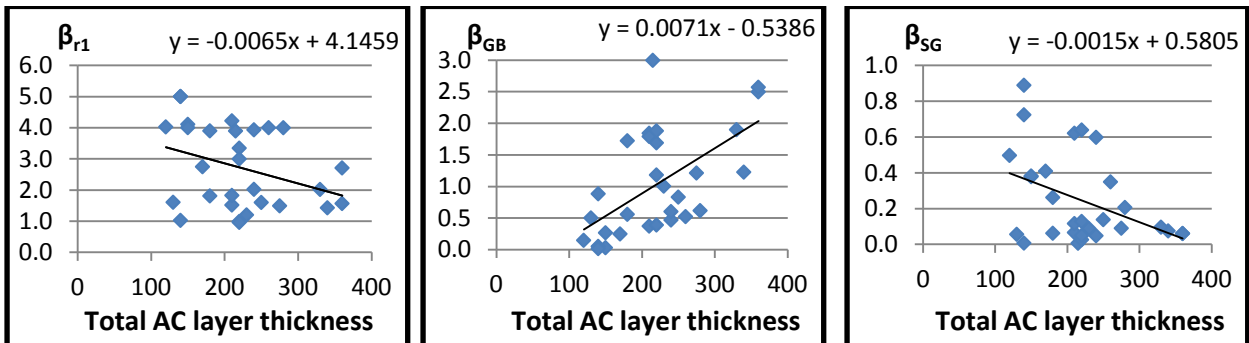


Figure 7.21: Effects of total AC layer thickness on calibration coefficients for Marshall mix

7.6.2.5 Total GB layer thickness

A regression analysis, as shown in Table 7.16, was performed by setting a hypothesis that there is no effect of total granular base (GB) layer thickness on calibration coefficients. The Figures 7.22 and 7.23 shows the relationship between total GB layer thickness and calibration coefficients. A negative relationship is established by general observation which is logical. The thick layer is more stiffer that protects itself from the rutting. From the test statistics, the effect is observed significant only for base layer.

Table 7.16: Summary of the regression analysis for effect of total GB layer thickness

Pavement type	N	Calibration coefficients	R ²	S _e	t-value	t-critical at 95%	P-value	Status of Null Hypothesis
Superpave	33	β_{r_1}	0.315	0.744	-1.851	2.039	0.074	Accepted
		β_{GB}	0.284	0.464	-2.645		0.010	Rejected
		β_{SG}	0.080	0.032	-0.448		0.657	Accepted
Marshall	29	β_{r_1}	0.007	1.337	-0.039	2.048	0.970	Accepted
		β_{GB}	0.686	0.616	-4.904		3.94E-05	Rejected
		β_{SG}	0.259	0.246	1.393		0.175	Accepted

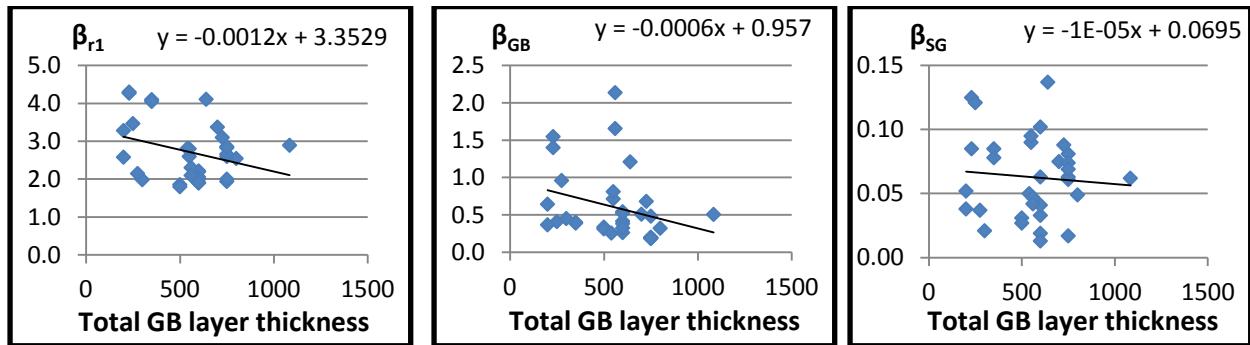


Figure 7.22: Effects of total GB layer thickness on calibration coefficients for Superpave mix

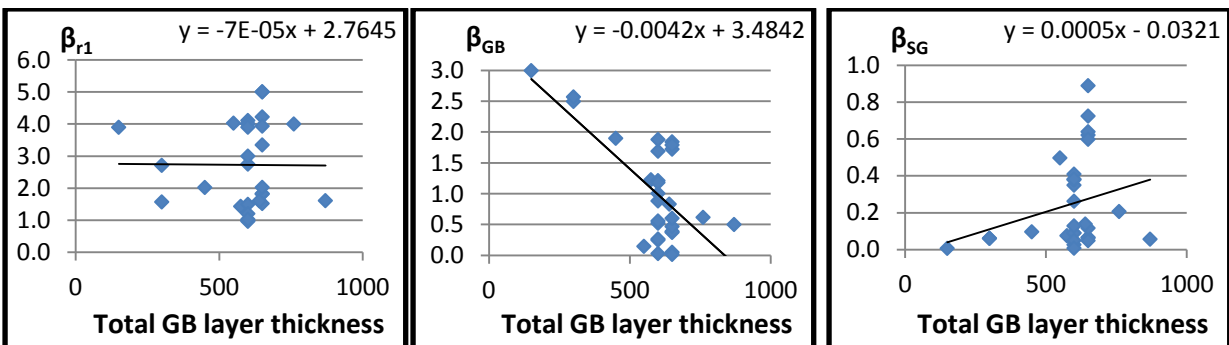


Figure 7.23: Effects of total GB layer thickness on calibration coefficients for Marshall mix

7.6.2.6 Sub-grade modulus

A regression analysis (refer to Table 7.17) was performed by setting a hypothesis that there is no effect of sub-grade modulus (M_{SG}) on calibration coefficients. The relationship of sub-grade modulus with calibration coefficients are presented in Figures 7.24 and 7.25. A positive relationship is observed with AC and sub-grade layer coefficients where as negative with base layer. Further, there are only two Superpave section having sub-grade modulus 80MPa. for more realistic representation, the analysis was performed by removing these two sections which shows that the effect is significant in sub-grade layer. However, the effect of sub-grade modulus on AC layer coefficient of Marshall type is not clear.

Table 7.17: Summary of the regression analysis for effect of sub-grade modulus

Pavement type	N	Calibration coefficients	R^2	S_e	t-value	t-critical at 95%	P-value	Status of Null Hypothesis
Superpave	31	β_{r_1}	0.135	0.803	0.733	2.039	0.469	Accepted
		β_{GB}	0.062	0.493	0.334		0.741	Accepted
		β_{SG}	0.375	0.031	2.176		0.038	Rejected
Marshall	29	β_{r_1}	0.555	1.112	3.465	2.048	0.002	Rejected
		β_{GB}	0.157	0.837	-0.824		0.417	Accepted
		β_{SG}	0.440	0.229	2.543		0.017	Rejected

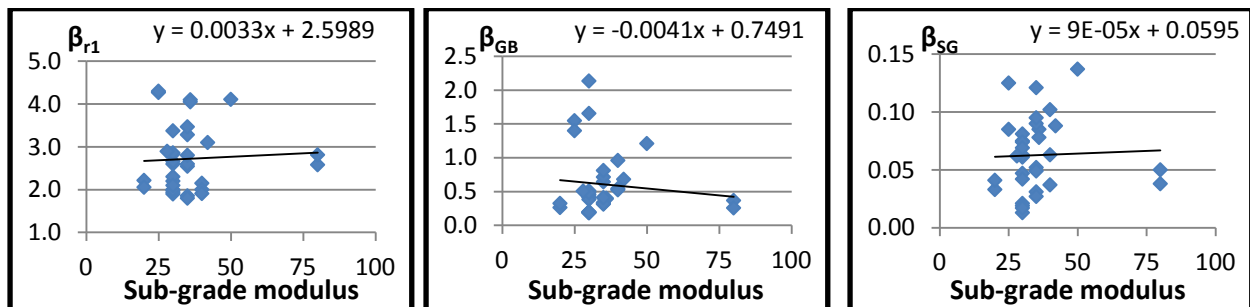


Figure 7.24: Effects of sub-grade modulus on calibration coefficients for Superpave mix

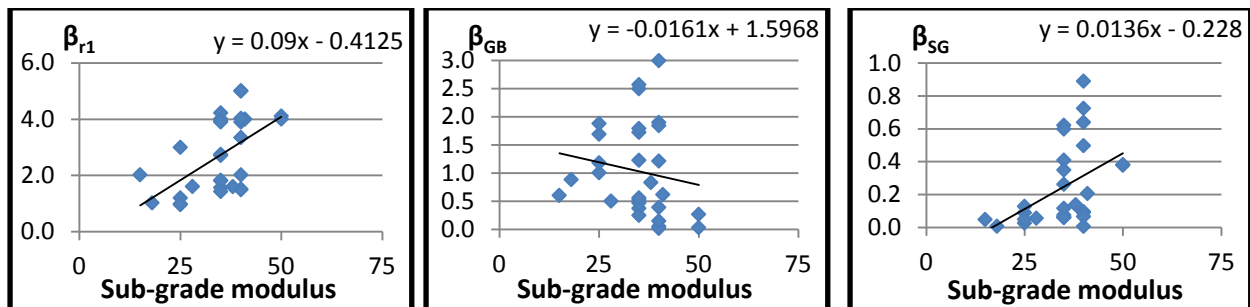


Figure 7.25: Effects of sub-grade modulus on calibration coefficients for Marshall mix

7.6.2.7 AADTT

A regression analysis, as shown in Table 7.18, was performed by setting a hypothesis that there is no effect of AADTT on calibration coefficients. The Figures 7.26 and 7.27 shows the relationship between total AADTT and calibration coefficients. The trend of effect is similar to both mix type. However, the test statistics shows a significant effect on Superpave base which is contradictory and non trustable because of poor distribution of traffic. Hence, no significant evidence is available to establish the relationship between them.

Table 7.18: Summary of the regression analysis for AADTT

Pavement type	N	Calibration coefficients	R ²	S _e	t-value	t-critical at 95%	P-value	Status of Null Hypothesis
Superpave	33	β_{r_1}	0.230	0.763	-1.315	2.039	0.198	Accepted
		β_{GB}	0.683	0.354	5.207		1.19E-05	Rejected
		β_{SG}	0.118	0.032	-0.661		0.513	Accepted
Marshall	29	β_{r_1}	0.155	1.320	-0.817	2.048	0.421	Accepted
		β_{GB}	0.249	0.821	1.334		0.193	Accepted
		β_{SG}	0.307	0.243	-1.677		0.105	Accepted

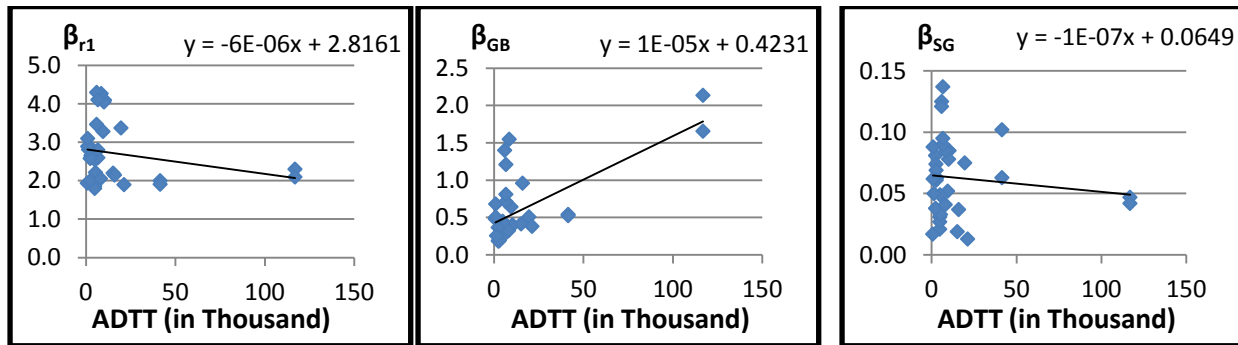


Figure 7.26: Effects of AADTT on calibration coefficients for Superpave mix

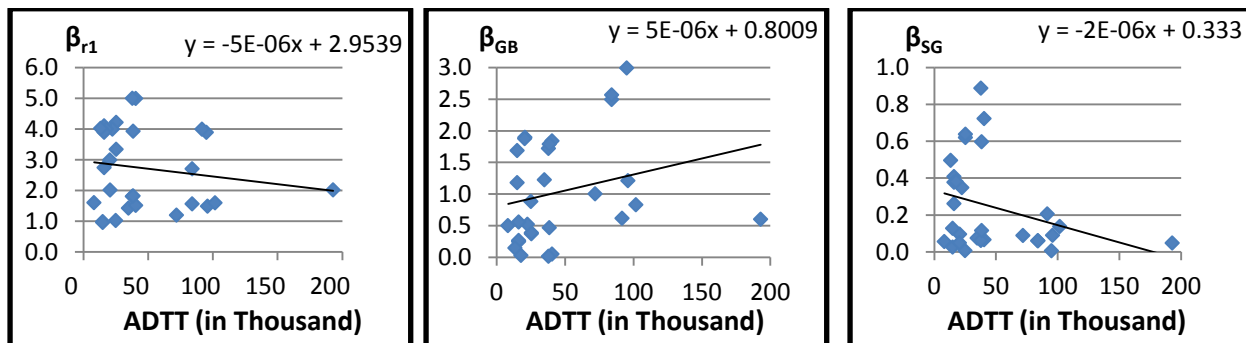


Figure 7.27: Effects of AADTT on calibration coefficients for Marshall mix

7.6.2.8 Summary

The summary of the effect of single factor on calibration coefficients are presented below. Based on the findings of the single factor analysis, it was aimed to develop a regression model through multiple regression analysis for the purpose of precise estimation of calibration coefficients which are required for design and maintenance practices within Ontario region. However, the results from this analysis are not sufficient to generalize the cause and effect relationship between them. Further, it is required to identify others factors, if any, and develop a relationship through an intensive study. But at this point, comprehensive effect analysis is not possible because of lack of layer specific information such as layer contribution to rutting and layer specific rutting coefficient for AC layer.

Table 7.19: Effects of single factors on calibration coefficients

Factors	Relationship with calibration coefficients						Remarks
	Superpave			Marshall			
	β_{r1}	β_{GB}	β_{SG}	β_{r1}	β_{GB}	β_{SG}	
Environment	NA	A	NA	NA	A	NA	Same effect on both mix type
Highway type	A	NA	NA	NA	NA	NA	Effect on Superpave β_{r1} is not trustable.
Top AC layer thickness	NA	(-)	NA	NA	NA	NA	Need further precise investigation
Total AC layer thickness	NA	(+)	(+)	NA	(+)	(-)	Need further precise investigation
Total GB layer thickness	NA	(-)	NA	NA	(-)	NA	Same effect on both mix type
Sub-grade modulus	NA	NA	(+)	(+)	NA	(+)	Need further intensive investigation
AADTT	NA	(+)	NA	NA	NA	NA	Effect on Superpave β_{GB} is not trustable

7.7 Methodological Comparison

A full study of cross-sectional and longitudinal calibration was performed in this study. The results showed that the both type of model calibration are better than the global models comparing in terms of standard error (refer to Table 6.3 and 7.8).

A comparative plot of residual errors (Figure 7.28 and 7.29) for total predicted rut depth showed that the residuals errors for longitudinal calibration were closely and equally scattered on both sides of zero line, whereas for cross-sectional calibration, they were widely scattered. On the other side, the section-by-section calibration gave very efficient results of R^2 value which shows great correlation between the predicted and observed values. But, in contrast, the cross-sectional calibration shows extremely poor correlation with relatively high standard error. The similar result is observed from a comparative longitudinal plot of total rutting to some typical Superpave and Marshall type sections from Ontario's highways (refer to Figure 7.30). The model can be further improved by using layer by layer calibration strategy that requires the information of layer contribution to rutting which is still unknown to Ontario's roads. Thus, there is an urgent need of trench analysis for precise investigation.

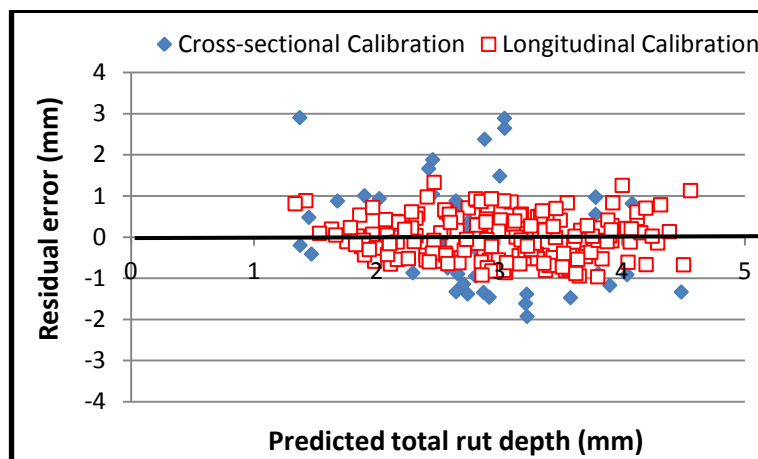


Figure 7.28: Residual error for total predicted rut depth for Superpave sections

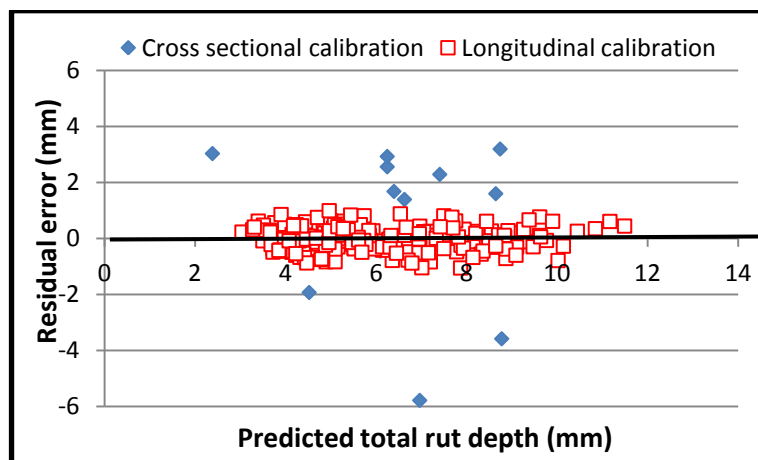


Figure 7.29: Residual error for total predicted rut depth for Marshall mix sections

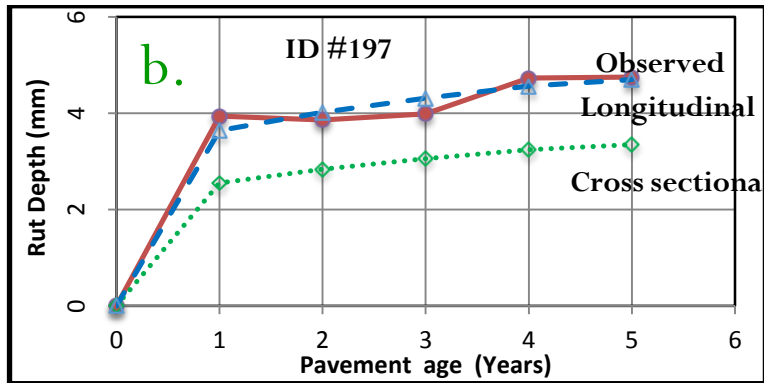
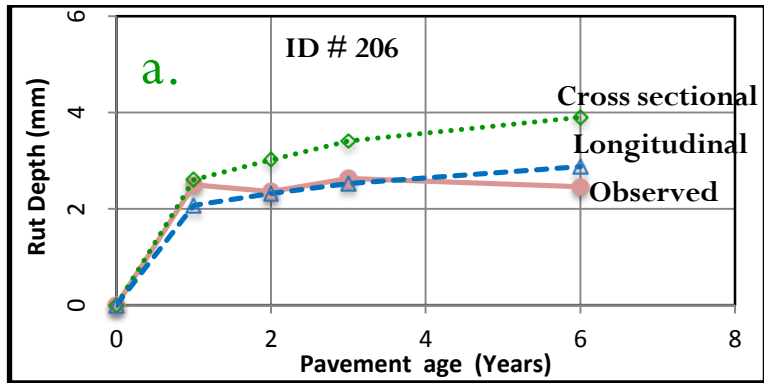


Figure 7.30: Typical longitudinal trend of rutting for (a) Superpave (b) Marshall

CHAPTER 8 SUMMARY, CONCLUSIONS AND RECOMMENDATIONS

This chapter summarizes the work of the local calibration study of the empirical rutting models of MEPDG method under Ontario's condition, draws conclusions from the analyses, and presents recommendations for future studies.

8.1 Summary

This thesis represents the third study at Ryerson University on the local calibration of the MEPDG distress models for Ontario's roadways. The study focuses on the rutting models and covers both the Superpave and Marshall mix sections. The study was partly funded by the MTO HIIFP (2013-2015).

A comprehensive literature review was performed on previous efforts for local calibration. The study investigated the needs and challenges involved in the local calibration process. These issues were resolved based on a solid analyses of literature and statistical tests. Cross-sectional and longitudinal types of model calibration strategies were used for calibration of the rutting models. The results were compared, verified and proposed for the design and maintenance practices within Ontario.

In addition to the first local calibration database developed by Jannat (2012), another local calibration database for Superpave sections under MTO's jurisdiction was developed and used them for calibration. The study of the behavior of rutting models raised a specific issues of indeterminacy and interdependency between the models during the full local calibration. To deal with this issue, the traffic and temperature exponents were prefixed to 0.30 and 1.5606, respectively, based on statistical analyses of the calibration results presented in NCHRP Report 719. Moreover, two different local calibration methods were developed: cross-sectional calibration to balance the section coverage issue and longitudinal calibration to satisfy the rutting trend tracking need. Both methods were used to calibrate the selected Superpave and Marshall mix pavement sections by considering equal weight for each observed rut depth. Further, a sensitivity study was performed with different value of traffic exponent during the longitudinal calibration to observe the prediction performance of the models based on standard error. The

results from both cross-sectional and longitudinal calibration methodology were compared with the results from global calibration and validated separately.

Clustering analysis was performed based on Ontario zone, Highway functional class, Sub-grade modulus, Top layer material and its performance grade to determine the possible cluster groups that improve the performance of the model. Further, factor analysis was also performed to see the possible causes of variation in calibration parameters during the longitudinal calibration.

8.2 Conclusions

Based on this study, the following conclusions are drawn:

- 1) The default, global rutting models consistently overestimate rutting in Ontario's existing flexible highways. This result echoes many previous calibration studies in U.S. and Canada.
- 2) The cross-sectional calibration reduces the residual standard deviation to a value of 1.20 mm and 2.21 mm for Superpave and Marshall mix sections, respectively, and 2.40 when calibrated jointly. The overall residual standard deviation is still less than the result from the global calibration. This implies that the cross-sectional calibration results can be used as level 3 input for Ontario's roads.
- 3) The large difference of the residual standard deviations in Superpave and Marshall mix sections suggests that the two types of materials should be separated and two rutting models be used.
- 4) The cross-sectional clustering analysis provides inconsistent and unconvincing results. While clustering based on environmental zone and sub-grade modulus seems to improve significantly the prediction performance of the rutting models for Marshall mix pavement sections, for Superpave pavement sections top layer material and top layer performance grade improve the model performance.
- 5) The sensitivity analyses suggested that the AC rutting model with the traffic exponent value of 0.30 obtains the lowest value of residual standard deviation.
- 6) The cross-sectional calibration fails to capture the longitudinal trend of evolution of rutting to Ontario's highway.

- 7) The longitudinal calibration parameters of Superpave pavement sections spread over a wide range. In particular, AC scaling parameter (β_{r_1}) varied from 1.801 to 4.300, granular base scaling parameters (β_{GB}) varied from 0.185 to 2.137 and fine soil scaling parameters (β_{SG}) varied from 0.013 to 0.137. Using an average value of calibration parameters (2.717, 0.604 and 0.063) results in a standard error of 1.761 mm, comparable to the result from the global calibration. Hence, these average values will be appropriate as level 3 input for Ontario.
- 8) The longitudinal calibration parameters of Marshall mix pavement sections also spread over a wide range, where AC scaling parameter (β_{r_1}) varied from 0.962 to 5.005, granular base scaling parameters (β_{GB}) varied from 0.017 to 2.996 and fine soil scaling parameters (β_{SG}) varied from 0.006 to 0.889. Using an average value of calibration parameters (2.723, 1.036 and 0.246) results in a standard error of 2.254 which is as good as to the result from the global calibration. Hence, these average values will be appropriate as level 3 input for Ontario.
- 9) From the results of longitudinal calibration, it is concluded that the pavement sections should be treated separately by different mixes types including Superpave and Marshall mixes during the database management for pavement management system.

8.3 Recommendations

Based on the local calibration findings, the following important recommendations are made by the author for the further local calibration practices of the rutting models in Ontario.

- For a more solid full local calibration study, it is recommended to take core and forensic investigation of the Ontario's pavements to determine the layer contribution to rutting. Solving linear regression equations sometimes complicates the optimization problem resulting negative values for the calibration coefficients which should never be the case. On the other side, the calculated layer contribution highly fluctuate. Thus, this confirms the value of layer contribution to rutting.
- This research utilized only a limited number of new, reconstructed and rehabilitated pavement sections. Hence, the number of sections with long

historical data should be increased for local calibration practices ones retrieved from the MTO database.

- It is recommended to collect the detailed material characterization data as level 1 input to robust the prediction performance of the models.
- The scope of this research was limited to King's highways and no pavement sections from secondary highways were selected in the calibration, although they are included in the database. Hence, further calibration for the secondary highways is needed.
- It is important to understand that many other asphalt materials were excluded during this research (e.g., stone-matrix asphalt or SMA). Hence, the scope of the study could be expanded by incorporating such SMA pavement sections in future local calibration of the MEPDG models for Ontario.
- It is better to understand that the results from section-by-section longitudinal calibration are more precise but less adaptable to design practices. Therefore to enhance the adaptability, it is recommended to develop a relationship between factors and the calibration coefficients by using highest accuracy level for material characterization and layer specific rutting coefficients before recalibration of the MEPDG rutting models for Ontario.

APPENDIX A: DERIVED PLASTIC DEFORMATION COEFFICIENTS UNDER NCHRP PROJECT 9-30A

Table A.1: Field-derived plastic deformation coefficient for AC overlay test sections (source: NCHRP Report 719, Table 9)

S. No.	Test Sections	Traffic Exponent ($m = k_{r3}\beta_{r3}$)
1	Arizona SPS-0506	0.300
2	Arizona SPS-0507	0.300
3	Arizona SPS-0503	0.280
4	Arizona SPS-0508	0.280
5	Montana SPS-0504	0.310
6	Montana SPS-0507	0.310
7	Montana SPS-0508	0.310
8	Colorado, no RAP	0.250
9	Colorado, with RAP	0.250
10	Texas SPS-0504	0.350
11	Texas SPS-0507	0.350
12	Texas SPS-0503	0.250
13	Texas SPS-0508	0.250
14	Mississippi SPS-0507	0.550
15	Mississippi SPS-0504	0.550
16	Missouri SPS-0504	0.175
17	Missouri SPS-0507	0.175
18	Missouri SPS-0509	0.230
19	Missouri SPS-0508	0.230
20	Alabama SPS-0607	0.290
21	Alabama SPS-0608	0.290
22	Alabama SPS-0662	0.290
23	Alabama SPS-0663	0.290

Table A.2: Field-derived plastic deformation coefficient for new construction test sections
(source: NCHRP Report 719, Table 8)

S. No.	Test Sections	Traffic Exponent ($m = k_{r3}\beta_{r3}$)
1	FHWA ALF; neat, 10-2	0.317
2	FHWA ALF; Styrelf, 7-2	0.245
3	FHWA ALF; Novophalt 8-2	0.180
4	California, modified, 609HB	0.350
5	California, RHMA, 611HB	0.250
6	Florida; modified, 1B-50	0.335
7	Florida; neat, 5B-50	0.450
8	WesTrack 05; coarse grading	0.310
9	WesTrack 03; fine grading	0.280
10	NCAT S02; SBS, PG 76-22	0.350
11	NCAT E06; neat, PG 67-22	0.450
12	NCAT; Florida, neat	0.230
13	NCAT; Florida, modified	0.200
14	NCAT; Florida, base	0.275
15	Indiana, 7A	0.290
16	Indiana 7B	0.250
17	Indiana 8A	0.255
18	Indiana 8B	0.230
19	Missouri N-10, surface	0.235
20	Missouri N-10, base	0.245
21	Oklahoma N-9, surface	0.310
22	Oklahoma N-9, base	0.360
23	Oklahoma N-9, rich layer	0.400
24	MnROADs 04; AC 120/150	0.350
25	MnROADs 17; AC-20	0.335
26	Arizona SPS-0116; surface	0.310
27	Arizona SPS-0116; binder	0.310
28	Arizona SPS-0116; ATB	0.230
29	Montana SPS-0116; surface	0.320
30	Montana SPS-0116; binder	0.320
31	Montana SPS-0116; ATB	0.230
32	Kansas SPS-0116; surface	0.370
33	Kansas SPS-0116; binder	0.370
34	Kansas SPS-0116; ATB	0.310
35	Wisconsin SPS-0116; surface	0.250
36	Wisconsin SPS-0116; binder layer	0.300
37	Wisconsin SPS-0116; ATB layer	0.500

Table A.3: Laboratory-derived plastic deformation coefficient from repeated-load tests of reconstituted specimens (source: NCHRP Report 719, Table 24 and Table 25)

S. No.	Test Section and Mixture Identification	Triaxial Tests		Shear Tests	
		Traffic Exponent (m)	Temperature Exponent (n)	Traffic Exponent (m)	Temperature Exponent (n)
1	Alabama SPS-6 polymer-modified mix	0.251	2.530	0.380	5.200
2	Arizona SPS-5, without RAP	0.281	3.150	0.390	8.500
3	Arizona SPS-5, with RAP	0.265	1.740	0.334	4.650
4	California, perpetual pavement, CA-47	0.211	2.850	0.160	5.800
5	California, perpetual pavement, CA-47M	0.185	2.100	0.221	3.600
6	California, perpetual pavement, CA-52	0.260	2.890	0.181	6.100
7	Colorado, binder layer with RAP	0.201	1.940	0.285	4.900
8	Colorado, binder layer without RAP	0.126	2.050	0.313	6.000
9	Florida PMA mix (NCAT N1 section)	0.251	3.000	0.242	10.100
10	Florida Neat mix (NCAT N2 section)	0.182	2.300	0.245	9.500
11	Florida base mix	0.139	2.300	0.262	9.800
12	Indiana low void mix (NCAT Section 7A)	0.237	2.200	0.280	7.500
13	Indiana low void mix (NCAT Section 7B)	0.238	1.300	0.245	7.300
14	Indiana wearing surface mix (Section 8B)	0.207	1.500	0.216	6.800
15	Mississippi SPS-5, without RAP	0.343	3.000	0.433	9.700
16	Missouri; SPS-5 binder mix with RAP	0.178	4.000	0.407	8.000
17	Missouri; SPS-5 binder mix without RAP	0.183	3.500	0.333	8.800
18	Missouri; SPS-5 wearing surface	0.216	4.250	0.370	9.000
19	Montana SPS-5 without RAP	0.365	3.900	0.259	9.800
20	Montana SPS-5 with RAP	0.288	3.400	0.236	9.300
21	Wisconsin; SPS-1 wearing surface	0.159	2.800	0.237	6.200
22	Wisconsin SPS-1 ATB mix	0.159	2.400	0.510	10.700
23	Wisconsin SPS-1 binder mix	0.264	1.200	0.334	10.300

APPENDIX B: PAVEMENT SECTIONS SELECTED FOR ANALYSIS

Table B.1: Summary of the Superpave pavement sections from western region

S. No.	Section ID	HWY	Direction	Construction type	Begin chainage	End chainage	Remarks
1	77	3	B	Rehab/Resur	12020+1.30	12036+0.00	LC, LV and CSC
2	78	3	B	Rehab/Resur	12036+0.00	12038+0.00	LC, LV and CSV
3	79	3	B	Rehab/Resur	12038+0.00	12045+0.00	LC, LV and CSV
4	80	3	B	Rehab/Resur	12045+0.00	12050+0.02	LC, LV and CSC
5	114	6	B	Rehab/Resur	13640+2.10	13650+2.46	CSC
6	115	6	B	Rehab/Resur	13650+2.46	13650+11.44	CSV
7	197	7	E	Rehab/Resur	14612+0.88	14620+6.00	LC, LV and CSC
8	206	7	W	Rehab/Resur	14612+0.88	14620+6.00	LC, LV and CSV
9	219	8	B	Rehab/Resur	15970+1.30	15980+0.00	CSC
10	221	8	B	Reconst	16000+1.00	16010+11.70	CSC
11	252	10	B	Rehab/Resur	16580+0.80	16590+0.00	LC, LV and CSC
12	253	10	B	Rehab/Resur	16590+0.00	16600+0.00	LC, LV and CSV
13	587	21	B	Reconst	24030+0.00	24030+12.97	CSC
14	589	21	B	Rehab/Resur	24050+5.20	24060+0.10	CSV
15	600	21	B	Reconst	24142+0.10	24142+13.00	CSC
16	613	23	B	Reconst	24600+0.00	24605+1.00	LC
17	629	26	B	Rehab/Resur	25700+2.80	25710+2.80	-
18	678	40	B	Reconst	29110+0.00	29110+6.20	-
19	679	40	B	Reconst	29110+6.20	29120+0.00	-
20	835	93	B	Reconst	39119+0.00	39132+0.00	LC and CSC
21	1217	402	E	Reconst	48140+2.00	48150+6.43	CSC
22	1230	402	W	Reconst	48140+2.00	48150+6.43	CSV
23	1240	403	E	Rehab/Resur	48335+0.00	48342+1.00	LC, LV and CSC
24	1255	403	W	Rehab/Resur	48335+0.00	48342+1.00	LC, LV and CSV

Table B.2: Summary of the Superpave pavement sections from central region

S. No.	Section ID	HWY	Direction	Construction type	Begin chainage	End chainage	Remarks
1	105	6	B	New Const	13465+0.00	13515+0.00	LC, LV and CSV
2	424	12	B	Rehab/Resur	19380+0.00	19390+0.00	-
3	425	12	B	Rehab/Resur	19390+0.00	19410+0.69	CSC
4	426	12	B	Rehab/Resur	19410+0.69	19420+0.00	CSV
5	670	35	N	Resur	27816+0.00	27822+0.00	LC, LV and CSV
6	673	35	S	Resur	27816+0.00	27822+0.00	LC, LV and CSC
7	719	58	B	New (Reconst)	32740+0.00	32746+0.00	LC, LV and CSC

8	825	89	B	New (Reconst)	38620+5.27	38630+0.24	CSC
9	826	89	B	New (Reconst)	38630+0.24	38635+0.00	CSV
10	1052	401	E	Rehab/Resur	47603+0.00	47607+0.00	CSV
11	1139	401	W	Rehab/Resur	47603+0.00	47607+0.00	CSC
12	1245	403	N	Rehab/Resur	48250+1.65	48255+1.65	CSC
13	1246	403	N	Rehab/Resur	48255+1.65	48270+1.00	CSV
14	1247	403	S	Rehab/Resur	48250+1.65	48255+1.65	CSC
15	1248	403	S	Rehab/Resur	48255+1.65	48270+1.00	CSC
16	1260	403	N	Rehab/Resur	48250+1.65	48255+1.65	CSV
17	1261	403	S	Rehab/Resur	48250+1.65	48255+1.65	CSC
18	1282	406	B	New (Reconst)	48652+0.63	48660+2.46	CSC
19	1287	406	S	New (Reconst)	48652+1.33	48660+2.46	CSV
20	1297	410	N	New (Exten)	49076+0.00	49085+0.00	LC, LV and CSV
21	1301	410	S	New (Exten)	49076+0.00	49085+0.00	LC, LV and CSC
22	1298	410	N	New (Reconst)	49085+0.00	49085+4.00	CSC
23	1302	410	S	New (Reconst)	49085+0.00	49085+4.00	CSV

Table B.3: Summary of the Superpave pavement sections from eastern region

S. No.	Section ID	HWY	Direction	Construction type	Begin chainage	End chainage	Remarks
1	144	7	B	New (Reconst)	14024+0.00	14040+0.00	-
2	156	7	B	Rehab/Resur	14180+6.90	14195+2.63	LC and CSC
3	158	7	B	Rehab/Resur	14200+0.30	14200+8.00	CSC
4	159	7	B	Rehab/Resur	14200+8.00	14210+0.80	CSV
5	166	7	B	Rehab/Resur	14270+0.00	14270+8.70	LC, LV and CSC
6	436	15	B	Rehab/Resur	20010+0.00	20020+3.82	-
7	437	15	B	Rehab/Resur	20020+3.82	20035+0.80	LC, LV and CSC
8	697	41	B	Rehab/Resur	29580+2.80	29590+3.90	LC, LV and CSV
9	698	41	B	Rehab/Resur	29590+3.90	29590+11.30	LC, LV and CSC
10	727	60	B	Rehab/Resur	33240+0.00	33240+7.85	CSV
11	728	60	B	Rehab/Resur	33240+7.85	33250+1.60	CSC
12	752	62	B	Rehab/Resur	33710+6.31	33720+7.20	CSC
13	887	118	B	Rehab/Resur	42620+0.00	42640+0.00	CSV
14	1016	401	E	Rehab/Resur	47200+0.00	47220+0.00	CSV
15	1103	401	W	Rehab/Resur	47200+0.00	47220+0.00	CSC
16	1038	401	E	New (Reconst)	47494+9.13	47500+6.98	-
17	1125	401	W	New (Reconst)	47494+9.13	47500+6.98	-
18	1331	417	E	Rehab/Resur	49500+0.00	49540+0.00	CSC
19	1332	417	E	Rehab/Resur	49540+0.00	49550+0.00	CSV
20	1813	1000	B	Rehab/Resur	99998+27.50	99999+0.00	-

Table B.4: Summary of the Superpave pavement sections from northeast region

S. No.	Section ID	HWY	Direction	Construction type	Begin chainage	End chainage	Remarks
1	265	11	B	Rehab/Resur	17285+18.20	17293+0.00	CSC
2	271	11	B	Rehab/Resur	17360+3.90	17380+0.00	CSC
3	368	11	N	New (Reconst)	17130+1.00	17148+1.00	-
4	404	11	S	New (Reconst)	17130+1.00	17148+1.00	-
5	477	17	B	Rehab/Resur	20940+2.10	20950+16.20	LC, LV and CSV
6	760	63	B	Rehab/Resur	34120+0.00	34133+4.77	CSC
7	764	64	B	Rehab/Resur	34320+0.00	34330+0.80	CSV
8	775	65	B	Rehab/Resur	34560+8.20	34570+8.50	-
9	782	66	B	Rehab/Resur	34770+0.00	34770+17.20	-
10	791	69	B	New (Reconst)	35550+14.30	35560+1.10	CSC
11	842	101	B	Rehab/Resur	40260+0.00	40270+5.60	-
12	843	101	B	Rehab/Resur	40270+5.60	40270+15.30	-
13	951	144	B	Rehab/Resur	46105+24.70	46130+9.90	LC, LV and CSC
14	952	144	B	Rehab/Resur	46130+9.90	46140+0.00	LC, LV and CSC
15	976	400	N	Rehab/Resur	46969+0.00	46972+0.00	CSC
16	977	400	N	Rehab/Resur	46972+0.00	46977+6.20	CSV
17	978	400	N	Rehab/Resur	46977+6.20	46981+2.22	CSC
18	1001	400	S	Rehab/Resur	46969+0.00	46972+0.00	CSC
19	1002	400	S	Rehab/Resur	46972+0.00	46977+6.20	CSC
20	1003	400	S	Rehab/Resur	46977+6.20	46981+2.22	CSV

Table B.5: Summary of the Superpave pavement sections from northwest region

S. No.	Section ID	HWY	Direction	Construction type	Begin chainage	End chainage	Remarks
1	312	11	B	Rehab/Resur	17960+0.00	17970+0.00	CSC
2	313	11	B	Rehab/Resur	17970+0.00	17970+2.21	CSC
3	314	11	B	Rehab/Resur	17970+2.21	17980+0.66	CSV
4	323	11	B	Rehab/Resur	18030+14.43	18040+13.99	LC, LV and CSC
5	328	11	B	Rehab/Resur	18105+0.00	18120+0.00	CSC
6	334	11	B	Rehab/Resur	18190+12.20	18205+4.00	LC, LV and CSC
7	337	11	B	Rehab/Resur	18240+0.20	18240+16.00	CSC
8	342	11	B	Rehab/Resur	18270+20.91	18280+6.99	-
9	563	17	B	Rehab/Resur	22220+13.79	22228+6.35	CSV
10	574	17	B	Rehab/Resur	22250+0.00	22255+0.00	LC, LV and CSC
11	575	17	B	Rehab/Resur	22255+0.00	22260+0.00	LC, LV and CSV
12	576	17	B	Rehab/Resur	22260+0.00	22260+6.00	LC, LV and CSC
13	577	17	B	Rehab/Resur	22260+6.00	22270+0.30	LC, LV and CSC
14	578	17	B	Rehab/Resur	22270+0.30	22272+0.00	LC, LV and CSC
15	868	105	B	Rehab/Resur	41060+1.90	41080+7.69	-

Table B.6: Summary of the Marshall mix pavement sections

S. No.	Section ID	HWY	Direction	Construction type	Begin chainage	End chainage	Remarks
1	9	1	E	New (Reconst)	10066+1.82	10083+2.07	LC, LV and CSV
2	43	1	W	New (Reconst)	10066+1.82	10083+2.07	LC, LV and CSC
3	139	6	S	Rehab/Resur	13605+0.00	13607+0.00	LC and CSC
4	191	7	E	New (Reconst)	14610+0.00	14612+0.50	LC, LV and CSV
5	217	8	E	Rehab/Resur	15864+0.00	15871+0.00	LC, LV and CSC
6	347	11	N	Rehab/Resur	16950+0.00	16950+7.59	LC, LV and CSV
7	348	11	N	Rehab/Resur	16950+7.59	16970+0.00	LC, LV and CSC
8	349	11	N	Rehab/Resur	16970+0.00	17000+0.00	LC, LV and CSC
9	350	11	N	Rehab/Resur	17000+0.00	17000+2.66	LC, LV and CSC
10	353	11	N	Rehab/Resur	17010+6.90	17025+0.00	LC, LV and CSV
11	356	11	N	Rehab/Resur	17030+0.00	17035+0.98	LC and CSC
12	357	11	N	Rehab/Resur	17035+0.98	17040+0.00	LC, LV and CSC
13	358	11	N	Rehab/Resur	17040+0.00	17060+0.00	LC, LV and CSV
14	361	11	N	Rehab/Resur	17073+7.40	17080+0.00	LC, LV and CSC
15	376	11	N	New (Reconst)	18060+0.00	18060+4.10	LC, LV and CSC
16	377	11	S	Rehab/Resur	16950+0.00	16950+7.59	LC, LV and CSC
17	378	11	S	Rehab/Resur	16950+7.59	16970+0.00	LC, LV and CSC
18	379	11	S	Rehab/Resur	16970+0.00	17000+0.00	LC, LV and CSV
19	386	11	S	Rehab/Resur	17030+0.00	17035+0.98	LC, LV and CSC
20	803	85	N	Rehab/Resur	38460+0.00	38470+0.00	LC, LV and CSC
21	811	85	S	Rehab/Resur	38450+0.00	38460+0.00	LC and CSV
22	951	400	N	Rehab/Resur	46827+0.00	46830+0.00	LC and CSV
23	981	400	S	Rehab/Resur	46930+0.00	46941+0.00	LC and CSC
24	1049	401	E	New (Reconst)	47710+1.00	47715+0.00	LC, LV and CSC
25	1053	401	E	New (Reconst)	47725+0.00	47730+0.00	LC and CSV
26	1188	402	E	New (Reconst)	48123+1.90	48123+9.60	LC and CSC
27	1189	402	E	New (Reconst)	48123+9.60	48127+3.70	LC and CSC
28	1200	402	W	New (Reconst)	48123+1.90	48123+7.00	LC and CSC
29	1311	417	E	New (Reconst)	49590+0.00	49593+0.90	LC, LV and CSV

Note: LC = Longitudinal Calibration
 LV = Longitudinal validation
 CSC = Cross-sectional calibration
 CSV = Cross-sectional validation

APPENDIX C: TRAFFIC DATA FOR AASHTOWARE ANALYSIS

Table C.1: Recommended percentage of truck in design lane for Ontario

Number of lanes in one direction	Average annual daily traffic, AADT (both direction)	Lane distribution factors
1	All	1.0
2	< 15,000	0.9
	> 15,000	0.8
3	< 25,000	0.8
	25,000 - 40,000	0.7
	> 40,000	0.6
4	< 40,000	0.7
	> 40,000	0.6
5	< 50,000	0.6
	> 50,000	0.6

Table C.2: Standard speed for different highway class in Ontario

Facility type	Speed (Km/hr)
Freeway	100
Arterial	80
Collector	60
Local	50

Table C.3: Summary of TTC and FHWA vehicle class distribution used in AASHTOWare

TTC group	Bus (%)	Multi-trailer (%)	TTC description	FEWA vehicle class									
				4	5	6	7	8	9	10	11	12	13
1	>2	<2	Predominantly single-trailer trucks	1.3	8.5	2.8	0.3	7.6	74	1.2	3.4	0.6	0.3
2	>2	<2	Predominantly single-trailer trucks with a low percentage of single-unit trucks	2.4	14	4.5	0.7	7.9	66	1.4	2.2	0.3	0.2
3	<2	2-10	Predominantly single-trailer trucks	0.9	12	3.6	0.2	6.7	62	4.8	2.6	1.4	6.2
4	>2	<2	Predominantly single-trailer trucks with a low to moderate amount of single-unit trucks	2.4	23	5.7	1.4	8.1	55	1.7	2.2	0.2	0.4
5	<2	>10	Predominately single-trailer trucks	0.9	14	3.5	0.6	6.9	54	5	2.7	1.2	11
6	>2	<2	Mixed truck traffic with a higher percentage of single-unit trucks	2.8	31	7.3	0.8	9.3	45	2.3	1	0.4	0.3
7	<2	2-10	Mixed truck traffic with a higher percentage of single-trailer trucks	1	24	4.2	0.5	10	42	5.8	2.6	1.3	8.4
8	<2	>10	High percentage of single-trailer truck with some single-unit trucks	1.7	19	4.6	0.9	6.7	45	6	2.6	1.6	12
9	>2	<2	Mixed truck traffic with about equal percentages of single-unit and single-trailer trucks	3.3	34	12	1.6	9.9	36	1	1.8	0.2	0.3
10	<2	2-10	Mixed truck traffic with about equal percentages of single-unit and single-trailer trucks	0.8	31	6.9	0.1	7.8	38	3.7	1.2	4.5	6.7
11	<2	>10	Mixed truck traffic with a higher percentage of single-trailer trucks	1.8	25	7.6	0.5	5	31	9.8	0.8	3.3	15
12	>2	<2	Mixed truck traffic with a higher percentage of single-unit trucks	3.9	41	12	1.5	12	25	2.7	0.6	0.3	1.3
13	<2	>10	Mixed truck traffic with about equal percentages of single-unit and single-trailer trucks	0.8	34	6.2	0.1	7.9	26	11	1.4	3.2	10
14	>2	<2	Predominantly single-unit trucks	2.9	57	10	3.7	9.2	15	0.6	0.3	0.4	0.3
15	<2	2-10	Predominantly single-unit trucks	1.8	57	8.5	1.8	6.2	14	5.4	0	0	5.7
16	<2	>10	Predominantly single-unit trucks	1.3	48	11	1.9	6.7	13	4.3	0.5	0.1	13
17	>25	<2	Mixed truck traffic with about equal single-unit and single-trailer trucks	36	15	13	0.5	15	18	0.5	0.8	0.1	1.5

Table C.4: Axial per truck for southern Ontario

FHWA class	Singles	Tandems	Tridems	Quads	Total
4	1.620	0.390	0.000	0.000	2.400
5	2.000	0.000	0.000	0.000	2.000
6	1.010	0.993	0.000	0.000	2.996
7	1.314	0.989	0.030	0.000	3.382
8	2.163	0.845	0.000	0.000	3.853
9	1.055	1.968	0.003	0.000	5.000
10	1.466	1.234	0.700	0.088	6.366
11	4.546	0.168	0.000	0.000	4.882
12	2.857	1.526	0.000	0.000	5.909
13	1.201	2.058	0.848	0.024	7.957

Table C.5: Axial per truck for northern Ontario

FHWA class	Singles	Tandems	Tridems	Quads	Total
4	1.620	0.390	0.000	0.000	2.400
5	2.000	0.000	0.000	0.000	2.000
6	1.014	0.993	0.000	0.000	3.000
7	1.244	0.962	0.043	0.000	3.297
8	2.414	0.674	0.000	0.000	3.762
9	1.048	1.955	0.014	0.000	5.000
10	1.358	1.165	0.840	0.044	6.384
11	3.849	0.538	0.000	0.000	4.925
12	2.910	1.514	0.021	0.000	6.001
13	1.100	2.012	0.945	0.011	8.003

Table C.6: Single axial load distribution for southern Ontario

Axle weight, kg		Frequency of a given axle weight range as a percentage									
Min	Max	4	5	6	7	8	9	10	11	12	13
0	1360	1.8	0.07	0.19	0.28	0.42	0.04	0.39	0.1	0.02	0.44
1361	1814	0.96	0.33	0.14	0.08	0.42	0.1	0.17	0.09	1.1	0.62
1815	2267	2.91	5.4	0.89	0.45	2.13	0.62	0.44	0.57	0.02	0.85
2268	2721	3.99	7.52	0.73	0.7	2.43	0.43	0.89	1.69	3.23	1.22
2722	3175	6.8	6.65	0.95	0.87	3.56	0.44	0.93	6.75	8.18	1.14
3176	3628	12	11.31	2.12	0.96	7.82	0.62	1.44	5.58	8.74	1.01
3629	4082	11.7	13.95	4.73	1.5	7.21	1.22	1.48	4.29	8.71	0.99
4083	4535	11.4	13.96	13.97	3.13	19.14	10.41	4.39	11.04	14.5	4.92
4536	4989	10.3	10.71	18.4	5.11	13.03	22.57	12.87	14.92	15.76	12.6
4990	5443	9	10.46	24.83	8.09	11.19	40.88	28.9	11.07	14.99	33.62
5444	5896	7.4	5.04	10.68	3.7	3.97	14.53	15.16	7.08	6.41	17.87
5897	6350	5.7	4.37	8.58	9.63	6.09	3.05	6.91	10.43	5.52	8.99
6351	6803	4.3	2.28	4.56	11.06	5.69	1.04	3.37	7.9	4.17	3.33
6804	7257	3.2	1.96	3.66	13.64	3.76	0.92	3.46	6.16	2.13	2.34
7258	7711	2.58	1.65	1.45	11.37	2.13	0.9	3.14	3.66	1.42	1.29
7712	8164	1.8	1.25	1.53	7	3.03	0.83	3.46	2.96	1.03	1.58
8165	8618	1.4	0.8	1.37	5.94	1.45	0.49	2.87	1.75	0.32	1.08
8619	9071	1	0.73	0.42	3.87	1.58	0.28	3.12	0.87	0.83	2.33
9072	9525	0.75	0.5	0.35	5.89	1.41	0.16	1.96	0.66	0	0.72
9526	9979	0.5	0.51	0.23	2.29	0.95	0.13	1.55	0.38	0.1	0.99
9980	10432	0.25	0.27	0.04	1.74	0.59	0.11	1.15	0.14	0.08	0.47
10433	10886	0.15	0.08	0.05	0.23	0.26	0.06	0.38	0.43	0.11	0.21
10887	11339	0.1	0.06	0.02	0.25	0.18	0.03	0.35	0.19	0.19	0.18
11340	11793	0	0.07	0.04	0.46	0.3	0.03	0.23	0	0.7	0.08
11794	12246	0	0.02	0	0.04	0.12	0.01	0.11	0.75	1.27	0.17
12247	12700	0	0.01	0	0.18	0.11	0.01	0.1	0	0	0.06
12701	13154	0	0.01	0	0.11	0.06	0.01	0.13	0.18	0.24	0.18
13155	13607	0	0.01	0	0	0.32	0	0.1	0.07	0	0
13608	14061	0	0.01	0.05	0.06	0.11	0.01	0.05	0.18	0	0.09
14062	14515	0	0.01	0	0.22	0.12	0.01	0.13	0	0	0.24
14516	14968	0	0	0	0.13	0.05	0.01	0.1	0.04	0	0.1
14969	15422	0	0	0	0.02	0.14	0.01	0.04	0.03	0	0
15423	15875	0	0	0	0.23	0.13	0.01	0.07	0	0	0.1
15876	16329	0	0	0	0.09	0.08	0.02	0.04	0.04	0	0
16330	16782	0	0	0	0	0	0	0.01	0	0	0.12
16783	17236	0	0	0	0.37	0.02	0	0.03	0	0	0.01
17237	17690	0	0	0.02	0.06	0	0	0.01	0	0	0.04
17691	18143	0.01	0	0	0.16	0	0.01	0.04	0	0.23	0
18144	20412	0	0	0	0.09	0	0	0.03	0	0	0.02
Total		100	100	100	100	100	100	100	100	100	100

Table C.7: Single axial load distribution for northern Ontario

Axle weight, kg		Frequency of a given axle weight range as a percentage									
Min	Max	Min	Max	Min	Max	Min	Max	Min	Max	Min	Max
0	1360	1.8	0.2	0.22	0	2.13	0.06	0.63	5.54	0.58	0.15
1361	1814	0.96	0.61	0	0	1.88	0.09	0.2	0	0	0.45
1815	2267	2.91	11.58	0.47	0.26	5.41	0.61	0.66	0	2.58	0.58
2268	2721	3.99	10.37	0.36	0	6.2	0.42	0.66	0	1.27	0.61
2722	3175	6.8	8.26	0.09	0.03	7.42	0.22	1.61	5.54	2.51	1.04
3176	3628	12	11.4	7.07	0.17	9.95	0.77	2.06	0	6.42	1.13
3629	4082	11.7	11.52	8.12	0.33	13.52	1.2	2.21	1.93	4.28	1.47
4083	4535	11.4	12.32	10.22	3.28	13.61	4.72	3.17	6.96	12.66	3.71
4536	4989	10.3	8.79	14.41	5.51	7.22	11.71	9.34	17.18	5.81	12.37
4990	5443	9	8.64	30.23	3.8	8.17	42.47	27.56	4.45	22.22	33.58
5444	5896	7.4	3.72	9.15	9.29	2.61	23.52	19.4	10.07	14.3	25.58
5897	6350	5.7	2.32	5.2	23.78	4.01	4.64	8.64	1.93	6.63	10.57
6351	6803	4.3	3.04	4.35	9.4	3.74	2.47	3.75	13.93	8.88	1.6
6804	7257	3.2	1.53	3.12	17.47	4.88	1.94	3.57	13.42	1.45	1.41
7258	7711	2.58	0.62	2.29	4.59	3	1.4	3	0	0	0.91
7712	8164	1.8	1.66	1.45	2.23	1.26	0.66	3.31	7.05	1.04	1.67
8165	8618	1.4	1.14	1.62	4.84	0.73	0.69	3.19	0	3.25	0.85
8619	9071	1	0.91	1.41	4.01	1.42	0.38	2.37	7.05	0	0.91
9072	9525	0.75	0.51	0	6.21	0.17	0.24	1.1	3.02	0	0.23
9526	9979	0.5	0.12	0	1.78	0	0.25	1.19	0	0	0.21
9980	10432	0.25	0.05	0	1.17	0.79	1.2	0.76	0	3.25	0
10433	10886	0.15	0.42	0.22	0.29	0.74	0.08	0.27	0	1.25	0.06
10887	11339	0.1	0.15	0	0.25	0	0.04	0.1	1.93	0.58	0
11340	11793	0	0.12	0	1.15	0	0.06	0.29	0	0	0.07
11794	12246	0	0	0	0	0	0	0.35	0	1.04	0
12247	12700	0	0	0	0	0	0.02	0.17	0	0	0
12701	13154	0	0	0	0	0	0.01	0.07	0	0	0
13155	13607	0	0	0	0	0.82	0.02	0.04	0	0	0.28
13608	14061	0	0	0	0	0	0.03	0.08	0	0	0
14062	14515	0	0	0	0	0.32	0.01	0.09	0	0	0
14516	14968	0	0	0	0.02	0	0	0.05	0	0	0.11
14969	15422	0	0	0	0	0	0.02	0.01	0	0	0
15423	15875	0	0	0	0.13	0	0.02	0.05	0	0	0.12
15876	16329	0	0	0	0	0	0.02	0.01	0	0	0.23
16330	16782	0	0	0	0	0	0.01	0	0	0	0.03
16783	17236	0	0	0	0	0	0	0	0	0	0.07
17237	17690	0	0	0	0.01	0	0	0	0	0	0
17691	18143	0.01	0	0	0	0	0	0.03	0	0	0
18144	20412	0	0	0	0	0	0	0.01	0	0	0
Total		100	100	100	100	100	100	100	100	100	100

Table C.8: Tandem axial load distribution for southern Ontario

Axle weight, kg		Frequency of a given axle weight range as a percentage									
Min	Max	Min	Max	Min	Max	Min	Max	Min	Max	Min	Max
0	2721	5.28	0	1.47	0.73	4.03	0.24	0.35	0	0.25	0.54
2722	3628	10	0	4.13	0.75	3.89	0.52	0.87	7.64	1.16	3.2
3629	4535	11.9	0	23.53	1.24	3.99	2.44	1.45	10.37	2.59	6.79
4536	5442	9.63	0	5.97	2.43	16.72	7.61	2.61	11.48	9.52	5.33
5443	6350	8	0	7.9	4.81	16.55	8.85	6.74	6.64	10.48	7.18
6351	7257	7.8	0	8.95	13.22	16.89	7.84	9.28	5.02	9.4	4.82
7258	8164	6.8	0	8.93	12.24	10.76	7.95	7.71	9.86	13.5	3.36
8165	9071	6.15	0	8.54	9.01	10.57	8.23	5.65	9.45	11.9	2.91
9072	9979	5.8	0	5.77	4	6.36	7.44	4.61	13.19	13.83	2.51
9980	10885	5.3	0	5.72	7.14	3.29	6.63	3.67	8.56	6.92	2.11
10886	11793	4.7	0	4.03	6.9	1.64	5.86	3.41	0	4.29	2.3
11794	12700	4.1	0	2.98	3.49	1.47	5.6	3.98	4.17	6.09	3.05
12701	13607	3.33	0	2.95	2.48	1.17	5.79	5.04	4.61	2.2	2.97
13608	14514	3.91	0	1.75	2.11	0.6	7.32	5.7	1.77	1.72	4.46
14515	15422	2.22	0	1.65	3.48	0.67	8.91	7.03	1.59	1.34	6.64
15423	16329	1.84	0	1.96	1.83	0.89	5.61	8.49	3.51	1.02	10.12
16330	17236	1.44	0	0.54	2.12	0.35	1.71	7.61	0	0.38	10.97
17237	18143	0.9	0	0.77	5.32	0.09	0.77	6.04	0	1.32	9.81
18144	19051	0.5	0	0.51	4.91	0	0.31	4.56	1.44	1.62	5.24
19052	19957	0.3	0	0.52	3.63	0.07	0.15	2.11	0	0.43	1.87
19958	20865	0.1	0	0.54	3.53	0	0.09	1.12	0.7	0	1.35
20866	21772	0	0	0.41	1.47	0	0.05	0.72	0	0	0.61
21773	22679	0	0	0.28	1.44	0	0.04	0.3	0	0	0.43
22680	23587	0	0	0.09	0.35	0	0.01	0.21	0	0	0.41
23588	24493	0	0	0.01	0.12	0	0.01	0.11	0	0	0.43
24494	25401	0	0	0	0.36	0	0.01	0.2	0	0	0.29
25402	26308	0	0	0.03	0.27	0	0.01	0.14	0	0	0.04
26309	27215	0	0	0	0.08	0	0	0.09	0	0.04	0.02
27216	28122	0	0	0	0.31	0	0	0.03	0	0	0.05
28123	29029	0	0	0.03	0	0	0	0.09	0	0	0
29030	29937	0	0	0	0.16	0	0	0.01	0	0	0
29938	30844	0	0	0.04	0	0	0	0.01	0	0	0.01
30845	31751	0	0	0	0	0	0	0.02	0	0	0.01
31752	32659	0	0	0	0	0	0	0.02	0	0	0
32659	33566	0	0	0	0	0	0	0.01	0	0	0.03
33567	34473	0	0	0	0	0	0	0	0	0	0
34474	35380	0	0	0	0.03	0	0	0	0	0	0.01
35381	36287	0	0	0	0	0	0	0	0	0	0.03
36288	38556	0	0	0	0.04	0	0	0.01	0	0	0.1
Total		100	0	100	100	100	100	100	100	100	100

Table C.9: Tandem axial load distribution for northern Ontario

Axle weight, kg		Frequency of a given axle weight range as a percentage									
Min	Max	4	5	6	7	8	9	10	11	12	13
0	2721	5.28	0	0	0.07	5.8	0.1	0.51	0	0	0.92
2722	3628	10	0	2.54	2.81	3.77	0.29	1.2	0	1.12	4.36
3629	4535	11.9	0	24.63	0.32	11.98	1.26	1.78	0	0	6.47
4536	5442	9.63	0	9.79	0.81	16.32	3.61	2.37	39.76	3.7	4.45
5443	6350	8	0	3.94	24.58	27.48	4.76	3.98	60.24	6.17	7.05
6351	7257	7.8	0	8.61	10.06	12.06	5.48	7.6	0	7.24	5.44
7258	8164	6.8	0	10.85	6.22	0.83	4.86	6.11	0	10.13	1.86
8165	9071	6.15	0	10.83	19.04	6.21	6.4	6.43	0	17.37	1.75
9072	9979	5.8	0	3.29	2.01	4.91	6.58	3.44	0	19.34	1.45
9980	10885	5.3	0	2.29	0.77	1.98	8.89	4.85	0	6.55	1.7
10886	11793	4.7	0	0.67	1.69	1.98	8.71	3.85	0	3.85	1.33
11794	12700	4.1	0	5.02	1.15	0.62	8.43	3.85	0	5.46	2.28
12701	13607	3.33	0	2.54	0.84	0	6.32	5.2	0	5.34	3.17
13608	14514	3.91	0	1.35	1.18	0	8.48	5.62	0	0	4.46
14515	15422	2.22	0	0.83	0.66	5.54	10.66	6.55	0	6.26	10.31
15423	16329	1.84	0	3.29	3.6	0	7.85	9.16	0	0	11.82
16330	17236	1.44	0	2.64	5.48	0.52	3.73	7.84	0	6.26	14.12
17237	18143	0.9	0	1.23	1.82	0	1.71	6.42	0	0	9.13
18144	19051	0.5	0	1.65	3.33	0	0.61	5.47	0	0	3.66
19052	19957	0.3	0	1.86	3.68	0	0.34	2.61	0	0	1.32
19958	20865	0.1	0	0.7	2.58	0	0.23	1.34	0	0	0.67
20866	21772	0	0	0.32	0.26	0	0.23	1.65	0	0	0.37
21773	22679	0	0	0.77	2.59	0	0.23	0.37	0	0	0.32
22680	23587	0	0	0.36	1.19	0	0.08	0.41	0	0	0.13
23588	24493	0	0	0	0.06	0	0.11	0.22	0	0	0.33
24494	25401	0	0	0	2.52	0	0.01	0.59	0	0	0.07
25402	26308	0	0	0	0.27	0	0.02	0.33	0	0	0.85
26309	27215	0	0	0	0.19	0	0.01	0	0	1.21	0.05
27216	28122	0	0	0	0	0	0.01	0.1	0	0	0.09
28123	29029	0	0	0	0	0	0	0.04	0	0	0.06
29030	29937	0	0	0	0.22	0	0	0.06	0	0	0
29938	30844	0	0	0	0	0	0	0	0	0	0
30845	31751	0	0	0	0	0	0	0	0	0	0.01
31752	32659	0	0	0	0	0	0	0	0	0	0
32659	33566	0	0	0	0	0	0	0	0	0	0
33567	34473	0	0	0	0	0	0	0	0	0	0
34474	35380	0	0	0	0	0	0	0	0	0	0
35381	36287	0	0	0	0	0	0	0	0	0	0
36288	38556	0	0	0	0	0	0	0.05	0	0	0
Total		100	0	100	100	100	100	100	100	100	100

Table C.10: Tridem axial load distribution for southern Ontario

Axle weight, kg		Frequency of a given axle weight range as a percentage									
Min	Max	4	5	6	7	8	9	10	11	12	13
0	5443	0	0	0	4.27	0	39.91	4.98	0	0	6.5
5444	6803	0	0	0	9.25	0	7.59	9.66	0	0	11.03
6804	8164	0	0	0	10.95	0	19.97	9.53	0	0	6.55
8165	9525	0	0	0	0.28	0	5.9	7.21	0	0	3.69
9526	10886	0	0	0	14.25	0	0.67	5.22	0	0	2.44
10887	12246	0	0	0	1.96	0	5.32	5.06	0	0	2.3
12247	13607	0	0	0	4.52	0	2.18	4.38	0	0	2.18
13608	14968	0	0	0	2.1	0	8.21	4.32	0	0	4.16
14969	16329	0	0	0	12.3	0	3.59	4.56	0	0	4.46
16330	17690	0	0	0	0.64	0	1.73	4.82	0	0	4.54
17691	19050	0	0	0	0	0	3.42	5.87	0	0	3.9
19051	20411	0	0	0	0.5	0	1.22	5.44	0	0	7.33
20412	21772	0	0	0	0	0	0	6.96	0	0	11.94
21773	23133	0	0	0	9.85	0	0	6.31	0	0	14.85
23134	24494	0	0	0	2.99	0	0.29	5.68	0	0	8.24
24495	25854	0	0	0	6.69	0	0	4.5	0	0	3.49
25855	27215	0	0	0	9.35	0	0	2.2	0	0	1.43
27216	28576	0	0	0	4.55	0	0	1.25	0	0	0.34
28577	29937	0	0	0	5.55	0	0	0.6	0	0	0.35
29938	31298	0	0	0	0	0	0	0.32	0	0	0.16
31299	32658	0	0	0	0	0	0	0.31	0	0	0.04
32659	34019	0	0	0	0	0	0	0.25	0	0	0.01
34020	35380	0	0	0	0	0	0	0.28	0	0	0.06
35381	36741	0	0	0	0	0	0	0.11	0	0	0
36742	38102	0	0	0	0	0	0	0.04	0	0	0
38103	39462	0	0	0	0	0	0	0.05	0	0	0
39463	40823	0	0	0	0	0	0	0.09	0	0	0.01
40824	42184	0	0	0	0	0	0	0	0	0	0
42185	43545	0	0	0	0	0	0	0	0	0	0
43546	44906	0	0	0	0	0	0	0	0	0	0
44907	47628	0	0	0	0	0	0	0	0	0	0
Total		0	0	0	100	0	100	100	0	0	100

Table C.11: Tridem axial load distribution for northern Ontario

Axle weight, kg		Frequency of a given axle weight range as a percentage									
Min	Max	4	5	6	7	8	9	10	11	12	13
0	5443	0	0	0	0	0	7.02	5.25	0	0	5.62
5444	6803	0	0	0	20.17	0	5.16	7.54	0	100	13.66
6804	8164	0	0	0	0	0	0	8.65	0	0	6.55
8165	9525	0	0	0	44.49	0	0.19	6.67	0	0	2.23
9526	10886	0	0	0	9.56	0	0.86	4.91	0	0	2.02
10887	12246	0	0	0	0	0	5.33	4.48	0	0	1.16
12247	13607	0	0	0	0	0	1.05	4.85	0	0	1.75
13608	14968	0	0	0	0	0	77.01	5.07	0	0	2.42
14969	16329	0	0	0	0	0	0.13	5.21	0	0	3.41
16330	17690	0	0	0	0	0	0	4.96	0	0	4.28
17691	19050	0	0	0	0	0	2.78	7.72	0	0	4.74
19051	20411	0	0	0	0	0	0	6.04	0	0	10.07
20412	21772	0	0	0	13.2	0	0	5.54	0	0	13.11
21773	23133	0	0	0	12.58	0	0.28	6.9	0	0	17.58
23134	24494	0	0	0	0	0	0.19	5.39	0	0	6.99
24495	25854	0	0	0	0	0	0	4.26	0	0	2.47
25855	27215	0	0	0	0	0	0	2.05	0	0	0.51
27216	28576	0	0	0	0	0	0	1.57	0	0	0.48
28577	29937	0	0	0	0	0	0	0.98	0	0	0.27
29938	31298	0	0	0	0	0	0	0.87	0	0	0.07
31299	32658	0	0	0	0	0	0	0.47	0	0	0.55
32659	34019	0	0	0	0	0	0	0.29	0	0	0.06
34020	35380	0	0	0	0	0	0	0.18	0	0	0
35381	36741	0	0	0	0	0	0	0.09	0	0	0
36742	38102	0	0	0	0	0	0	0.04	0	0	0
38103	39462	0	0	0	0	0	0	0	0	0	0
39463	40823	0	0	0	0	0	0	0	0	0	0
40824	42184	0	0	0	0	0	0	0	0	0	0
42185	43545	0	0	0	0	0	0	0.02	0	0	0
43546	44906	0	0	0	0	0	0	0	0	0	0
44907	47628	0	0	0	0	0	0	0	0	0	0
Total		0	0	0	100	0	100	100	0	100	100

Table C.12: Quad axial load distribution for southern Ontario

Axle weight, kg		Frequency of a given axle weight range as a percentage									
Min	Max	4	5	6	7	8	9	10	11	12	13
0	5443	0	0	0	0	0	0	1.24	0	0	4.29
5444	6803	0	0	0	0	0	0	4.17	0	0	8.96
6804	8164	0	0	0	0	0	0	6.18	0	0	13.81
8165	9525	0	0	0	0	0	0	6.07	0	0	5.32
9526	10886	0	0	0	0	0	0	4.72	0	0	0.76
10887	12246	0	0	0	0	0	0	5.88	0	0	0
12247	13607	0	0	0	0	0	0	3.56	0	0	2.2
13608	14968	0	0	0	0	0	0	2.04	0	0	2.95
14969	16329	0	0	0	0	0	0	2.87	0	0	13.86
16330	17690	0	0	0	0	0	0	2.37	0	0	0.82
17691	19050	0	0	0	0	0	0	3.58	0	0	3.17
19051	20411	0	0	0	0	0	0	3.03	0	0	8.65
20412	21772	0	0	0	0	0	0	5.41	0	0	2.04
21773	23133	0	0	0	0	0	0	6.93	0	0	5.77
23134	24494	0	0	0	0	0	0	8.53	0	0	11.66
24495	25854	0	0	0	0	0	0	6.93	0	0	7.89
25855	27215	0	0	0	0	0	0	4.36	0	0	0.23
27216	28576	0	0	0	0	0	0	3.85	0	0	0.39
28577	29937	0	0	0	0	0	0	3.72	0	0	0
29938	31298	0	0	0	0	0	0	3.79	0	0	0
31299	32658	0	0	0	0	0	0	3.13	0	0	3.09
32659	34019	0	0	0	0	0	0	3.6	0	0	4.14
34020	35380	0	0	0	0	0	0	1.5	0	0	0
35381	36741	0	0	0	0	0	0	0.79	0	0	0
36742	38102	0	0	0	0	0	0	0.35	0	0	0
38103	39462	0	0	0	0	0	0	1.02	0	0	0
39463	40823	0	0	0	0	0	0	0.16	0	0	0
40824	42184	0	0	0	0	0	0	0.06	0	0	0
42185	43545	0	0	0	0	0	0	0.16	0	0	0
43546	44906	0	0	0	0	0	0	0	0	0	0
44907	47628	0	0	0	0	0	0	0	0	0	0
Total		0	0	0	0	0	0	100	0	0	100

Table C.13: Quad axial load distribution for northern Ontario

Axle weight, kg		Frequency of a given axle weight range as a percentage									
Min	Max	4	5	6	7	8	9	10	11	12	13
0	5,443	0	0	0	0	0	0	3.18	0	0	5.81
5,444	6,803	0	0	0	0	0	0	5.33	0	0	9.56
6,804	8,164	0	0	0	0	0	0	10.25	0	0	3.09
8,165	9,525	0	0	0	0	0	0	5.2	0	0	0
9,526	10,886	0	0	0	0	0	0	1.99	0	0	0
10,887	12,246	0	0	0	0	0	0	3.35	0	0	0
12,247	13,607	0	0	0	0	0	0	2.62	0	0	3.09
13,608	14,968	0	0	0	0	0	0	2.12	0	0	6.47
14,969	16,329	0	0	0	0	0	0	4.23	0	0	3.84
16,330	17,690	0	0	0	0	0	0	2.48	0	0	9.37
17,691	19,050	0	0	0	0	0	0	1.01	0	0	0
19,051	20,411	0	0	0	0	0	0	0.23	0	0	0
20,412	21,772	0	0	0	0	0	0	7.56	0	0	3.37
21,773	23,133	0	0	0	0	0	0	3.05	0	0	2.44
23,134	24,494	0	0	0	0	0	0	4.18	0	0	45.93
24,495	25,854	0	0	0	0	0	0	7.42	0	0	0.09
25,855	27,215	0	0	0	0	0	0	3.19	0	0	6.94
27,216	28,576	0	0	0	0	0	0	5.91	0	0	0
28,577	29,937	0	0	0	0	0	0	6.43	0	0	0
29,938	31,298	0	0	0	0	0	0	5.29	0	0	0
31,299	32,658	0	0	0	0	0	0	4.38	0	0	0
32,659	34,019	0	0	0	0	0	0	8.45	0	0	0
34,020	35,380	0	0	0	0	0	0	1.64	0	0	0
35,381	36,741	0	0	0	0	0	0	0	0	0	0
36,742	38,102	0	0	0	0	0	0	0	0	0	0
38,103	39,462	0	0	0	0	0	0	0	0	0	0
39,463	40,823	0	0	0	0	0	0	0.51	0	0	0
40,824	42,184	0	0	0	0	0	0	0	0	0	0
42,185	43,545	0	0	0	0	0	0	0	0	0	0
43,546	44,906	0	0	0	0	0	0	0	0	0	0
44,907	47,628	0	0	0	0	0	0	0	0	0	0
Total		0	0	0	0	0	0	100	0	0	100

Table C.14: Ontario's traffic information for Superpave pavement sections from western region

S. No.	Section ID	HWY	Zone	Design Life (Years)	Total AADTT	No. of lanes	Facility Type	TTC Class
1	77	3	SO	11	10400	2	Arterial	11
2	78	3	SO	11	10100	2	Arterial	11
3	79	3	SO	14	8550	2	Arterial	11
4	80	3	SO	14	6000	2	Arterial	11
5	114	6	SO	7	5500	2	Arterial	11
6	115	6	SO	7	5500	2	Arterial	11
7	197	7	SO	9	21300	2	Arterial	11
8	206	7	SO	9	21300	2	Arterial	11
9	219	8	SO	6	3900	2	Arterial	11
10	221	8	SO	6	5900	2	Arterial	11
11	252	10	SO	10	4900	2	Arterial	11
12	253	10	SO	10	4900	2	Arterial	11
13	587	21	SO	6	6900	2	Arterial	11
14	589	21	SO	11	3750	2	Arterial	11
15	600	21	SO	5	4200	2	Arterial	11
16	613	23	SO	9	5950	2	Arterial	11
17	835	93	SO	12	8150	2	Arterial	11
18	1217	402	SO	12	17600	2	Freeway	11
19	1230	402	SO	12	17600	2	Freeway	11
20	1240	403	SO	9	41500	2	Freeway	11
21	1255	403	SO	9	41500	2	Freeway	11

Table C.15: Ontario's traffic information for Superpave pavement sections from central region

S. No.	Section ID	HWY	Zone	Design Life (Years)	Total AADTT	No. of lanes	Facility Type	TTC Class
1	105	6	SO	12	7500	2	Arterial	11
2	425	12	SO	8	10900	2	Arterial	11
3	426	12	SO	5	11200	2	Arterial	11
4	670	35	SO	10	6700	2	Arterial	11
5	673	35	SO	10	6700	2	Arterial	11
6	719	58	SO	7	16000	2	Arterial	11

7	825	89	SO	11	13200	2	Arterial	11
8	826	89	SO	5	11900	2	Arterial	11
9	1052	401	SO	6	157700	4	Freeway	11
10	1139	401	SO	6	157700	4	Freeway	11
11	1245	403	SO	12	180100	4	Freeway	11
12	1246	403	SO	5	165700	4	Freeway	11
13	1247	403	SO	12	180100	4	Freeway	11
14	1248	403	SO	5	165700	4	Freeway	11
15	1260	403	SO	12	180100	3	Freeway	11
16	1261	403	SO	12	180100	3	Freeway	11
17	1282	406	SO	8	21100	2	Freeway	11
18	1287	406	SO	8	21100	2	Freeway	11
19	1297	410	SO	8	116900	3	Freeway	11
20	1301	410	SO	8	116900	3	Freeway	11
21	1298	410	SO	6	116900	3	Freeway	11
22	1302	410	SO	6	116900	3	Freeway	11

Table C.16: Ontario's traffic information for Superpave pavement sections from eastern region

S. No.	Section ID	HWY	Zone	Design Life (Years)	Total AADTT	No. of lanes	Facility Type	TTC Class
1	156	7	SO	8	4850	2	Arterial	11
2	158	7	SO	5	7450	2	Arterial	11
3	159	7	SO	7	8000	2	Arterial	11
4	166	7	SO	11	9550	2	Arterial	11
5	437	15	SO	12	5350	2	Arterial	11
6	697	41	SO	7	2400	2	Arterial	11
7	698	41	SO	8	1450	2	Arterial	11
8	727	60	SO	7	2600	2	Arterial	11
9	728	60	SO	7	2150	2	Arterial	11
10	752	62	SO	7	4750	2	Arterial	11
11	887	118	SO	7	1500	2	Arterial	11
12	1016	401	SO	10	18100	2	Freeway	11
13	1103	401	SO	10	18100	2	Freeway	11
14	1331	417	SO	5	94600	2	Freeway	11
15	1332	417	SO	9	65800	2	Freeway	11

Table C.17: Ontario's traffic information for Superpave pavement sections from northeast region

S. No.	Section ID	HWY	Zone	Design Life (Years)	Total AADTT	No. of lanes	Facility Type	TTC Class
1	265	11	NO	7	4150	2	Freeway	11
2	271	11	NO	6	5000	2	Arterial	11
3	477	17	NO	10	6700	2	Freeway	11
4	760	63	NO	7	2800	2	Arterial	11
5	764	64	NO	7	1750	2	Arterial	11
6	791	69	NO	7	6400	2	Freeway	11
7	951	144	NO	11	990	2	Arterial	11
8	952	144	NO	11	990	2	Arterial	11
9	976	400	NO	8	9850	2	Freeway	11
10	977	400	NO	8	9300	2	Freeway	11
11	978	400	NO	8	8150	2	Freeway	11
12	1001	400	NO	8	9850	2	Freeway	11
13	1002	400	NO	8	9300	2	Freeway	11
14	1003	400	NO	8	8150	2	Freeway	11

Table C.18: Ontario's traffic information for Superpave pavement sections from northwest region

S. No.	Section ID	HWY	Zone	Design Life (Years)	Total AADTT	No. of lanes	Facility Type	TTC Class
1	312	11	NO	5	4600	2	Freeway	11
2	313	11	NO	5	4350	2	Freeway	11
3	314	11	NO	5	4350	2	Freeway	11
4	323	11	NO	10	5050	2	Freeway	11
5	328	11	NO	5	4800	2	Freeway	11
6	334	11	NO	9	750	2	Freeway	11
7	337	11	NO	6	780	2	Freeway	11
8	563	17	NO	6	4400	2	Freeway	11
9	574	17	NO	9	2400	2	Freeway	11
10	575	17	NO	9	2650	2	Freeway	11
11	576	17	NO	9	2850	2	Freeway	11
12	577	17	NO	9	3100	2	Freeway	11
13	578	17	NO	9	2750	2	Freeway	11

Table C.19: Ontario's traffic information for the Marshall mix pavement sections

S. No.	Section ID	HWY	Zone	Design Life (Years)	Total AADTT	No. of lanes	Facility Type	TTC Class
1	9	1	SO	14	84100	3	Freeway	11
2	43	1	SO	14	84100	3	Freeway	11
3	139	6	SO	10	34900	2	Arterial	11
4	191	7	SO	10	20700	2	Freeway	11
5	217	8	SO	12	96000	4	Freeway	11
6	347	11	SO	14	40500	2	Arterial	11
7	348	11	SO	14	37900	2	Arterial	11
8	349	11	SO	13	38500	2	Freeway	11
9	350	11	SO	14	25400	2	Arterial	11
10	353	11	SO	14	25400	2	Arterial	11
11	356	11	NO	13	16100	2	Arterial	11
12	357	11	NO	14	22500	2	Arterial	11
13	358	11	NO	14	16100	2	Arterial	11
14	361	11	NO	12	17800	2	Arterial	11
15	376	11	NO	12	8250	2	Arterial	11
16	377	11	SO	14	40500	2	Arterial	11
17	378	11	SO	14	37900	2	Arterial	11
18	379	11	SO	13	38500	2	Freeway	11
19	386	11	NO	13	16100	2	Arterial	11
20	803	85	SO	11	72000	2	Freeway	11
21	811	85	SO	11	95100	2	Freeway	11
22	951	400	SO	14	91700	3	Freeway	11
23	981	400	SO	14	13400	2	Freeway	11
24	1049	401	SO	12	101800	3	Freeway	11
25	1053	401	SO	11	193000	3	Freeway	11
26	1188	402	SO	12	15000	2	Freeway	11
27	1189	402	SO	12	15000	2	Freeway	11
28	1200	402	SO	13	20500	2	Freeway	11
29	1311	417	SO	13	25050	2	Freeway	11

APPENDIX D: CLIMATIC DATA FOR AASHTOWARE ANALYSIS

Table D.1: Ontario's weather stations

Station	Station name	Location	Latitude	Longitude	Elevation
15801	Armstrong	Armstrong Airport	50.294	-88.905	322
94932	Atikokan	Atikokan	48.750	-91.617	395
15806	Big Trout Lake	Big Trout Lake	53.833	-89.867	224
94862	Chapleau	Chapleau	47.833	-83.433	428
94797	Earlton	Earlton Airport	47.700	-79.850	243
94864	Geraldton	Geraldton	49.700	-86.950	331
94888	Geraldton	Geraldton Airport	49.783	-86.931	349
94803	Gore Bay	Gore Bay Airport	45.883	-82.567	194
14998	Graham	Graham Airport	49.267	-90.583	503
4797	Hamilton	Hamilton Airport	43.172	-79.934	238
14899	Kapuskasing	Kapuskasing Airport	49.414	-82.468	226
14999	Kenora	Kenora Airport	49.790	-94.365	410
94799	Killaloe	Killaloe	45.567	-77.417	174
94805	London	London Airport	43.033	-81.151	278
94857	Mount Forest	Mount Forest	43.983	-80.750	415
15804	Nakina	Nakina Airport	50.183	-86.700	325
4705	North Bay	North Bay Airport	46.364	-79.423	370
4772	Ottawa	Macdonald-Cartier International Airport	45.323	-75.669	114
4706	Ottawa	Ottawa Rockcliff Airport	45.450	-75.633	54
54706	Petawawa	Petawawa Airport	45.950	-77.317	130
94842	Sault Ste Marie	Sault Ste Marie Airport	46.483	-84.509	192
94858	Simcoe	Simcoe	42.850	-80.267	240
15909	Sioux Lookout	Sioux Lookout Airport	50.117	-91.900	383
4713	Stirling	Stirling	44.317	-77.633	139
94828	Sudbury	Sudbury Airport	46.625	-80.799	347
94804	Thunder Bay	Thunder Bay Airport	48.369	-89.327	199
94831	Timmins	Victor Power Airport	48.570	-81.377	295
54753	Toronto	Buttonville Airport	43.862	-79.370	198
94791	Toronto	Lester B. Pearson International Airport	43.677	-79.631	173
4715	Trenton	Trenton Airport	44.117	-77.533	86
94808	White River	White River	48.600	-85.283	379
94809	Warton	Warton Airport	44.746	-81.107	222
94810	Windsor	Windsor Airport	42.276	-82.956	190
15807	Winisk	Winisk Airport	55.233	-85.117	13

Table D.2: Location parameters for selected Superpave pavement sections from western region

S. No.	Section ID	HWY	Latitude	Longitude	Elevation (m)
1	77	3	42.77844	-81.14647	233.874
2	78	3	42.78940	-81.14682	245.149
3	79	3	42.80313	-81.20982	229.832
4	80	3	42.80301	-81.25256	232.832
5	114	6	43.88480	-80.61130	460.000
6	115	6	43.96120	-80.72460	425.000
7	197	7	43.40913	-80.54814	363.170
8	206	7	43.40913	-80.54814	363.170
9	219	8	43.52190	-81.32030	335.000
10	221	8	43.66140	-81.61830	269.000
11	252	10	44.31670	-80.79465	377.000
12	253	10	44.45594	-80.89764	294.000
13	587	21	43.30790	-81.76020	185.000
14	589	21	43.34740	-81.72740	187.000
15	600	21	44.26700	-81.54400	240.000
16	613	23	43.91320	-80.87155	385.000
17	835	93	44.71885	-79.89745	219.000
18	1217	402	42.99160	-82.00270	223.000
19	1230	402	42.99160	-82.00270	223.000
20	1240	403	43.18866	-80.09823	212.000
21	1255	403	43.18866	-80.09823	212.000

Table D.3: Location parameters for selected Superpave pavement sections from central region

S. No.	Section ID	HWY	Latitude	Longitude	Elevation (m)
1	105	6	43.20427	-79.96635	242.842
2	425	12	44.25800	-79.06300	264.000
3	426	12	44.48990	-79.15370	223.000
4	670	35	43.95255	-78.60636	124.896
5	673	35	43.95255	-78.60636	124.896
6	719	58	43.11507	-79.18576	174.973
7	825	89	44.15350	-79.90270	236.000
8	826	89	44.12610	-79.96880	265.000
9	1052	401	43.83920	-79.07040	90.000

10	1139	401	43.83920	-79.07040	90.000
11	1245	403	43.62170	-79.63670	148.000
12	1246	403	43.60040	-79.64470	156.000
13	1247	403	43.62170	-79.63670	148.000
14	1248	403	43.60040	-79.64470	156.000
15	1260	403	43.62170	-79.63670	148.000
16	1261	403	43.62170	-79.63670	148.000
17	1282	406	43.04580	-79.23570	182.000
18	1287	406	43.04580	-79.23570	182.000
19	1297	410	43.75674	-79.79863	257.842
20	1301	410	43.75674	-79.79863	257.842
21	1298	410	43.71140	-79.83140	249.000
22	1302	410	43.71140	-79.83140	249.000

Table D.4: Location parameters for selected Superpave pavement sections from eastern region

S. No.	Section ID	HWY	Latitude	Longitude	Elevation (m)
1	156	7	44.46738	-77.72179	205.000
2	158	7	44.43300	-77.89380	216.000
3	159	7	44.38190	-77.98030	203.000
4	166	7	44.29889	-78.56030	252.738
5	437	15	44.47235	-76.24013	97.606
6	697	41	44.39601	-79.68255	255.000
7	698	41	44.39221	-79.70049	240.000
8	727	60	45.58770	-77.34070	178.000
9	728	60	45.55430	-77.42540	190.000
10	752	62	44.43400	-77.46210	186.000
11	887	118	44.99230	-78.15110	427.000
12	1016	401	45.13700	-74.49590	50.000
13	1103	401	45.13700	-74.49590	50.000
14	1331	417	45.32450	-75.87600	100.000
15	1332	417	45.31330	-75.89880	94.000

Table D.5: Location parameters for selected Superpave pavement sections from northeast region

S. No.	Section ID	HWY	Latitude	Longitude	Elevation (m)
1	265	11	47.26780	-79.77330	378.000
2	271	11	47.89290	-79.94360	255.000
3	477	17	46.36407	-79.67950	204.000
4	760	63	46.38620	-79.25710	270.000
5	764	64	46.13050	-80.43170	217.000
6	791	69	46.62500	-80.79900	347.000
7	951	144	47.47800	-81.84931	407.000
8	952	144	47.54397	-81.85467	398.00
9	976	400	44.84530	-79.73580	195.000
10	977	400	44.87780	-79.74710	190.000
11	978	400	44.92830	-79.77500	199.000
12	1001	400	44.84530	-79.73580	195.000
13	1002	400	44.87780	-79.74710	190.000
14	1003	400	44.92830	-79.77500	199.000

Table D.6: Location parameters for selected Superpave pavement sections from northwest region

S. No.	Section ID	HWY	Latitude	Longitude	Elevation (m)
1	312	11	49.02110	-88.28690	252.000
2	313	11	49.02210	-88.29820	269.000
3	314	11	48.96010	-88.33480	229.000
4	323	11	48.48020	-89.18770	243.000
5	328	11	48.40170	-89.61410	284.000
6	334	11	48.37906	-89.44588	224.000
7	337	11	48.72500	-91.59840	427.000
8	563	17	49.7427	-95.11330	365.000
9	574	17	49.76397	-94.32793	373.000
10	575	17	49.80032	-94.40758	336.000
11	576	17	49.78924	-94.54697	317.000
12	577	17	49.76973	-94.63829	354.000
13	578	17	49.73336	-94.65752	342.000

Table D.7: Location parameters for Marshall mix pavement sections

S. No.	Section ID	HWY	Latitude	Longitude	Elevation (m)
1	9	1	43.08924	-79.11903	198.120
2	43	1	43.08925	-79.11881	197.206
3	139	6	43.70005	-80.37318	406.908
4	191	7	43.39606	-80.63884	363.322
5	217	8	43.41522	-80.40606	304.495
6	347	11	44.43490	-79.64348	258.775
7	348	11	44.43490	-79.64348	290.170
8	349	11	44.57118	-79.44331	225.857
9	350	11	44.6441	-79.42114	242.926
10	353	11	44.77184	-79.33462	220.370
11	356	11	44.90746	-79.36159	250.241
12	357	11	44.93859	-79.34096	259.690
13	358	11	44.99535	-79.30609	270.053
14	361	11	45.27612	-79.28038	298.399
15	376	11	48.48353	-89.18184	251.765
16	377	11	44.43125	-79.64854	247.802
17	378	11	44.46613	-79.56471	290.170
18	379	11	44.7118	-79.44331	225.857
19	386	11	44.90746	-79.36159	250.241
20	803	85	43.47389	-80.48445	323.698
21	811	85	43.46202	-80.47127	322.174
22	951	400	43.84686	-79.54849	227.990
23	981	400	44.55246	-79.74560	250.241
24	1049	401	43.48557	-79.99804	297.790
25	1053	401	43.41816	-80.290352	317.297
26	1188	402	42.93355	-81.48001	248.717
27	1189	402	42.96690	-81.5553	236.220
28	1200	402	42.93369	-81.47968	248.717
29	1311	417	45.27215	-75.98257	130.150

APPENDIX E: PAVEMENT MATERIAL AND STRUCTURAL DATA FOR AASHTOWARE ANALYSIS

Table E.1: Ontario's typical superpave and SMA properties

Asphalt Layer	Unit Weight (Kg/m ³)	Region	Effective Binder Content (%)	Air Voids (%)	Sieve Passing %			
					19 mm	9.5 mm	4.75 mm	0.075 mm
SP 12.5	2460	All	11.8	4	100	83.2	54	4
SP 12.5 FC1	2530	WR	11.8	4	100	83.2	54	4
	2520	CR						
	2390	ER						
	2520	NR						
SP 12.5 FC2	2530	WR	10.8	4	100	83.2	54	4
	2520	CR						
	2390	ER						
	2520	NR						
SP 19.0	2460	All	11.2	4	96.9	72.5	52.8	3.9
SP 25.0	2469	All	10.4	4	89.1	63.3	49.3	3.8
SMA 12.5	2530	WR	14.6	4	100	73.1	29.7	9.3
	2520	CR						
	2390	ER						
	2520	NR						

Table E.2: Ontario's typical Marshall mix properties

Asphalt Layer	Unit Weight (Kg/m ³)	Region	Effective Binder Content (%)	Air Voids (%)	Sieve Passing %			
					19 mm	9.5 mm	4.75 mm	0.075 mm
DFC	2520	All	12.4	3.5	100	82.5	52.5	2.5
HDBC & HDB	2460		10.9	4	97	63	43.5	3
MDBC	2500		12.3	4	97	63	40	3
HL-1	2520		12.4	4	100	82.5	55	2.5
HL-2	2410		14.2	5	100	100	92.5	5.5
HL-3	2520		12.4	4	100	82.5	55	2.5
HL-4	2480		12.2	4	100	72	53.5	3
HL-5	2520		10.9	4	97	72	53.5	3
HL-6	2460		10.9	4	97	72	53.5	3
HL-8	2460		10.9	4	97	63	42.5	3

Table E.3: Ontario's recommended asphalt stabilized material properties

Asphalt Layer	Unit Weight (Kg/m ³)	Region	Effective Binder Content (%)	Air Voids (%)	Sieve Passing %			
					19 mm	9.5 mm	4.75 mm	0.075 mm
CIR	2240	All	12.5	9	100	83	63	6
CIREAM	2110		13.5	13.5	100	83	63	6
EAS	2170		11.7	10	97	73	58	7

Table E.4: Ontario's typical granular material properties

Granular Type	Resilient Modulus (MPa)	Liquid Limit	Plasticity Index		Sieve Passing %			
					25 mm	19 mm	9.5 mm	4.75 mm
Granular A	250	6	0	100	92.5	61.5	45	5
Granular B-I	150	11	0	75	-	-	60	4
Granular B-II	200	11	0	75	-	-	37.5	5
Granular O	200	6	0	100	97.5	70	60	2.5

Table E.5: Ontario's typical chemically stabilized base material properties

Material Type	Unit Weight (Kg/m ³)	Poison Ratio	Modulus of Rupture (MPa)	Resilient Modulus (MPa)	Thermal Conductivity (watt/meter-Kelvin)	Heat capacity (J/kg-K)
OGDL	1700	0.4	4.5	400	2.16	1172
CTB	2400	0.2	4.5	690	2.16	1172

Table E.6: Ontario's typical fine sub-grade soil properties

Granular Type	Resilient Modulus (MPa)	Liquid Limit	Plasticity Index		Sieve Passing %			
					19 mm	9.5 mm	4.75 mm	0.075 mm
CL	20	26	12	100	99	97	80	30
CI	20	41	21	100	100	99	88	37
CH	20	67	43	100	100	99	92	60
CL - ML	22	22	6	100	99	98	84	16
ML	25	26	3	100	100	96	74	11
MI	25	42	15	100	100	100	82	25
MH	20	53	21	100	100	100	84	40
SM	35	18	4	98	94	90	29	8
SC	30	22	10	100	100	93	32	13

Table E.7: Material and structural information for the selected Superpave sections from western region

S. No.	Section ID	Activity	HWY	Layer Thickness (mm)					Layer Material					Sub-grade	Resilient Modulus (MPa)
				Lay 1	Lay 2	Lay 3	Lay 4	Lay 5	Lay 1	Lay 2	Lay 3	Lay 4	Lay 5		
1	77	Recon_ Ac3	3	40	60	70	200	150	SP12.5 FC2 (58-28)	SP19 (58-28)	SP19 (58-28)	Granular A	Granular B	CI	36
2	78														
3	79	Mil + Ovly2	3	40	60	150	230	-	SP12.5 FC2 (64-28)	SP19 (64-28)	HL-4	Granular B-I	-	CL- ML	30
4	80														
5	114	FDR + Ovly3	6	40	50	50	225	-	SP12.5 FC1 (58-28)	SP19 (58-28)	SP19 (58-28)	Granular A	-	SM	35
6	115														
7	197	Mil + Ovly2	7	40	60	60	300	300	SP12.5 FC2 (58-28)	SP19 (58-28)	SP19 (58-28)	Granular A	Granular B-I	SM	30
8	206														
9	219	EAS_ Ovly2	8	40	80	300	200	350	SP12.5 (58-28)	SP12.5 (58-28)	Granular A	Granular A	Granular B-I	CL- ML	25
10	221	CIR + Ovly1	8	50	120	300	200	-	SP12.5 FC1 (58-28)	CIR	Granular A	Granular A	-	CL- ML	25
11	252	HM Ovly1	10	50	100	200	300	-	SP12.5 FC1 (58-28)	SP19 (58-28)	Granular A	Granular B-I	-	SM	35
12	253														
13	587	CIR + Ovly1	21	50	110	180	-	-	SP12.5 FC1 (58-28)	CIR	Granular B	-	-	SM	40
14	589	Recon_ Ac3	21	60	75	320	-	-	SP12.5 (58-28)	SP19 (58-28)	Granular A	-	-	CL- ML	30
15	600	CIR + Ovly1	21	40	110	100	200	560	SP12.5 (58-28)	SP19 (58-28)	Granular A	Granular A	Granular B-I	MI	35
16	613	FDR + Ovly3	23	40	50	50	100	150	SP12.5 FC1 (58-28)	SP19 (58-28)	SP19 (58-28)	Granular A	Granular B-I	CI	35
17	835	FDR + Ovly3	93	40	100	150	450	-	SP12.5 FC1 (58-28)	SP19 (58-28)	Granular A	Granular B-I	-	CL	20
18	1217	Recon_ Ac5F	402	40	120	80	100	550	SP12.5 FC2 (64-28)	SP19 (64-28)	SP25 (58-28)	SP25 (58-28)	Granular A	CL- ML	27
19	1230														
20	1240	Mil + Ovly2	403	40	100	120	225	375	SP12.5 FC2 (64-28)	SP19 (64-28)	HL-4	Granular A	Granular B	SM	40
21	1255														

Table E.8: Material and structural information for the selected Superpave sections from central region

S. No.	Section ID	Activity	HWY	Layer Thickness (mm)					Layer Material					Sub-grade	Resilient Modulus (MPa)
				Lay 1	Lay 2	Lay 3	Lay 4	Lay 5	Lay 1	Lay 2	Lay 3	Lay 4	Lay 5		
1	105	Recon_Ac3	6	40	50	110	150	250	SP12.5 FC2 (64-28)	SP19 (58-28)	SP19 (58-28)	Granular A	Granular B-I	CL-ML	30
2	425	Mil + Ovly1	12	50	125	30	325	610	SP12.5 FC2 (58-28)	CIREAM	HL-8	Granular A	Granular B-I	CL-ML	35
3	426														
4	670	Mil + Ovly1	35	40	50	130	550	-	SP12.5 FC2 (64-28)	SP19 (64-28)	HL-8	Granular B-I	-	SM	35
5	673														
6	719	Recon_Ac3	58	50	100	50	225	-	SP12.5 FC2 (58-28)	SP19 (58-28)	Granular A	Granular A	-	CI	40
7	825	EAS_Ovly1	89	40	110	130	290	240	SP12.5 FC2 (64-28)	SP19 (64-28)	EAS	Granular A	Granular B-I	CL-ML	25
8	826														
9	1052	Mil + Ovly1	401	40	50	160	320	550	SP12.5 FC2 (70-28)	SP19 (70-28)	HL-3	Granular A	Granular B-I	CL-ML	30
10	1139														
11	1245	Mil + Ovly1F	403	40	40	200	300	-	SP12.5 FC2 (64-28)	SP19 (64-28)	HDBC	Granular A	-	MI	35
12	1246														
13	1247														
14	1248														
15	1260														
16	1261														
17	1282	Recon_Ac5	406	40	60	100	450	-	SP12.5 FC2 (64-28)	SP19 (64-28)	SP25 (58-28)	Granular A	-	CL	35
18	1287														
19	1297	Recon_PCCF	410	40	100	100	100	150/410	SP12.5 FC2 (64-28)	SP19 (64-28)	SP25 (58-28)	OGDL	Granular A / B-I	CL-ML	30
20	1301		410												
21	1298		410	40	100	80	100	150/410	SP12.5 FC2 (64-28)	SP19 (64-28)	SP25 (58-28)	OGDL	Granular A / B-I	CL-ML	30
22	1302														

Table E.9: Material and structural information for the selected Superpave sections from eastern region

S. No.	Section ID	Activity	HWY	Layer Thickness (mm)					Layer Material					Sub-grade	Resilient Modulus (MPa)
				Lay 1	Lay 2	Lay 3	Lay 4	Lay 5	Lay 1	Lay 2	Lay 3	Lay 4	Lay 5		
1	156	FDR + Ovly3	7	40	50	50	300	-	SP12.5 FC1 (58-34)	SP19 (58-34)	SP19 (58-34)	Granular A	-	SM	30
2	158	HM Ovly1	7	40	125	180	-	-	SP12.5 FC1 (58-34)	CIR	Granular B-I	-	-	SM	50
3	159	CIR + Ovly1	7	60	70	90	220	-	SP12.5 FC1 (58-34)	CIR	HL-4	Granular B-I	-	SM	50
4	166	FDR + Ovly3	7	40	50	50	40	200	SP12.5 FC1 (58-34)	SP19 (58-34)	SP19 (58-34)	HL-4	Granular B-I	SM	35
5	437	Recon_Ac3	15	40	60	60	150	450	SP12.5 FC1 (58-28)	SP19 (58-28)	SP19 (58-28)	Granular A	Granular B-I	CH	20
6	697	HM Ovly2	41	40	50	200	-	-	SP12.5 (58-28)	SP19 (58-34)	Granular A	-	-	SM	80
7	698	HM Ovly2	41	40	50	200	190	150	SP12.5 (58-28)	SP19 (58-34)	Granular A	Granular A	Granular B-I	SM	80
8	727		60	50	150	145	150	-	SP12.5 (58-28)	HL-4	Granular B-I	Granular A	-	ML	80
9	728														
10	752		62	40	50	300	490	-	SP12.5 (58-34)	SP19 (58-34)	Granular A	Granular B-I	-	ML	50
11	887	FDR + Ovly2	118	300	30	150	250	250	SP12.5 (58-28)	SP12.5 (58-28)	Granular A	Granular B-I	Granular A	SM	35
12	1016	Mil + Ovly1	401	40	50	225	300	-	SP12.5 FC2 (64-34)	SP19 (64-34)	HL-8	Granular A	-	SM	35
13	1103														
14	1331	Mil + Ovly1	417	40	100	40	185	225	SP12.5 FC2 (64-34)	SP19 (64-34)	HDB	HL-4	Granular A	CL-ML	31
15	1332														

Table E.10: Material and structural information for the selected Superpave sections from northeast region

S. No.	Section ID	Activity	HWY	Layer Thickness (mm)					Layer Material					Sub-grade	Resilient Modulus (MPa)
				Lay 1	Lay 2	Lay 3	Lay 4	Lay 5	Lay 1	Lay 2	Lay 3	Lay 4	Lay 5		
1	265	CIR + Ovly2	11	60	60	110	250	320	SP12.5 (58-34)	CIR	HL-4	Granular A	Granular B-I	CL-ML	45
2	271	CIR + Ovly1	11	40	50	110 / 140	200	700	SP12.5 (58-34)	SP19 (58-34)	CIREAM / HL-4	Granular A	Granular B-I	CL-ML	40
3	477	CIR + Ovly2	17	40	50	75	200	640	SP12.5 (58-34)	SP19 (58-34)	CIR	HL-4	Granular A	SM	50
4	760	EAS_ Ovly1	63	40	50	175	100	625	SP12.5 (58-34)	SP19 (58-34)	EAS	Granular A	Granular B-I	CL-ML	45
5	764	FDR+ Ovly1	64	30	30	200	120	600	SP12.5 (52-34)	SP12.5 (52-34)	Granular A	Granular A	Granular B-I	CL-ML	35
6	791	Mil+ Ovly1	69	50	90	150	150	-	SP12.5 FC1 (58-34)	SP25 (58-34)	Granular A	Granular B-II	-	CL-ML	90
7	951	EAS_ Ovly1	144	50	150	50	90	994	SP12.5 (52-34)	EAS	HL-4	Granular A	Granular B-I	SM	28
8	952	EAS_ Ovly1	144	50	150	50	115	612	SP12.5 (52-34)	EAS	HL-4	Granular A	Granular B-I	SM	42
9	976	CIR + Ovly2	400	40	50	100	40	420	SP12.5 FC2 (64-34)	SP19 (58-34)	CIR	HL-4	Granular A	CL-ML	35
10	977														
11	978														
12	1001	CIR + Ovly2	400	40	50	100	170	540	SP12.5 FC2 (64-34)	SP19 (58-34)	CIR	HL-4	Granular A	CL-ML	70
13	1002														
14	1003														

Table E.11: Material and structural information for the selected Superpave sections from northwest region

S. No.	Section ID	Activity	HWY	Layer Thickness (mm)					Layer Material					Sub-grade	Resilient Modulus (MPa)
				Lay 1	Lay 2	Lay 3	Lay 4	Lay 5	Lay 1	Lay 2	Lay 3	Lay 4	Lay 5		
1	312	Mil+ Ovly1	11	60	130	150	700	-	SP12.5 (58-34)	EAS	Granular A	Granular B-I	-	SC	30
2	313														
3	314														
4	323	FDR + Ovly2	11	55	75	150	700	300	SP12.5 (64-34)	SP19 (64-34)	Granular A	Granular A	Granular B-I	SM	35
5	328	FDR + Ovly3	11	50	90	150	600	-	SP12.5 FC1 (64-34)	SP25 (64-34)	Granular A	Granular B-III	-	SM	35
6	334	FDR + Ovly1	11	50	150	150	600	-	SP12.5 (58-34)	EAS	Granular A	Granular B	-	SC	30
7	337	FDR + Ovly1	11	30	30	300	100	300	SP12.5 (58-34)	SP12.5 (58-34)	Granular A	Granular A	Granular B-I	SM	35
8	563		17	60	70	300	100	300	SP12.5 (58-34)	SP19 (58-34)	Granular A	Granular A	Granular B-I	CL-ML	25
9	574	HM Ovly1	17	50	50	150	600	-	SP12.5 (58-34)	SP19 (58-34)	Granular A	Granular B	-	SC	30
10	575														
11	576														
12	577														
13	578														

Table E.12: Material and structural information for the Marshall mix pavement sections

S. No.	Section ID	Activity	HWY	Layer Thickness (mm)					Layer Material					Sub-grade	Resilient Modulus (MPa)
				Lay 1	Lay 2	Lay 3	Lay 4	Lay 5	Lay 1	Lay 2	Lay 3	Lay 4	Lay 5		
1	9	Recon_ Ac5	1	40	90	130	100	300	DFC	HDB	HL 8	OGDL	Granular A	CI	35
2	43														
3	139	HM Ovly2	6	40	50	40 / 100	150	425	HL 1	HL 4B	HL 1 / HL 3	Granular A	Granular B-I	CI	35
4	191	Recon_ Ac3	7	40	50	40 / 200	150	300	HL 1	MDB	HL 1 / HL 4B	Granular A	Granular B-I	CI	40
5	217	HM Ovly2	8	40	100	35 / 100	150	450	DFC	HDB	HL 1 / HL 4B	Granular A	Granular B-I	CH	40
6	347	HM Ovly2	11	40	70	40 / 60	250	400	HL 1	HL 8	HL 1 / HL 8	Granular A	Granular B-I	CH	40
7	348	HM Ovly2	11	40	50	60 / 30	250	400	HL 1	HL 8	HL 3 / HL 8	Granular A	Granular B-I	CH	35
8	349	HM Ovly1	11	40	70	40 / 60	250	400	HL 1	HL 8	HL 1 / HL 8	Granular A	Granular B-I	CI	35
9	350	HM Ovly2	11	40	70	40 / 60	250	400	HL 1	HL 8	HL 1 / HL 8	Granular A	Granular B-I	CI	35
10	353	HM Ovly2	11	40	50	70 / 60	250	400	HL 1	HL 8	HL 3 / HL 8	Granular A	Granular B-I	CI	40
11	356	CIR + Ovly1	11	50	90	30	150	450	HL 3M	CIR	HL 2	Granular A	Granular B-I	CH	35
12	357	HM Ovly1	11	50	30	140 / 40	150	450	HL 3	HL 1	HL 4B / HL 1	Granular A	Granular B-I	CI	35
13	358	HM Ovly1	11	40	76	30	150	450	HL 1	HL 4B	HL 2	Granular A	Granular B-I	CH	50
14	361	HM Ovly1	11	40	76	30	150	450	HL 1	HL 4B	HL 2	Granular A	Granular B-I	CH	50
15	376	FDR + Ovly3	11	40	90	-	270	600	HL 1	HL 8	-	Granular A	Granular B-I	CI	28

16	377	HM Ovly2	11	40	30	40 / 30	250	400	HL 1	MDB	HL 4S / HL 8	Granular A	Granular B-I	CH	40
17	378	HM Ovly2	11	40	30	40 / 30	250	400	HL 1	MDB	HL 4S / HL 8	Granular A	Granular B-I	CH	40
18	379	HM Ovly2	11	40	80	80 / 40	250	400	HL 1	MDB	HL 8 / HL 1	Granular A	Granular B-I	CI	35
19	386	HM Ovly1	11	30	40	80 / 30	150	450	HL 3M	DFC	HL 4 / HL 2	Granular A	Granular B-I	CI	35
20	803	Recon_ Ac5F	85	40	50	40 / 100	150	450	DFC	HDB	HL 1 / HL 4B	Granular A	Granular B-I	CI	25
21	811	HM Ovly2	85	40	50	95 / 30	150	-	DFC	HDB	HL 4B / HL 8	Granular A	-	CH	40
22	951	HM Ovly2	400	40	50	190	150	610	DFC	HDB	HL 6	Granular A	Granular B-I	CI	41
23	981	HM Ovly2	400	40	50	30	150	400	HL 1	MDB	HL 2	Granular A	Granular B-I	CH	40
24	1049	Recon_ AcF	401	40	210	-	640	-	DFC	HDB	-	Granular O	-	SM	38
25	1053	Recon_ Ac5F	401	40	200	-	150	500	DFC	HL 4S	-	Granular A	Granular B-I	SM	15
26	1188	Recon_ Ac5F	402	40	80	100	150	450	HL 1	MDB	HL 4B	Granular A	Granular B-I	SM	25
27	1189	Recon_ Ac5F	402	40	80	100	150	450	HL 1	MDB	HL 4B	Granular A	Granular B-I	SM	25
28	1200	Recon_ Ac5F	402	40	80	100	150	450	HL 1	MDB	HL 4B	Granular A	Granular B-I	SM	25
29	1311	Recon_ Ac5F	417	40	40	60	150	450	HL 1	HDB	HDB	Granular O	Granular B-I	CI	18

REFERENCE LIST

AASHTO (2008). *Mechanistic-Empirical Pavement Design Guide: A Manual of Practice*, American Association of State Highway and Transportation Officials, Washington DC.

AASHTO (2010). *Guide for the Local Calibration of the Mechanical-Empirical Pavement Design Guide*, American Association of State Highway and Transportation Officials, Washington DC.

AASHTO (2011). *AASHTOWare DARWin-ME SOFTWARE HELP SYSTEM*

AASHTO (2014). *AASHTOWare Pavement ME Design Release Notes*

Agardh, S. (2005). "Rut Depth Prediction on Flexible Pavement- Calibration and Validation of Incremental Recursive Model." *Doctoral Thesis, Lund Institute of Technology, Sweden*.

Ahmed, M. A., Kass, S., Hilderman, S., and Tang, W. K. S. (2011). "MEPDG Implementation: Manitoba Experience." *Annual Conference of the Transportation Association of Canada, Edmonton, Alberta*.

Banerjee, A., Aguiar-Moya, J. P., Smit, A. de F., and Prozzi, J. A. (2008). "Development of the Texas Flexible Pavements Database." *Center for Transportation Research, Austin, Report No. FHWA/TX-10/0-5513-2*.

Banerjee, A., Aguiar-Moya, J. P., and Prozzi, J. A. (2009). "Calibration of Mechanistic-Empirical Pavement Design Guide Permanent Deformation Models." *Transportation Research Record, Journal of Transportation Research Board, (No.2094), pp. 12-20*.

Banerjee, A., Prozzi, J. A., and Aguiar-Moya, J. P., (2010). "Calibration of MEPDG Permanent Deformation Performance Model for Different Maintenance and Rehabilitation Strategies." *Transportation Research Board Paper 10-2355*.

Bayomy, F., El-Badawy, S., and Awed, A., (2012). "Implementation of the MEPDG for Flexible Pavements in Idaho." *Idaho Transportation Department Research Program, FHWA-ID-12-193*.

Boone, J. N. (2013). "Comparison of Ontario Pavement Designs Using the AASHTO 1993 Empirical Method and the Mechanistic-Empirical Pavement Design Guide Method." MASC, University of Waterloo, Canada.

Caliendo, C. (2012). "Local calibration and implementation of the mechanistic-empirical pavement design guide for flexible pavement design." *Journal of Transportation Engineering*, 138(3), 348-360.

Crawford, G. (2009). "National Trends in Pavement Design." Southeastern States Pavement Management Association, Pavement Management and Design, New Orleans, Louisiana.

Crovetti, J. A., and Hall, K. T. (2012). "Local Calibration of the Mechanistic Empirical Pavement Design Software for Wisconsin." SPR #0092-09-30, SPR # 0092-09-31 Wisconsin Department of Transportation Research & Library Unit, 4802 Sheboygan Ave. Madison, WI 53707.

Darter, M. I., Titus-Glover, L., and VonQuintus, H. L. (2009). "Implementation of the Mechanistic–Empirical Pavement Design Guide in Utah: Validation, Calibration, and Development of the UDOT MEPDG User's Guide.", *Utah Department of Transportation, Report No. UT--09.11*.

Donahue, J. (2008). "Local calibration of the MEPDG for HMA pavements in Missouri." *Journal of the Association of Asphalt Paving Technologists, Volume: 77, Asphalt Paving Technology 2008*, 975-984.

Dzotepe, G. A., and Ksaibati, K. (2011). "The Effects of Environmental Factors on the Implementation of the Mechanistic-Empirical Pavement Design Guide (MEPDG)." *Department of Transportation, University Transportation Center Program, University of Wyoming.*

Flintsch, G., McGHEE, K.K., (2009). "Quality Management of Pavement Condition Data Collection- A Synthesis of Highway Practice." NCHRP Synthesis 401,TRB

Glover, L. T., and Mallela, J. (2009). "Guidelines for Implementing NCHRP 1-37A M-E Design Procedures in Ohio: Volume 4 - MEPDG Models Validation and Recalibration." *Applied Research Associates, Inc., Report No. FHWA/OH-2009/9D.*

Gramling, W. L., Hunt, J. E., and Suzuki, G. S. (1991). "Rational Approach to Cross-Profile and Rut Depth Analysis." *Transportation Research Record*, (1311), 173-179.

Hajek, J. J., Musgrove, G., and Kazmierowski, T. J. (1998). "Measurement, Management and Utilization of Rutting Data." Ontario Ministry of Transportation, 4th International Conference on Managing Pavements, 17 to 21 May 1998, Durban, South Africa, Vol. 1, pp. 226-237.

Hall, K. D., Xiao, D. X., and Wang, K. C. P. (2010). "Calibration of the mechanistic-empirical pavement design guide for flexible pavement design in Arkansas." *Transportation Research Board 2011 Annual Meeting.*

He, W., Juhasz, M., Crockett, J., and Lakkavalli, V. (2011). "Evaluation of DARWin-ME Pavement Rutting Prediction Models Using Data from Alberta's Pavement Management System." *Annual Conference of the Transportation Association of Canada* Edmonton, Alberta.

Hoegh, K., Khazanovich, L., and Jensen, M. (2010). "Local Calibration of Mechanistic-Empirical Pavement Design Guide Rutting Model for Minnesota Road Research Project Test Sections." *Transportation Research Record*, (2180), pp. 130-141.

Huang, Y. H. (2004). *Pavement Analysis and Design*, Pearson Prentice Hall, Pearson Prentice Hall Upper Saddle River, NJ 07458.

Hussan, S., Kamal, M. A., Khan, M. B., Irfan, M., and Hafeez, L. (2013). "Determining the Contribution of Different Structural Layers of Asphalt Pavement System to Rutting Using Transverse Profile Analysis." *American Journal of Civil Engineering and Architecture*, Vol. 1, No. 6, pp. 174-180.

Jadoun, F. M. (2011). "Calibration of the Flexible Pavement Distress Prediction Models in the Mechanistic-Empirical Pavement Design Guide (MEPDG) for North Carolina." *Doctor of Philosophy, North Carolina State University, North Carolina*.

Jannat, G. (2012). "Database Development for Ontario's Local Calibration of Mechanistic-Empirical Pavement Design Guide (MEPDG) Distress Model." *MASc, Ryerson University, Canada*.

Kazmierowski, T., He, Z., and Kerr, B. (2001). "A Second Generation PMS for the Ministry of Transportation of Ontario." *Ontario Ministry of Transportation, 5th International Conference on Managing Pavements, August 2001, Seattle, WA*.

Khan, K. M. (2008). "Impact of Superpave Mix Design Method on Rutting Behaviour of Flexible Pavements." *Doctor of Philosophy, University of Engineering and Technology Taxila*.

Kim, Y. R., Jadoun, F. M., Hou, T., and Muthadi, N. (2001). "Local Calibration of the MEPDG for Flexible Pavement Design." *Final Report submitted to the North Carolina Department of Transportation, Research Project No. HWY-2007-07*.

Korczak, R. C. (2013). "Utilizing the Canadian Long-Term Pavement Performance (C-LTPP) Database for Asphalt Dynamic Modulus Prediction." *MASc, University of Waterloo, Canada*.

Lenngren, C. A. (1988). "Some Approaches in Treating Automatically Collected Data for Rutting." *Transportation Research Record*, (1196), pp. 20-26.

Li, N. (2011). "Quality Assurance of Pavement Profile Measurements in Managing Ontario Provincial Highway Network." *Ministry of Transportation of Ontario*.

Li, N. and Kazmierowski, T. (2008). "Engineering tools and standards applied in preserving Ontario's provincial highways." 7th conference on managing pavements and other roadway assets, Calgary, Alberta, Canada.

Li, J., Pierce, L. M., and Uhlmeier, J. (2009). "Calibration of Flexible Pavement in Mechanistic-Empirical Pavement Design Guide for Washington State." *Transportation Research Record*, (2095), pp. 73-83.

Mallela, J., Glover, L. T., Sadasivam, S., Bhattacharya, B., Darter, M. I., and VonQuintus (2013). "Implementation of the AASHTO Mechanistic-Empirical Pavement Design Guide for Colorado." *Colorado Department of Transportation, Applied Research Associates, Inc.*, Report No. CDOT-2013-4.

Mallela, J., Glover, L. T., and Darter, M. I. (2009). "Guidelines for Implementing NCHRP 1-37A M-E Design Procedures in Ohio: Volume 1— Summary of Findings, Implementation Plan, and Next Steps ", Ohio Department of Transportation, and the U.S. Department of Transportation, Federal Highway Administration, Applied Research Associates, Inc.

Momin, S. A. (2011). "Local Calibration of Mechanistic-Empirical Pavement Design Guide for North Eastern United States." *MASc, The University of Texas at Arlington*.

Monismith, C. L. (2004). "Evolution of Long-Lasting Asphalt Pavement Design Methodology: A Perspective." International Society for Asphalt Pavements, International Symposium on Design and Construction of Long Lasting Asphalt Pavement, June 7-9, 2004, Auburn University, Alabama, USA.

MTO, M. E. R. O. (2012). "Ontario's Default Parameters for AASHTOWare Pavement ME Design Interim Report."

NCHRP (2004). "Guide for Mechanistic Empirical Design of New and Rehabilitated Pavement Structures." ARA, Inc., ERES Division 505 West University Avenue Champaign, Illinois 61820.

NCHRP (2006). "Research Results Digest 307 Independent Review of the Mechanistic-Empirical Pavement Design Guide and Software." Transportation Research Board, Washington, D.C.

NCHRP (2006). "Research Results Digest 308 Changes to the Mechanistic-Empirical Pavement Design Guide Software Through Version 0.900, July 2006." Transportation Research Board, Washington, D.C.

NCHRP (2013). "Research Results Digest 372 Sensitivity Evaluation of MPDG Performance Prediction." Transportation Research Board, Washington, D.C.

Rada, G. R., Jones, D. J., Harvey, J. T., Senn, K. A., and Thomas, M. (2013). "NCHRP REPORT 747 Guide for Conducting Forensic Investigations of Highway Pavements." Transportation Research Board, American Association of State Highway and Transportation, National Research Council, Washington, D.C.

Salama, H. K., Chatti, K., and Haider, S. W. "Backcalculation of permanent deformation parameters using time series rut data from in-service pavements." Proc., Pavement Rehabilitation, Strength and Deformation Characteristics, and Surface Properties-Vehicle Interaction 2006, National Research Council, 98-109.

Schram, S. A., and Abdelrahman, M. (2010). "Integration of Mechanistic-Empirical Pavement Design Guide Distresses with Local Performance Indices", *Transportation Research Record*, (2153), pp. 13-23.

Schwartz, C. W., Li, R., Kim, S. H., Ceylan, H., and Gopalakrishnan, K. (2011). "Sensitivity Evaluation of MEPDG Performance Prediction." National Cooperative Highway Research Program, Transportation Research Board of the National Academies, Project 1-47.

Schwartz, C. W., Carvalho, R. L., (2007). "Implementation of the NCHRP 1-37A -Design Guide: Evaluation of Mechanistic-Empirical Design Procedure." Maryland State Highway Administration, Final Report Volume 2, MDSHA Project No. SP0077B41 UMD FRS No. 430572.

Simpson, L. A., Daleiden, J. F., and Hadley, W. O. (1995). "Rutting Analysis from a Different Perspective." *Transportation Research Record*, (1473), pp. 9-16.

Siraj,N., (2008). "Verification of Asphalt Concrete Performance Prediction using Level 2 and Level 3 inputs of Mechanistic-Empirical Pavement Design Guide for Flexible Pavements of the State of New Jersey.", *MASc*, Rowan University.

Siraj, N., Mehta, Y. A., Muriel, K. M., and Sauber, R. W. "Verification of Mechanistic-Empirical pavement design guide for the state of New Jersey." Proc., 8th International Conference on the Bearing Capacity of Roads, Railways and Airfields, BCR2A'09, June 29, 2009 - July 2, 2009, CRC Press, 921-930.

Souliman, M. I., Mamlouk, M. S., El-Basyouny, M. M., and Zapata, C. E. "Calibration of the AASHTO MEPDG for flexible pavement for Arizona conditions." Proc., 89th Annual Meeting of the Transportation Research Board, Transportation Research Board.

Tarefder, R., and Rodriguez-Ruiz, J. (2013). "Local Calibration of MEPDG for Flexible Pavements in New Mexico." *Journal of Transportation Engineering*, Volume 139(10), 981-991.

Tighe, S. L., McLeod, N. W., and Juhasz, M. (2011). "Development of the New 2011 Canadian Pavement Asset Design and Management Guide: A Brief Summary of Canadian State-of-the-

Practice." *Ontario Ministry of Transportation, 8th International Conference on Managing Pavement Assets, November 15-19, 2011, Santiago, Chile.*

Torres-Machi, C., Chamorro, A., Videla, C., Pellicer, E., and Yepes, V. (2012). "Optimization and Prioritization Methods for Pavement Network Management." *Research and Department of Solutions for Urban Pavement Management in Chile.*

Villiers, C., Reynaldo, R., and Dietrich, B. (2005). "Interpretation of Transverse Profiles to Determine the Source of Rutting Within an Asphalt Pavement System." *Transportation Research Record, Volume 1905, 73-81.*

VonQuintus, H. L., Mallela, J., Bonaquist, R., Schwartz, C. W., and Carvalho, R. L. (2012). "NCHRP REPORT 719 Calibration of Rutting Models for Structural and Mix Design." *Transportation Research Board, American Association of State Highway and Transportation, National Research Council, Washington, D.C.*

VonQuintus, H. L., and Moulthrop, J. S. (2007). "Mechanistic–Empirical Pavement Design Guide Flexible Pavement Performance Prediction Models for Montana.", *Montana Department of Transportation, Helena, Montana.*

Waseem, A. (2013). "Methodology Development and Local Calibration of MEPDG Permanent Deformation Models for Ontario's Flexible Pavements." *MASc, Ryerson University, Canada.*

Werkmeister, S. (2002). "Permanent deformation behaviour of unbound granular materials." *Ph.D, University of Technology Dresden.*

Werkmeister, S., Dawson, A. R., and Wellner, F. (2005). "Permanent Deformation Behaviour of Granular Materials." *Road Materials and Pavement Design, 31-51.*

White, T. D., Haddock, J. E., Hand, A. J. T., and Fand, H. (2002). "NCHRP REPORT 468 Contributions of Pavement Structural Layers to Rutting of Hot Mix Asphalt Pavements."

Transportation Research Board, American Association of State Highway and Transportation, National Research Council, Washington. D.C.

Williams, D. R. C., and Shaidur, R. (2013). "Mechanistic-Empirical Pavement Design Guide Calibration for Pavement Rehabilitation." SPR 718 Institute for Transportation Iowa State University, 2711 South Loop Drive, Suite 4700 Ames, IA 50010-8664

Xu, T., and Huang, X. (2012). "Investigation into Causes of in-place Rutting in Asphalt Pavement." *Research Article, Construction and Building Materials, Volume 28, Issue 1*. pp. 525-530